A satellite-based approach to estimating spatially distributed groundwater recharge rates in a tropical wet sedimentary region despite cloudy conditions

Luís Romero Barbosa[a,b,c,1], Victor Hugo R. Coelho[d,*,1], Ana Claudia V. e L. Gusmão[c], Lucila A. Fernandes[c], Bernardo B. da Silva[e], Carlos de O. Galvão[f], Nelson O. L. Caicedo[a], Adriano R. da Paz[a], Yunqing Xuan[g], Guillaume F. Bertrand[h], Davi de C. D. Melo[i], Suzana M. G. L. Montenegro[c], Sascha E. Oswald[b], Cristiano das N. Almeida[a]

[a] Department of Civil and Environmental Engineering, Federal University of Paraíba, João Pessoa, Brazil

[b] Institute of Environmental Science and Geography, University of Potsdam, Potsdam, Germany

[c] Department of Civil Engineering, Federal University of Pernambuco, Recife, Brazil

[d] Department of Geosciences, Federal University of Paraíba, João Pessoa, Brazil

[e] Department of Atmospheric Sciences, Federal University of Campina Grande, Campina Grande, Brazil

[f] Department of Civil Engineering, Federal University of Campina Grande, Campina Grande, Brazil

[g] College of Engineering, Swansea University, Swansea, UK

[h] Laboratory of Chrono-Environment, University of Bourgogne Franche-Comté, Besançon, France

[i] Department of Soils and Rural Engineering, Federal University of Paraíba, Areia, Brazil

[1] These authors contributed equally to this work.

*Corresponding author. Tel.: +55 83 32167432. E-mail address: victor.coelho@academico.ufpb.br

ABSTRACT: Groundwater recharge (GWR) is one of the most challenging water fluxes to estimate, as it relies on observed data that are often limited in many developing countries. This study developed an innovative water budget method using satellite products for estimating the spatially distributed GWR at monthly and annual scales in tropical wet sedimentary regions despite cloudy conditions. The distinctive features proposed in this study include the capacity to address 1) evapotranspiration estimations in tropical wet regions frequently overlaid by substantial cloud cover; and 2) seasonal root-zone water storage estimations in sedimentary regions prone to monthly variations. The method also utilises satellite-based information of the precipitation and surface runoff. The GWR was estimated and validated for the hydrologically contrasting years 2016 and 2017 over a tropical wet sedimentary region located in North-eastern Brazil, which has substantial potential for groundwater abstraction. This study showed that applying a cloud-cleaning procedure based on monthly compositions of biophysical data enables the production of a reasonable proxy for evapotranspiration able to estimate groundwater by the water budget method. The resulting GWR rates were 219 (2016) and 302 (2017) mm yr^{-1}, showing good correlations (CC = 0.68 to 0.83) and slight underestimations (PBIAS = -13 to -9%) when compared with the referenced estimates obtained by the water table fluctuation method for 23 monitoring wells. Sensitivity analysis shows that water storage changes account for +19% to -22% of our monthly evaluation. The satellite-based approach consistently demonstrated that the consideration of cloud-cleaned evapotranspiration and root-zone soil water storage changes are essential for a proper estimation of spatially distributed GWR in tropical wet sedimentary regions because of their weather seasonality and cloudy conditions.

Keywords: Remote sensing, water balance, groundwater recharge, water table fluctuation, tropical climate, sedimentary aquifer.

1. Introduction

Understanding the factors constraining groundwater recharge (GWR) is important for management and planning purposes of this water resource that is only slowly renewed (Cuthbert et al., 2019). In some regions, for instance, the abstracted groundwater over the past decades are taken from non-renewable groundwater (Döll et al., 2014), which increases, even more, the need for a better understanding of such factors. These abstractions need to be regionally regulated (Aeschbach-Hertig and Gleeson, 2012), since groundwater serves as the key strategic reserve for supplying water to societies during long-lasting droughts (Famiglietti, 2014). Such regulation, in turn, requires accurate information about the spatiotemporal distribution of natural GWR rates (Jasechko et al., 2014), including their variability and uncertainty in estimations, which are strongly sensitive to climate forcing factors, land uses and covers, watershed geomorphology and local hydrogeology (Moeck et al., 2020).

Since GWR is a key component used in many hydrological models to assess groundwater resource worldwide (Graaf et al., 2017; Wada et al., 2010), its accurate estimation constitutes a priority for stakeholders and a research challenge for the scientific community (Jasechko et al., 2014; Mohan et al., 2018). Many methods have been developed to estimate natural GWR at various spatiotemporal scales, with a wide range of complexity (Walker et al., 2019), given that GWR cannot be directly measured (Melo et al., 2015). Making use of these methods often depends on data availability, desired spatiotemporal resolution, and result representations (Walker et al., 2019).

The following five methods are commonly used to estimate GWR: 1) tracer techniques, which estimate aquifer renewal via substances in the water or specific concentrations of chemical elements, such as the chloride mass-balance method (e.g., Brunner et al., 2004; Hornero et al., 2016); 2) groundwater level monitoring in unconfined aquifers, which include examples such as water table fluctuation method (e.g., Cai and Ofterdinger, 2016; Wendland et al., 2007) and cumulative rainfall departure methods (e.g., Ahmadi et al., 2015; Weber and Stewart, 2004); 3) Darcy's law application, which allows calculating the velocity of soil water percolation and requires knowledge of hydraulic gradient and vertical hydraulic conductivity (e.g., Callahan et al., 2012; Yin et al., 2011); 4) numerical modelling, which consists of a mathematical representation of the GWR process (e.g., Melo et al., 2015; Melo and Wendland, 2017); and 5) the water balance method, which considers the main variables of the hydrological cycle as inputs and outputs of the system (e.g., Hornero et al., 2016; Wendland et al., 2007).

Most of the aforementioned methods are based on point-scale observations (e.g., meteorological stations or boreholes), which may cause serious issues when spatial variability in the regions of concern is great (e.g., Melo and Wendland, 2017). Although such a problem can be simply ignored for regions with extremely dense observation networks, it remains persistent in most regions worldwide, especially in developing countries. For instance, in Brazil, the national ground-based monitoring network consists of about 400 wells distributed over the country, complemented by a small number of observation wells monitored in only 21 active experimental basins (Melo et al., 2020). Therefore, the chief challenge for many hydrologists is to find and utilise alternative sources of data to estimate the spatial information of GWR (Brunner et al., 2007).

The use of cutting-edge satellite-derived remote sensing technology has played a crucial role in assimilating valuable distributed observation and in modelling water resources, which would otherwise be impossible with relatively sparse ground-based measurements alone (Famiglietti et al., 2015). However, the remote sensing contributions are rather inconsistent at quantifying and estimating GWR because all current data from satellite data can only detect patterns and processes related to water resources on and above the surface (Brunner et al., 2007; Coelho et al., 2017; Lucas et al., 2015). Satellite-based observations of time-variable gravity, such as the joint mission of the Gravity Recovery and Climate Experiment (GRACE), are sensitive to variations of terrestrial water storage, including the groundwater storage changes (Tapley et al., 2004; Vasco et al., 2019; Wahr et al., 2004). Unfortunately, the low spatial resolution of GRACE-derived data limits its ability to provide localised groundwater information at an appropriate scale (Alley and Konikow, 2015; Lakshmi et al., 2018). Thus, an innovative use of satellite data to estimate GWR at local and regional scales has been recently proposed, where most of data are applied to a simplified water budget approach that uses precipitation and evapotranspiration products (e.g., Crosbie et al., 2015; Gokmen et al., 2013; Lucas et al., 2015; Munch et al., 2013; Szilágyi et al., 2012; Szilagyi et al., 2011). This approach disregards other water balance components, such as surface runoff and soil water storage changes, which could considerably alter the estimation accuracy of GWR in some regions for short time scales (e.g., monthly).

In this context, some studies also have considered uniform surface runoff (Khalaf and Donoghue, 2012), as well as spatially distributed information about surface runoff (Coelho et al., 2017) and irrigation (Usman et al., 2015). The aforementioned studies used different remote sensing products and algorithms, but all of them were developed in regions with arid, semiarid, continental or Mediterranean climate

conditions where the cloud cover is limited (Coelho et al., 2017). For some tropical regions such as Brazil, the estimation of GWR using this approach remains challenging, mainly because of the difficulties in obtaining continuous information of actual evapotranspiration data by remote sensing without substantial cloud cover. In parallel, soil moisture information from satellite observations is currently available at the global scale and can provide valuable data to update the water budget approach with information regarding water storage changes in unsaturated soil layers (Reichle et al., 2018). Accounting for this component is particularly important for understanding GWR in sedimentary aquifers, where the unsaturated vadose zone width may vary from thin to thick soil layers (Rossetti et al., 2012). Unfortunately, some satellite-based datasets are only recently available, but some applications require earlier data.

Based on this information, this study develops an innovative water budget method using satellite-based data for estimating natural spatially distributed GWR rates at annual and monthly scales in tropical wet sedimentary regions, taking into account cloudy conditions. Accordingly, this study hypothesizes that such an approach enables local and regional scale perspectives in ungauged tropical wet regions. The general and transferable strategy would be relevant to account for 1) the substantial cloud cover and 2) the water storage changes in sedimentary regions prone to monthly variations. The method also utilises spatially distributed information on precipitation and surface runoff estimated from satellite products. The major limitation of this residual approach is that the accuracy of the GWR depends on the accuracy of the other components considered in the water balance (Scanlon et al., 2002), i.e., its application is appropriated when the errors of these components are small relative to the water flux. This limitation, when a satellite-based approach is considered, is mainly identified in regions that present ground-truth measurements discrepant with the estimated products used in the water balance, especially the main input (precipitation) and output (evapotranspiration) of the system. On the other hand, ground-based evaluations are punctual and representative of small areas, hardly integrating the spatial heterogeneity of meteorological processes, especially in urban areas (Maier et al., 2020). This study used ground-truth measurements to assess the two main estimated components of the water balance (i.e., precipitation and evapotranspiration) and the GWR rates.

2. Materials and methods

2.1 Study area

The study was carried out over an area of 1,032 km^2 in João Pessoa (JPA) (Paraíba, NE Brazil), which includes the metropolitan region and surrounding rural areas (Fig. 1). It consists in 1) the Gramame river basin (589.1 km^2; 57.1% of the area), and 2) the right bank of the Baixo Paraíba river basin (442.9 km^2; 42.9% of the area). The main source of water of the JPA metropolitan region (~1 million inhabitants) is the Gramame-Mamuaba reservoir, with maximum volume capacity of 56.9 hm^3. The water supply is complemented by more than 756 wells (CPRM – Geological Service of Brazil, 2020), pumped mostly for the public, industry, and irrigation, which are essential during periods of surface water shortage.

INSERT FIG. 1 HERE

Fig. 1. Location of (a) Brazil, (b) Paraíba state, and (c) João Pessoa (JPA) study area with the monitoring network, (d) land use and land cover, and (e) soil types.

The JPA has a tropical wet climate with a dry summer (i.e., As, according to the Köppen climate classification), with a mean temperature of 26°C and well-distinguished rainy and dry seasons (Alvares et al., 2013). The average annual precipitation is 1,700 mm, of which ~70% occurs from March to August during the austral autumn and winter. The potential evapotranspiration is relatively high in JPA, with mean annual values greater than 1,500 mm. The predominant land use and land cover (LULC) types in JPA are cropland (30.7%), Atlantic Forest (28.4%), pasture (26.3%), and urban areas (9.5%). The forest areas are Atlantic remnants, and the cropland areas contain mainly sugarcane and pineapple crops. Moreover, the main soil types in JPA are acrisols (58.7%), fluvisols (12.0%), podzols (10.8%), lixisols (9.1%) and histosols (5.5%). The fluvisols and histosols surround the rivers and the JPA urban area.

The hydrogeological framework mainly consists in 1) a coastal multi-layered sedimentary aquifer system near the littoral (i.e., the Paraíba Basin) and 2) a regional substratum that outcrops upstream in the more continental area (i.e., the Borborema Province). This latter corresponds to the crystalline regional basement that was affected by rifting processes due to the Cretaceos Atlantic aperture. This resulted in a graben that was progressively and sequentially filled by sediments as follows: 1) up to 360 m-thick fluvial sandstones of the Beberibe Formation from the Coniacian–Santonian age; 2) a 70 m-thick fossiliferous

calciferous sandstones and muddy siltstones of the Itamaracá Formation formed in marine transitional settings during the Santonian-Campanian age; 3) a 50-m thick phosphatic rocks and calciferous shales of the marine Gramame Formation from the Campanian-Maastrichtian age; and 4) a nearly 70 m-thick succession of fluvial sandstones and mudstones of the Barreiras Formation from the Early/Middle Miocene ages (Rossetti et al., 2012, 2011).

2.2 Satellite-based water budget approach

The actual GWR rates, defined as the rate at which water arrives at the table of an aquifer (Mathias et al., 2017), were spatially estimated from the residual terms of the water budget equation using satellite-based information. This estimation was performed for two hydrologically contrasting years 2016 and 2017, in which ground-based information was measured to evaluate the results. The GWR rates were then calculated at the monthly and annual scales by Eq. (1).

$$\mathrm{GWR} = \begin{cases} \mathrm{P} - \mathrm{ET} - \Delta\mathrm{S} - \mathrm{Q}\,, & \text{if } \mathrm{P} - \mathrm{ET} - \Delta\mathrm{S} - \mathrm{Q} > 0 \\ 0\,, & \text{if } \mathrm{P} - \mathrm{ET} - \Delta\mathrm{S} - \mathrm{Q} \leq 0 \end{cases} \quad (1)$$

where GWR is the groundwater recharge, P is the precipitation, ET is the actual evapotranspiration, ΔS is the water storage change at a root-zone scale (100-cm depth), and Q is the surface runoff. Other input and output water balance components were not investigated in this study because 1) they frequently represent relatively small contributions to the root zone (e.g., water pumping) or are implicitly considered in the aforementioned components (e.g., irrigation and interception), and 2) there are no reliable in situ data available for the JPA. Moreover, horizontal groundwater flow was also neglected because it refers to a slower GWR mechanism rather than the direct contribution of vertical infiltration (e.g., Coelho et al., 2017; Crosbie et al., 2015; Munch et al., 2013), since ~70% of the study area has terrain slope ranging from 0 to 92 m km^{-1}, which means that the topography predominantly presents weak slopes. All the used remote sensing products and other input data are summarised in Fig. 2 and described thoroughly in the next sub-items of this sub-section.

INSERT FIG. 2 HERE

Fig. 2. Satellite-based water budget approach showing the remote sensing products and other input data used to estimate the water balance components and groundwater recharge.

2.2.1 Precipitation

P was estimated by the Global Precipitation Measurement (GPM) mission, which is an international network of satellites undertaken by the National Aeronautics and Space Administration (NASA) of the USA and the Japanese Aerospace Agency (JAXA) (Huffman et al., 2018). This mission provides rainfall and snowfall information globally via the Integrated Multi-satellitE Retrievals for GPM (IMERG) products at 0.1° (~10 km) and 30-min resolutions (Huffman et al., 2018). IMERG is an algorithm that combines microwave and infrared estimates from the GPM constellation. This study used version V05B of the IMERG Final Run product. The IMERG Final Run product also incorporates monthly gauge observations from the Global Precipitation Climatology (GPCC) and other ancillary data to improve the satellite estimations (Skofronick-Jackson et al., 2017). This product is ready for use after 3.5 months of the data acquisition (Skofronick-Jackson et al., 2018). The advantage of IMERG is the high spatial resolution when compared to other satellite-based products. On the other hand, the weakness of this product is its latency (~3.5 months), which is inappropriate for real-time applications.

IMERG P is a valuable source of information for global and regional applications mainly because of its high spatiotemporal resolution. However, for medium- and small-scale hydrological studies, the spatial resolution of 0.1° of the IMERG product is still coarse (Sharifi et al., 2019). Due to the dimension of the study area, the IMERG data was downscaled to a resolution of 0.0045° (~500 m), similarly to Lu et al. (2019). The bilinear interpolation method was used to downscale the IMERG product, as it can provide consistent data disaggregation (Moghim et al., 2016). The 30-min IMERG data were accumulated aggregated to daily, monthly, and annual P scales.

The accuracy of remote sensing P products can be hampered by various factors, such as calculation algorithms and satellite sensor characteristics (Semire et al., 2012). The assessment carried out by Gadelha et al. (2019) found that in comparison with the ground-based rainfall data, the IMERG V05B effectively captures the P spatial patterns over most of the Brazilian territory, except for the entire coastal zone of NE Brazil, where underestimates occurs. For this reason, a linear-scaling bias correction procedure was applied (Lenderink et al., 2007), using a single correction factor per month calculated by the ratio between the monthly averages of rain gauges and the IMERG data (Le et al., 2018) rather than a grid-box correction (i.e., pixel-per-pixel) to preserve the original spatial distribution of the IMERG data.

P data measured from 16 rain gauges that are subjected to quality control were used for the IMERG bias correction and comparison purposes (Fig. 1c). The gridded observed rainfall data were estimated by

inverse distance weighting interpolation. For comparison purposes, Quantile-Quantile plots between the bias-corrected IMERG interpolated data (henceforth IMERG-C) and ground-based interpolated data were built at the monthly and annual scales for every 10% percentiles (i.e., 0, 10, …, 90, 100%). Over these estimates, the linear regressions were plotted, and their slope and y-intersect values were calculated. Moreover, the rain gauges interpolated data were used as input to spatially estimate the runoff and the GWR from the water budget equation. The estimates were then compared with the estimated components obtained from the satellite-based approach.

2.2.2 Actual evapotranspiration

The ET was estimated using the Penman-Monteith equation (Monteith, 1965), which was also adopted by Mu et al. (2007) to create the first global ET product (MOD16). The MOD16 is a product from NASA based on the MODerate Resolution Imaging Spectroradiometer (MODIS) sensors installed on two satellites (Terra and Aqua), as well as reanalysis-derived meteorological inputs. Currently, the MOD16 dataset provides ET at the global scale with a spatial resolution of 500 m and three different timescales (8-d, monthly, and annual scales). Unlike the algorithm used by Mu et al. (2011) to generate the current MOD16 product, this study calculated the ET based on the algorithm developed by Mu et al. (2007), using the biome-property-look-up-table shown by Running et al. (2017). The algorithm proposed by Mu et al. (2007) was based on Eq. (2) and assumes that night-time ET is small and in turn negligible.

$$\Lambda E = \Lambda E_{transp} + \Lambda E_{soil} = \frac{\Delta A + \rho C_p (e_s - e_a)/r_a}{\Delta + \gamma(1 + \frac{r_s}{r_a})} \quad (2)$$

where Λ is the latent heat of evaporation (=2.45 MJ kg^{-1}), ΛE is the latent heat flux density (W m^{-2}) consisting of the plant transpiration (ΛE_{transp}) and soil evaporation (ΛE_{soil}), i.e., the total daily ET (mm) after multiplying by the conversion factor (=3.53×10^{-2} mm d^{-1} W^{-1} m^{2}); A is the available energy commonly determined as the daily net radiation of the land surface (Rn) (W m^{-2}); ρ is the air density (=1.2 kg m^{-3}); C_p is the specific heat capacity of air at constant pressure (=1005 J kg^{-1} °C^{-1}); r_a is the aerodynamic resistance (s m^{-1}), r_s is the surface resistance (s m^{-1}); e_a is the actual water vapour pressure (kPa); e_s is the saturated water vapour pressure (kPa); Δ is the slope of the curve relating saturated water vapour pressure to the temperature (kPa °C^{-1}); and γ is the psychrometric constant (kPa °C^{-1}).

The MOD16 algorithm is only suitable to use under clear sky conditions, as MODIS satellite sensors cannot measure cloud base parameters (Sur et al., 2015). This occurs because the MOD16 generates the ET based on some 8-day MODIS products (i.e., pixels of the best observations from the last eight days) with 500-m spatial resolutions (e.g., MOD15A2H and MCD43A2/A3). These 8-d products remain insufficient to attenuate cloudy condition effects on ET estimations in some regions (Running et al., 2017).

The available MOD09Q1 (Terra) and MYD09Q1 (Aqua) reflectance products were used in this study due to their suitable 250-m and 8-d resolutions to obtain the biophysical data, namely, 1) the leaf area index (LAI) using the soil adjusted vegetation index (SAVI) (Bastiaanssen et al., 1998; Huete, 1988), 2) the vegetation cover fraction calculated by the enhanced vegetation index (EVI2) proposed by Jiang et al. (2008), and 3) the surface albedo (ALB) computed by the equation proposed by Teixeira et al. (2013). To address the shortcomings related to cloudy conditions, this study carried out monthly map compositions with 8-d grid biophysical inputs (i.e., EVI2, LAI, and ALB). The monthly compositions were based on the selection of pixels with higher values of LAI and EVI2 obtained from the eight images available per month (i.e., four MOD09Q1 and four MYD09Q1), assuming that lower or negative values of these two biophysical parameters were possibly contaminated by clouds. Conversely, for the monthly compositions of ALB, only the lower values per pixel from the eight images available per month were considered, assuming that higher values of albedo were possibly contaminated by clouds. These new data then assumed clear sky conditions to indicate fixed input parameters throughout a month and were used to generate daily ET data.

The MOD16 product also uses global LULC classification from MODIS land cover type (MCD12Q1) as an input to obtain information about canopy conductance and plant transpiration. However, the global representation of the MCD12Q1, which is associated with the limited number of classes (17), can misidentify some local and regional specificities of the vegetation and introduce considerable errors in the estimation of ET for medium and small areas (Ruhoff et al., 2013). Therefore, we used a regional LULC classification (SEEG/OC, 2015), namely, the MapBiomas Project (http://mapbiomas.org). MapBiomas provides Landsat-based annual LULC maps associated with 27 classes at a 30-m spatial resolution processed from 1985. In this study, MapBiomas LULC collection 3.1 was reclassified into six general classes (barren land, forest, cropland, pasture, urban, and water body) before being used to generate ET data.

The MOD16 product uses the global meteorological reanalysis data provided by NASA's Global Modelling and Assimilation Office (GMAO) at a 0.5° × 0.6° or 1.0° × 1.25° spatial resolution as inputs of

the original algorithm (Mu et al., 2011, 2007; Running et al., 2017). GMAO incorporates ground- and satellite-based observations to provide information with a 6-h temporal resolution. Unlike the MOD16 product, this study used the GLDAS NOAH L4 V2.1 meteorological product provided by the NASA Global Land Data Assimilation System (GLDAS) (Rodell et al., 2004). It allowed providing the following meteorological data with 3-h and 0.25° resolutions: downward shortwave radiation, air pressure, air temperature, and specific humidity. The meteorological data were retrieved from four pixels covering most of JPA and were averaged and used as inputs for the ET estimation.

The daily mean estimated ET was tested against the Penman-Monteith equation, which is considered the universal standard approach for calculating daily reference evapotranspiration (ET_0) (Allen et al., 1998). Such a comparison does not validate the estimates but only assess if both evapotranspiration time series oscillate and peak with similar amplitudes and magnitudes, respectively. The meteorological data used to calculate the ET_0 were acquired from a meteorological station inside JPA, which belongs to the Brazilian National Institute of Meteorology (INMET, acronym in Portuguese) (Fig. 1c). Additionally, the mean 8-day ET data from the original MOD16A2 product was also used to check the daily estimates using the cloud-cleaning procedure combined with a more fine-tuned dataset.

2.2.3 Soil water storage changes

The soil water storage changes were calculated using root-zone moisture information of the Soil Moisture Active Passive (SMAP) mission from NASA, estimated each 2 to 3 days since 2015 (Reichle et al., 2018). The SMAP Level 4 (L4) provides global near-surface (0-5 cm) and root-zone (0-100 cm) soil moisture with the SMAP L4 Surface and Root Zone Soil Moisture Analysis Update (SPL4SMAU) product (Reichle et al., 2017). The 100-cm root-zone SPL4SMAU soil moisture product (3-h temporal and 9-km spatial resolution), whose data result from the assimilation of L-band brightness temperature data into the NASA Catchment land surface model, was used to obtain the soil water storage by the soil moisture difference from one day to another multiplied by the root zone depth of 1,000 mm (Reichle et al., 2018).

Based on the SMAP orbit revisit time, the soil moisture data were scheduled to be retrieved at 6:00 a.m. and 6:00 p.m. (at the Legal Local Time). However, since the satellite takes 2 to 3 days to map the whole globe, some images over JPA were missing for a range of days of the year. Thus, similar to the study carried out by Souza et al. (2018), the soil moisture data were calculated in three ways: 1) if both orbits were completed on the same day, then both values were averaged; 2) if only one orbit had a valid value,

then this value was considered for that day; and 3) if no valid value was obtained in any orbit, then the soil moisture calculated for the previous day was repeated. Finally, the soil water storage changes were calculated by summing (positive or negative) daily differences in the SPL4SMAU root-zone data at the monthly and annual scales, which was performed after interpolating their images from a 9-km to a 500-m resolution through bilinear interpolation (same as that for P).

2.2.4 Surface runoff

The surface runoff was estimated using the Natural Resources Conservation Service–Curve Number (NRCS–CN) method (Hawkins et al., 1985). The NRCS–CN method combines climatic and physiographic characteristics in empirical formulas that convert basic descriptive data into numeric values to estimate the excess P that was not intercepted, stored, or infiltrated (Deshmukh et al., 2013). We implemented this estimation spatially with daily P. The daily runoff estimates were then summed pixel by pixel at monthly and annual scales, thus avoiding the overestimation errors that stem from its direct calculation at monthly and annual scales (Awadallah et al., 2017). We choose the NRCS-CN method because of its simplicity, ease of use and widespread acceptance (Ponce and Hawkins, 1996; Verma et al., 2017), focusing on scarce data regions in developing countries but taking advantage of freely available remote sensing data.

The NRCS–CN method is based on a water budget equation that assumes that P must exceed the initial abstraction (I_a), being a soil-dependent fraction (λ) of the maximum water storage capacity (S), before any direct runoff (Q) is triggered. A fixed value of λ equals to 0.20 is recommended by the original method and widely adopted in the United States (Hawkins et al., 1985). However, the initial losses depend on the local and regional characteristics of the watershed. Many studies, including some carried out in Brazilian catchments, indicated that the value proposed by the original method is too high for many parts of the world and recommended λ values of about 0.05 or less (e.g., Ajmal and Kim, 2015; Durán-Barroso et al., 2017; Shi et al., 2009; Valle Junior et al., 2019; Veeck et al., 2020). Recently, the studies by Lal et al. (2019, 2017) reviewed the values of λ for 63 watersheds worldwide with various LULC, finding 0.03 as a representative value, which was also used in our study. In this context, the new runoff and water storage capacity calculations under average wet conditions ($S_{II,\lambda=0.03}$) are shown in Eqs. (3) and (4).

$$Q = \begin{cases} \dfrac{\left(P - 0.03S_{II,\lambda=0.03}\right)^2}{\left(P + 0.97S_{II,\lambda=0.03}\right)} & , \quad \text{if } P \geq I_a = 0.03S \\ 0 & , \quad \text{if } P = 0 \end{cases} \tag{3}$$

$$S_{II,\lambda=0.03} = 0.654\left(\frac{25400}{CN_{II,\lambda=0.20}} - 254\right)^{1.248} \quad , \quad \text{for } 0 \leq CN_{II,\lambda=0.20} \leq 100 \tag{4}$$

CN values were selected from the (NRCS – Natural Resources Conservation Service, 2004) tables and spatially assigned to different hydrologic soil-cover complexes using a look-up table built in a GIS platform. The hydrologic soil-cover complexes refer to the different combinations of LULC and hydrological soil groups (HSGs) contained in a study area. The HSG information was created from the regional information about soil types provided by Araújo Filho et al. (2000). The HSG was assigned according to the soil type, following the methodology proposed by Sartori et al. (2005) that consists of 19 criteria based on a survey of 58 soil profiles and hydrodynamic data in Brazil. The LULC information was obtained from MapBiomas collection 3.1, the same used for estimating ET.

The potential runoff before a surface runoff event generated by the NRCS–CN method depends on the antecedent moisture condition (AMC) (Hawkins et al., 1985). The proper condition was identified through the 5-d antecedent cumulative P (P_{5d}, mm), which was calculated for each P grid cell. For this purpose, three intervals of P_{5d} were used, distinguishing between the growing season (GS, from March to July) and the dormant season (DS, from August to February) according to the AMC. Similar to those in Lal et al. (2017), the P_{5d} intervals in this study were defined as AMC-I (dry conditions): if $P_{5d} \leq 35.56$ mm (GS) or $P_{5d} \leq 12.7$ mm (DS); AMC-II (average conditions): if $35.56 < P_{5d} \leq 53.34$ mm (GS) or $12.70 < P_{5d} \leq 27.94$ mm (DS); and AMC-III (wet conditions): if $P_{5d} > 53.34$ mm (GS) or $P_{5d} > 27.94$ mm (DS). Moreover, the P_{5d} intervals of DS were considered for the urban and barren areas, whereas the P_{5d} intervals of GS were considered for the forest areas throughout all months of the year because of their active vegetation growing conditions. Finally, the CN_I and CN_{III} values were determined under AMC-I and AMC-III, respectively, based on Lal et al. (2019).

2.3 Evaluation of groundwater recharge estimates

The GWR rates were evaluated by the water table fluctuation (WTF) method (Healy and Cook, 2002; Scanlon et al., 2002). The ground-based GWR rates obtained from WTF (Eq. 5) were used to evaluate the spatially distributed GWR rates estimated by the water budget equation on a 1-km footprint around the

wells to comprehensively consider the surrounding characteristics. Their absolute (GWR, mm) and relative (GWR/P, %) estimates were compared through linear regressions.

$$R_{WTF} = S_y \frac{\Delta H}{\Delta t} \quad (5)$$

where R_{WTF} denotes the estimated recharge rate (mm/time step) using WTF, S_y represents the aquifer specific yield coefficient, ΔH is the cumulated rising piezometric level changes (mm), and Δt is the time from the beginning of the rise to the peak. ΔH corresponds to the sum of the actual groundwater rise and the potential groundwater decline for the same period, with the latter being obtained by extrapolating the antecedent recession curve (Healy and Cook, 2002; Wendland et al., 2007).

The groundwater fluctuation data were manually collected every 45 days from 16 (in 2016) and 23 monitoring wells (in 2017) located in the Barreiras Formation (Fig. 1c). Seven additional wells were drilled in 2017 in the urban area. These monitoring wells are well-distributed throughout the study area and, therefore, capable to characterise the local groundwater since they cover several soil types, depths (from shallow to deep) and LULC, from the coastline to the headwater. This monitoring network was carefully selected so as to have no groundwater pumping in or nearby the monitoring wells. The temporal variations of groundwater fluctuations were also used to compare the overall behaviour of the monthly satellite-based GWR estimates. The values of S_y equal to 0.10 (16 wells) and 0.24 (7 wells) were estimated by pumping tests in four wells and assigned to the others based on their similar local characteristics, including the groundwater level patterns.

2.4 Statistical metrics

Three statistical metrics were selected to evaluate the goodness-of-fit of the results. The first metric was the correlation coefficient (CC, Eq. (6)), which describes the relationship between variations in simulated and observed values. The other two metrics were the percent bias (PBIAS, Eq. (7)) and the relative root mean square error (RRMSE, Eq. (8)), both with perfect values equal to 0%, which were used to describe the bias and error between simulated and observed values, respectively.

$$CC(-) = \frac{\sum_{i=1}^{n}(G_i - \bar{G})(S_i - \bar{S})}{\sqrt{\sum_{i=1}^{n}(G_i - \bar{G})^2}\sqrt{\sum_{i=1}^{n}(S_i - \bar{S})^2}} \quad (6)$$

$$\mathrm{PBIAS}(\%) = \frac{\sum_{i=1}^{n}(S_i - G_i)}{\sum_{i=1}^{n} G_i} \times 100 \quad (7)$$

$$\mathrm{RRMSE}(\%) = \frac{\sqrt{(1/n)\sum_{i=1}^{n}(S_i - G_i)^2}}{\overline{G}} \times 100 \quad (8)$$

where S_i and G_i are the satellite- and ground-based data, respectively, and $\overline{S}$ and $\overline{G}$ are the mean values of the satellite- and ground-based data, respectively.

3. Results and discussion

3.1 Precipitation

The first set of analyses assessed the spatiotemporal distributions of the main input of the water balance (i.e., P) obtained from IMERG-C data and compared these with the ground-based interpolated data (henceforth Gauge) (Fig. 3). Annual P based on IMERG-C data gradually decreased from east to west, varying from 1,120 to 1,600 mm in 2016 and 1,050 to 2,300 mm in 2017. The maximum P based on Gauge observations was 1,630 mm in 2016 and 2,070 mm in 2017. Similarly, (Lu et al., 2019) showed consistent spatial patterns and maximum values of IMERG P after performing bias correction using monitoring data. P obtained in JPA from the IMERG-C data occurred mostly within the regular rainy season (i.e., from March to July), corresponding to 71% in 2016 and 77% in 2017 of the annual totals. The monthly variations in P in 2016 from the IMERG-C and Gauge data were similar (Fig. 3e,f), whereas the IMERG-C variation was larger than the Gauge variation in some months of 2017, particularly in June and July, when the 10-90% percentile ranges were 60% higher and double, respectively. Despite such differences, the average values obtained by IMERG-C were similar to those from the Gauge in most of the months, showing that IMERG-C was able to detect the temporal variation of P.

INSERT FIG. 3 HERE

Fig. 3. Spatially distributed precipitation in 2016 and 2017 estimated using (a and d) ground-based interpolated data and (b and e) IMERG-C data, with (c and f) monthly variations depicted by box plots with 10-90% percentiles. Histograms refer to the proportion of total cells.

389 The deviations between the IMERG-C and ground-based interpolated P were also assessed using
390 Quantile-Quantile plots (Fig. 4). At the monthly scale, a suitable correlation (CC = 0.97) and a reasonable
391 fit using linear regressions (slope = 1.01; y-intersect = -1.68) were found, with some deviations in March,
392 June, and July. Good correlations between the IMERG products and the observed dataset have been found
393 by other studies in tropical regions at the monthly scale (e.g., Satgé et al., 2017; Tan and Duan, 2017). The
394 monthly mean error was 23%, higher than the annual mean error (i.e., 8%). These values remained within
395 the acceptable ranges for satellite-based monthly P (Salles et al., 2019). Acceptable metrics were also found
396 at the annual scale, despite the slight deviation of the linear regression (slope = 1.20; y-intersect = -314
397 mm). Such a deviation probably occurred due to the larger variation of the ground-based P on the western
398 side of the study area in 2017, which likely stemmed from the limited number of rain gauges used on the
399 interpolation (see Fig. 1). According to Tang et al. (2016), the underestimation of this satellite-based P data
400 can occur over regions with wet climates and low latitudes. The results found in this analysis confirm that
401 the IMERG-C data enabled the mapping of the decreasing P gradient in the study area.

402 **INSERT FIG. 4 HERE**

403 **Fig. 4.** (a) Monthly and (b) annual Quantile-Quantile plots between the IMERG-C and ground-based
404 interpolated data at the 10% percentile. Shaded bounds: 95% confidence interval.

405 **3.2 Actual evapotranspiration**

406 The spatial ET distribution estimated by the modified MOD16 algorithm applying cloud cleaning
407 is shown in Fig. 5. Overall, the mean annual ET varied from 1,170 (in 2016) to 1,220 mm (in 2017). The
408 results were consistently distinguishable amongst the LULC types, with values smaller than 850 mm in the
409 urban areas and above 1,450 mm in the forest areas. At the monthly scale, the ranges of the average
410 estimates were similar between the studied years, varying from 73 to 119 mm in 2016 and 85 to 114 mm
411 in 2017. However, comparing the monthly mean estimates of 2017 with those of 2016, they were smaller
412 at the beginning, closer at the middle, and higher at the end of the year. In the rainy season, smaller
413 differences between high and low ET data were observed, showing monthly averages in the 10-90%
414 percentile ranges equal to 63 (in 2016) and 58 mm (in 2017) from April to August. On the other hand, larger
415 differences between high and low ET data occurred in the dry season, as shown by the monthly averages
416 in the 10-90% percentile ranges equal to 84 (in 2016) and 87 mm (in 2017) from September to March. Lima

417 and Ribeiro (2018) showed that such seasonable patterns can stem from the associations between
418 meteorological and evapotranspiration estimates by using the MapBiomas LULC and GLDAS
419 meteorological forcing data to calculate spatially distributed ET. Thus, variations in the ET throughout the
420 studied years in JPA were likely influenced by the combination of LULC diversity, weather seasonality and
421 cloudy conditions.

422 **INSERT FIG. 5 HERE**

423 **Fig. 5.** Spatially distributed actual evapotranspiration in (a) 2016 and (b) 2017, with (c) monthly variations
424 depicted by box plots with 10-90% percentiles. The MOD16 algorithm disregards the evaporation rates
425 from water bodies, which are white shown in the maps. Histograms refer to the proportion of total cells.

426 The mean daily ET obtained by the modified MOD16 algorithm ranged from 1.0 to 4.7 mm d^{-1}
427 during the whole study period, whereas the mean ET_0 varied from 3.0 to 7.0 mm d^{-1} (Fig. 6). The ET_0 was
428 as much as three times higher than the ET estimated by the proposed approach between August and
429 February (dry season) due to the lower soil water availability in these months. This difference is plausible
430 since ET_0 refers to the evapotranspiration of well-watered grass vegetation with active growth throughout
431 the year. Such a difference considerably shrunk during the rainy seasons, with the actual and reference
432 evapotranspiration following the same temporal behaviour, as expected.

433 **INSERT FIG. 6 HERE**

434 **Fig. 6.** Comparison between the daily actual evapotranspiration obtained by the modified MOD16
435 algorithm, the mean 8-day actual evapotranspiration data from the MOD16A2 product, and the daily
436 reference evapotranspiration.
437
438 The daily ET estimates obtained by the proposed methodology were greater than those acquired
439 by the mean 8-day MOD16A2 product for the studied period, which ranged from 1.9 to 3.9 mm d^{-1} (Fig.
440 6). Consequently, the mean annual ET estimated by the MOD16A2 was lower than those obtained by the
441 modified MOD16 algorithm for 2016 (895 mm) and 2017 (938 mm). The values of ET estimated by the
442 MOD16A2 product was also lower than those found by other studies using the Surface Energy Balance
443 Algorithm for Land (SEBAL) in river basins with similar characteristics in NE Brazil (e.g., Oliveira et al.,
444 2014). Although slightly higher, the ET estimates presented the same temporal patterns observed by the

original MOD16A2 product. The differences found between the original and the modified approaches can possibly be attributed to the following factors: 1) the missing data in some pixels of the MOD16A2 product because of the presence of cloud cover, 2) the use of a more fine-tuned LULC regional product, and 3) the use of a higher resolution input meteorological data. For instance, Ruhoff et al. (2013) identified that the misclassification of the LULC data used in the MOD16A2 product, combined with the low spatial resolution of the GMAO reanalysis meteorological information and the cloud cover contaminated pixels, were the largest contributors to over- or under-estimate the eddy covariance measurements in a humid tropical river basin located in south-eastern Brazil. Recently, a study carried by Melo et al. (2021) used 25 flux towers to evaluate four remote sensing-based ET algorithms in many ecoregions over South America, including the MOD16 model forced by ground-based meteorological data. An average uncertainty of ~10% was found for the MOD16 algorithm when considering all studied ecoregions, with relatively higher performance observed for wet climate regions. This overall uncertainty observed by Melo et al. (2021) for the MOD16 algorithm was similar to those found by Ruhoff et al. (2013) in two sites in Brazil after the MOD16 algorithm parameter fitting based on land use and land cover (i.e., without the use of the MOD12Q1 product).

3.3 Soil water storage changes

The annual water storage changes in the root zone throughout JPA varied from -27 to -6 mm during 2016 and from -40 to -12 mm during 2017 (Fig. 7). Annual water storage decreases suggest that the root zone released water during the studied period, which is in part due to vertical percolation to aquifers. Despite its original coarse resolution, SPL4SMAU consistently showed a water storage increase in the root zone mostly during the rainy season, likely because there is more water in the top layer after P. The water increase in the root zone in December 2016 likely stemmed from substantial P (Fig. 3e) when the South Atlantic Convergence Zone was positioned further eastward (Palharini and Vila, 2017). Moreover, as expected, the urban areas featured large water decreases in the root zone in both years, likely because of the lower infiltration caused by soil imperviousness, whereas the rural areas featured a larger spatial variation in water decreases. These results show that an above-average rainy condition is required for an annual water increase in the root zone, implying a susceptibility in JPA to water shortage.

INSERT FIG. 7 HERE

Fig. 7. Spatially distributed soil water storage changes in (a) 2016 and (b) 2017, with (c) monthly variations depicted by box plots with 10-90% percentiles. Histograms refer to the proportion of total cells.

3.4 Surface runoff

The mean annual surface runoff estimated from the IMERG-C data varied from 220 (in 2016) to 300 (in 2017) mm (Fig. 8). Due to soil imperviousness, urban areas produced annual runoff estimates greater than 450 mm. In 2017, higher values of surface runoff from IMERG-C data also occurred outside the urban area in relation to that from Gauge because of the high P in June and July. In the regular rainy season (i.e., from March to July), the mean annual surface runoff estimated with IMERG-C data accounted for 200 mm in 2016 and 265 mm in 2017. The sources of uncertainties surrounding the NRCS-CN method were analysed by Durán-Barroso et al. (2017), which include: 1) a significant weakness to select representative events for simulation with the NRCS CN parameters; and 2) the impossibility of determining an optimum value for λ but lower values are recommended instead of the original value. For instance, the study carried out by Veeck et al. (2020) in a Brazilian catchment found fitted initial losses lower than the original value for almost all simulated events, with relative errors below 12%. However, quantifying uncertainties of rainfall-runoff is a very complex issue in Brazil due to the lack of data.

INSERT FIG. 8 HERE

Fig. 8. Spatially distributed surface runoff in 2016 and 2017 estimated using (a and d) rain gauge and (b and e) IMERG-C data, with (c and f) monthly variations depicted by box plots with 10-90% percentiles. The surface runoff results over the water bodies were neglected in the NRCS–CN calculation, which are white shown in the maps. Histograms refer to the proportion of total cells.

3.5 Groundwater recharge

On average, the GWR rates ranged from 219 (in 2016) to 302 mm yr^{-1} (in 2017) (Fig. 9). These results remained within the range of the GWR rates of several tropical wet regions throughout the world (e.g., Malakar et al., 2019; Rodríguez-Huerta et al., 2020; Vu and Merkel, 2019). The urban area featured greater GWR rates than other areas despite its greater surface runoff, likely due to the combination of lower

498 ET and sandy soils (Minnig et al., 2018; O'Driscoll et al., 2010), as well as to the higher P estimates for the
499 coastline than for the headwaters. Consistently, Moeck et al. (2020) also showed that in the eastern part of
500 Brazil, high GWR rates can occur despite the annual potential evapotranspiration being greater than 1,500
501 mm because of the large amount and seasonality of P. At the monthly scale, GWR rates using IMERG-C
502 and Gauge data averaged 34.7 and 36.5 mm month^{-1} in 2016 and 47.7 and 51.4 mm month^{-1} in 2017,
503 respectively. These monthly estimates using IMERG-C data were similar to the Gauge estimates, although
504 the difference doubled in 2017 due to higher surface runoff estimated in June and July using IMERG-C
505 data. The differing GWR rates obtained for the Gauge data were likely influenced by the sensitivity of
506 modelled groundwater recharge estimates to the rain gauge network scale (Wiebe and Rudolph, 2020).

507 **INSERT FIG. 9 HERE**

508 **Fig. 9.** Spatially distributed GWR rates estimated in 2016 and 2017 by the water budget equation and WTF
509 method, using (a and d) rain gauge and (b and e) IMERG-C data, with (c and f) monthly variations depicted
510 by box plots with 10-90% percentiles. The GWR results over the water bodies were neglected in the water
511 budget equation, which are white shown in the maps. Histograms refer to the proportion of total cells.

512 The differences caused by disregarding the soil water storage changes were negligible at the annual
513 scale, reducing the mean relative GWR by less than -1% for the studied years, which likely occurred due
514 to the compensation of the water increases and decreases in the root zone throughout the rainy and dry
515 seasons. Conversely, at the monthly scale, neglecting the soil water storage changes would have
516 considerably impacted the GWR values, increasing their mean relative estimates by as much as +19 (in
517 2016) and +12% (in 2017) during the rainy season and decreasing their mean relative estimates by -22 (in
518 2016) and -13% (in 2017) during the dry season. Therefore, although other studies considering long-term
519 average recharge (e.g., 10 year period) have claimed that satisfactory estimations can be obtained by simply
520 applying the difference between P and ET satellite products in some semiarid, continental and
521 Mediterranean regions (e.g., Crosbie et al., 2015; Gokmen et al., 2013; Munch et al., 2013; Szilagyi et al.,
522 2011), this study demonstrated that tropical wet sedimentary regions also require the consideration of
523 surface runoff and soil water storage changes on a monthly and annual basis because their water cycles are
524 stressed by weather seasonality and hydrologic soil-cover complexes.

525 The annual GWR rates estimated by the WTF method varied from 110 to 370 mm yr^{-1} in 2016,
526 corresponding to 10 and 24% of the mean annual P obtained by the Gauge data, respectively (Table 1). Half

of these estimates ranged from 100 to 200 mm yr^{-1}, mostly obtained from the observation wells located upstream (Fig. 9). In 2017, the GWR rates varied from 90 to 550 mm yr^{-1}, corresponding to 7 and 29% of the mean annual P obtained by the Gauge data, respectively. More than half of these estimates ranged from 300 to 550 mm yr^{-1}, mostly obtained from observation wells located downstream (urban area).

INSERT TABLE 1 HERE

Table 1. Absolute and relative GWR estimates calculated by the WTF method in 2016 and 2017.

For evaluation purposes, the absolute and relative estimates of the GWR obtained by the water budget equation were plotted against the WTF results (Fig. 10). The correlations and mean errors of the absolute and relative GWR estimates based on the IMERG-C data varied from 0.68 to 0.83 and from 30 to 34%, respectively. These correlations and mean errors were fairly similar to the GWR ranges estimated using the Gauge data, whose correlations varied from 0.73 to 0.89, and the mean errors remained at 31%. Szilagyi et al. (2011) compared the GWR rates estimated by a satellite-based approach with chloride mass-balance rates, showing a spatial correlation of 0.57 at the annual scale. In our study, the GWR rates estimated by the water budget equation using the IMERG-C data tended to slightly underestimate the WTF data between -13 and -9%, whereas the Gauge scenario overestimated the WTF data between 8 and 11%. However, a good fit was found for the IMERG-C data by using linear regressions, showing decent slope and y-intersect values for the absolute (1.16 and -69 mm, respectively) and relative (0.82 and 0.79%, respectively) GWR, which confirmed the low underestimations. These negative biases could have been caused by neglecting the contribution of the irrigation input component in the water budget equation of this study, which is practically nil in the wettest period but can be significant in some sugarcane cultivated areas (i.e., corresponding to ~30% of the study area) during the four driest months. Usman et al. (2015) also found negative bias by applying a satellite-based approach to estimate GWR rates, showing that the consideration of irrigation considerably improves GWR estimates in comparison with WTF estimates. In this study, the GWR estimates based on the IMERG-C data were slightly lower than those calculated based on the WTF method, whose mean differences were 5 (in 2016) and -30 mm yr^{-1} (in 2017) at the absolute scale, as well as -0.8 (in 2016) and -1.8% (in 2017) at the relative scale, respectively. Crosbie et al. (2015) also found average underestimations of 45 mm yr^{-1} when comparing the GWR rates calculated by a satellite-based approach with the chloride mass-balance and WTF estimates.

INSERT FIG. 10 HERE

Fig. 10. Evaluation based on the WTF method of the annual GWR rates, estimated from rain gauge and IMERG-C data at (a, b, and e) absolute and (c, d, and f) relative scales.

Besides the biases possibly caused by disregarding the irrigation, the uncertainties in each water balance component (i.e., P with ~8% according to comparisons with on-ground gauge measurements; ET with ~10% based upon Melo et al. (2021); and Q with ~12% as found by Veeck et al. (2020)) used in the proposed approach might propagate to the residual term (i.e., the GWR). Uncertainty in time series of GWR estimated using the WTF method is associated with the difficulty in determining a representative Sy, which has a dependence on the depth to water table (Crosbie et al., 2019). For instance, the uncertainty in the GWR rates estimated from a satellite-based approach (P-ET) and the WTF method was analysed by Lucas et al. (2015), which found uncertainties ranging from 24 to 42% of the annual mean GWR. Actually, estimating GWR is a big challenge because it cannot be measured directly (Crosbie et al., 2019; Scanlon et al., 2002). Therefore, it is still difficult to assess the accuracy of any method (Crosbie et al., 2019; Healy and Cook, 2002), with no widely applicable methodology available that can directly and accurately quantify the volume of rainwater that reaches the water table (MacDonald et al., 2021). Because of this, it has been recommended over the last decades to use multiple methods when estimating the GWR (Crosbie et al., 2019; Scanlon et al., 2002). Unfortunately, in most developing countries and remote regions, groundwater measured data are scarce or unavailable, and rarely one or more than one method has been used to estimate GWR (Lucas et al., 2015). For such areas, satellite-based approaches, as proposed in this study for tropical wet regions, can be scientifically much more robust than considering, for instance, the estimations of GWR as a fixed percentage of rainfall, as often adopted by water managers in some tropical developing areas.

Fig. 11 shows the comparisons between the temporal variations of groundwater level fluctuations at 9 monitoring wells and the monthly satellite-based GWR estimates. The satellite-based GWR estimates presented similar peak variation patterns to those observed in the groundwater levels. This agreement between the peak variation patterns from the GWR and groundwater levels were observed to either shallower (e.g., W04, W9, and W13) and deeper (e.g., W15 and W16) monitoring wells. Although presenting similar peak variation patterns, it is possible to notice a monthly delay in the groundwater level fluctuations compared to the GWR amounts likely due to unsaturated zone transit which is not considered in the method, as it was already pointed out by Coelho et al. (2017) in a semiarid region.

584 **INSERT FIG. 11 HERE**

585 **Fig. 11**. Comparison between the observed groundwater levels and monthly groundwater recharge based
586 on IMERG-C data and interpolated rain gauge data.

587 **4. Summary and conclusions**

588 This study developed and evaluated an innovative satellite-based approach based on the water
589 budget equation to estimate the natural GWR over by only using freely available satellite-based data. The
590 proposed distinctive features include the capacity to address 1) ET estimations (MOD16 algorithm) in
591 tropical wet regions frequently overlaid by substantial cloud cover and 2) water storage change estimation
592 in the root zone (SPL4SMAU product) in sedimentary regions seasonably prone to monthly variations. The
593 proposed method, which also included P (IMERG product) and runoff (NRCS–CN method) information,
594 was assessed for two hydrologically contrasting years. The spatially distributed GWR rates were compared
595 with the measurements of groundwater levels and recharge estimates based on the WTF method applied to
596 the monitoring wells over the study area. Overall, the results of the proposed satellite-based water budget
597 approach performed consistently with the groundwater ground-based estimates. The monitoring wells used
598 to evaluate the groundwater recharge rates covered different soil types, LULC, and depths (from shallow
599 to deep). These features suggest that the proposed methodology may be reliable in characterising the spatial
600 heterogeneity of the studied area.

601 Concerning ET, the use of a cloud-cleaning procedure based on monthly map compositions of
602 biophysical data (i.e., LAI, EVI2, and ALB), combined with a more fine-tuned LULC regional product and
603 a set of GLDAS meteorological forcing data, suggested the production of a reasonable proxy for ET despite
604 cloudy conditions. The use of soil water storage changes calculated from the SPL4SMAU root-zone soil
605 moisture product was shown to provide essential spatially distributed information to be included in the
606 satellite-based approach, as the GWR estimates would vary considerably over JPA by disregarding this
607 component at the monthly scale.

608 Therefore, the satellite-based approach consistently demonstrated that the consideration of soil
609 water storage changes and the cloud cleaning procedure used to obtain ET are essential for a proper
610 estimation of the spatially distributed GWR rates in tropical wet sedimentary regions because of their
611 hydrologic soil-cover complexes, weather seasonality and cloudy conditions. However, some sources of

uncertainty in the satellite-based approach still require a better assessment, which includes: 1) a more detailed comparison of each component of the water balance (e.g., runoff, ET, and soil moisture) with ground-based measurements to identify the errors accumulated in the residual term (i.e., GWR); and 2) the impact of interception, irrigation, and pumping demands in the GWR estimates. Also, a better representation of S_y across the region, together with an analysis of errors associated with its estimates, which contribute to the overall uncertainty of the WTF method, need to be accounted for in further studies.

Acknowledgements: The authors would like to acknowledge the financial support granted by 1) the Research Support Foundation of Paraíba State (FAPESQ-PB) (Grant REF: 88887.142311/2017-00), which also funded the contribution from Yunqing Xuan, supported in partnership with the Newton Fund, via CONFAP – The UK Academies Research Mobility 2017/2018 (Grant REF: 039/2018); 2) the Brazilian Coordination for Improvement of Higher Education Personnel (CAPES) – Finance Code 001 (Grant REF: 88887.161412/2017-00); 3) the Brazilian National Council for Scientific and Technological Development (CNPq) (Grant REF: 160043/2019-0), which also funds the Universal MCTI/CNPq No. 28/2018 (Grant REF: 433801/2018-2); 4) the Brazilian Innovation Agency (FINEP) for funding the Brazilian Managed Aquifer Recharge (BRAMAR) research project (Grant REF: 01.13.0340.00); and 5) the German Research Foundation (DFG) for funding the Cosmic Sense research project – Research Unit No. FOR 2694 (Grant REF: 357874777). The authors also acknowledge the two anonymous reviewers and the editor for the constructive comments that allowed improving the quality of the manuscript.

References

Aeschbach-Hertig, W., Gleeson, T., 2012. Regional strategies for the accelerating global problem of groundwater depletion. Nature Geoscience 5, 853–861. https://doi.org/10.1038/ngeo1617

Ahmadi, T., Ziaei, A.N., Rasoulzadeh, A., Davary, K., Esmaili, K., Izady, A., 2015. Mapping groundwater recharge areas using CRD and RIB methods in the semi-arid Neishaboor Plain, Iran. Arabian Journal of Geosciences 8, 2921–2935. https://doi.org/10.1007/s12517-014-1321-2

Ajmal, M., Kim, T.-W., 2015. Quantifying Excess Stormwater Using SCS-CN–Based Rainfall Runoff Models and Different Curve Number Determination Methods. Journal of Irrigation and Drainage Engineering 141, 1–12. https://doi.org/10.1061/(ASCE)IR.1943-4774.0000805

Allen, R.G., Pereira, L.S., Raes, D., Smith, M., 1998. Crop evapotranspiration - Guidelines for computing crop water requirements, in: FAO Irrigation and Drainage Paper 56. FAO - Food and Agriculture Organization of the United Nations, Rome, Italy, pp. 1–15.

Alley, W.M., Konikow, L.F., 2015. Bringing GRACE down to Earth. Groundwater 53, 826–829. https://doi.org/https://dx.doi.org/10.1111/gwat.12379

Alvares, C.A., Stape, J.L., Sentelhas, P.C., De Moraes Gonçalves, J.L., Sparovek, G., 2013. Köppen's climate classification map for Brazil. Meteorologische Zeitschrift 22, 711–728. https://doi.org/10.1127/0941-2948/2013/0507

Araújo Filho, J.C., Burgos, N., Lopes, O.F., Silva, F.H.B.B. Da, Medeiros, L.A.R., Melo Filho, H.F.R. De, Parahyba, R.D.B.V., Cavalcanti, A.C., Oliveira Neto, M.B. De, Silva, F.B.R.E., Leite, A.P., Santos, J.C.P. Dos, Souza Neto, N.C. De, Silva, A.B. Da, Luz, L.R.Qu.P. Da, Lima, P.C. De, Reis, R.M.G., Barros, A.H.C., 2000. Levantamento de reconhecimento de baixa e média intensidade dos solos do Estado de Pernambuco. … de Janeiro, Embrapa Solos 382.

Awadallah, A.G., Farahat, M.S., Haggag, M., 2017. Discussion of "Interfacing the geographic information system , remote sensing, and the soil conservation service-curve number method to estimate curve number and runoff volume in the ASIR region of Saudi Arabia" by Fawzi S . Mohammad, Jan Adamowski. Arabian Journal of Geosciences 10, 1–10. https://doi.org/http:/dx.doi.org/10.1007/s12517-017-2984-2

Bastiaanssen, W.G.M., Pelgrum, H., Wang, J., Ma, Y., Moreno, J.F., Roerink, G.J., van der Wal, T., 1998. A remote sensing surface energy balance algorithm for land (SEBAL), Part 1: Formulation. Journal of Hydrology 212–213, 213–229. https://doi.org/10.1016/S0022-1694(98)00254-6

Brunner, P., Bauer, P., Eugster, M., Kinzelbach, W., 2004. Using remote sensing to regionalize local precipitation recharge rates obtained from the Chloride Method. Journal of Hydrology 294, 241–250. https://doi.org/10.1016/j.jhydrol.2004.02.023

Brunner, P., Hendricks Franssen, H.J., Kgotlhang, L., Bauer-Gottwein, P., Kinzelbach, W., 2007. How can remote sensing contribute in groundwater modeling? Hydrogeology Journal 15, 5–18. https://doi.org/10.1007/s10040-006-0127-z

Cai, Z., Ofterdinger, U., 2016. Analysis of groundwater-level response to rainfall and estimation of annual recharge in fractured hard rock aquifers, NW Ireland. Journal of Hydrology 535, 71–84. https://doi.org/10.1016/j.jhydrol.2016.01.066

Callahan, T.J., Vulava, V.M., Passarello, M.C., Garrett, C.G., 2012. Estimating groundwater recharge in lowland watersheds. Hydrological Processes 26, 2845–2855. https://doi.org/10.1002/hyp.8356

Coelho, V.H.R., Montenegro, S., Almeida, C.N., Silva, B.B., Oliveira, L.M., Gusmão, A.C. V, Freitas, E.S., Montenegro, A.A.A., 2017. Alluvial groundwater recharge estimation in semi-arid environment using remotely sensed data. Journal of Hydrology 548, 1–15. https://doi.org/10.1016/j.jhydrol.2017.02.054

CPRM – Geological Service of Brazil, 2020. SIAGAS – Groundwater Information System [WWW Document]. Law No. 9.433/1997.

Crosbie, R.S., Davies, P., Harrington, N., Lamontagne, S., 2015. Ground truthing groundwater-recharge estimates derived from remotely sensed evapotranspiration: a case in South Australia. Hydrogeology Journal 23, 335–350. https://doi.org/10.1007/s10040-014-1200-7

Crosbie, R.S., Doble, R.C., Turnadge, C., Taylor, A.R., 2019. Constraining the Magnitude and Uncertainty of Specific Yield for Use in the Water Table Fluctuation Method of Estimating Recharge. Water Resources Research 55, 7343–7361. https://doi.org/10.1029/2019WR025285

Cuthbert, M.O., Taylor, R.G., Favreau, G., Todd, M.C., Shamsudduha, M., Villholth, K.G., MacDonald, A.M., Scanlon, B.R., Kotchoni, D.O.V., Vouillamoz, J.-M., Lawson, F.M.A., Adjomayi, P.A., Kashaigili, J., Seddon, D., Sorensen, J.P.R., Ebrahim, G.Y., Owor, M., Nyenje, P.M., Nazoumou, Y., Goni, I., Ousmane, B.I., Sibanda, T., Ascott, M.J., MacDonald, D.M.J., Agyekum, W., Koussoubé, Y., Wanke, H., Kim, H., Wada, Y., Lo, M.-H., Oki, T., Kukuric, N., 2019. Observed controls on resilience of groundwater to climate variability in sub-Saharan Africa. Nature 572, 230–234. https://doi.org/http://dx.doi.org/10.1038/s41586-019-1441-7

Deshmukh, D.S., Chaube, U.C., Ekube Hailu, A., Aberra Gudeta, D., Tegene Kassa, M., 2013. Estimation and comparision of curve numbers based on dynamic land use land cover change, observed rainfall-

693 runoff data and land slope. Journal of Hydrology 492, 89–101.
694 https://doi.org/10.1016/j.jhydrol.2013.04.001

695 Döll, P., Schmied, H.M., Schuh, C., Portmann, F.T., Eicker, A., 2014. Global-scale assessment of
696 groundwater depletion and related groundwater abstractions: combining hydrological modeling
697 with information from well observations and GRACE satellites. Water Resources Research 50,
698 5698–5720. https://doi.org/http://dx.doi.org/10.1002/2014WR015595

699 Durán-Barroso, P., González, J., Valdés, J.B., 2017. Sources of uncertainty in the NRCS CN model:
700 Recognition and solutions. Hydrological Processes 31, 3898–3906.
701 https://doi.org/10.1002/hyp.11305

702 Famiglietti, J.S., 2014. The global groundwater crisis. Nature Climate Change 4, 945–948.
703 https://doi.org/http://dx.doi.org/10.1038/nclimate2425

704 Famiglietti, J.S., Cazenave, A., Eicker, A., Reager, J.T., Rodell, M., Velicogna, I., 2015. Satellites
705 provide the big picture. Science 349, 684–685. https://doi.org/10.1126/science.aac9238

706 Gadelha, A.N., Coelho, V.H.R., Xavier, A.C., Barbosa, L.R., Melo, D.C.D., Xuan, Y., Huffman, G.J.,
707 Petersen, W.A., Almeida, C.N., 2019. Grid box-level evaluation of IMERG over Brazil at various
708 space and time scales. Atmospheric Research 218, 231–244.
709 https://doi.org/10.1016/j.atmosres.2018.12.001

710 Gokmen, M., Vekerdy, Z., Lubczynski, M.W., Timmermans, J., Batelaan, O., Verhoef, W., 2013.
711 Assessing Groundwater Storage Changes Using Remote Sensing–Based Evapotranspiration and
712 Precipitation at a Large Semiarid Basin Scale. Journal of Hydrometeorology 14, 1733–1753.
713 https://doi.org/10.1175/JHM-D-12-0156.1

714 Graaf, I.E.M., Beek, R.L.P.H. Van, Gleeson, T., Moosdorf, N., Schmitz, O., Sutanudjaja, E.H., Bierkens,
715 M.F.P., Engineering, C., 2017. Advances in Water Resources A global-scale two-layer transient
716 groundwater model: Development and application to groundwater depletion. Advances in Water
717 Resources 102, 53–67. https://doi.org/10.1016/j.advwatres.2017.01.011

718 Hawkins, R.H., Hjelmfelt, A.T., Members, A., Zevenbergen, A.W., 1985. Runoff probability, storm
719 depth, and curve numbers. Journal of Irrigation and Drainage Engineering 111, 330–340.
720 https://doi.org/http://dx.doi.org/10.1061/(ASCE)0733-9437(1985)111:4(330)

721 Healy, R.W., Cook, P.G., 2002. Using groundwater levels to estimate recharge. Hydrogeology Journal 10,
722 91–109. https://doi.org/10.1007/s10040-001-0178-0

723 Hornero, J., Manzano, M., Ortega, L., Custodio, E., 2016. Integrating soil water and tracer balances,
724 numerical modelling and GIS tools to estimate regional groundwater recharge: Application to the
725 Alcadozo Aquifer System (SE Spain). Science of the Total Environment 568, 415–432.
726 https://doi.org/10.1016/j.scitotenv.2016.06.011

727 Huete, A.R., 1988. A soil-adjusted vegetation index (SAVI). Remote Sensing of Environment 25, 295–
728 209. https://doi.org/10.1016/0034-4257(88)90106-X

729 Huffman, G.J., Bolvin, D.T., Nelkin, E.J., 2018. Integrated Multi-satellitE Retrievals for GPM (IMERG)
730 Technical Documentation.

731 Jasechko, S., Birks, S.J., Gleeson, T., Wada, Y., Fawcett, P.J., Sharp, Z.D., McDonnell, J.J., Welker,
732 J.M., 2014. The pronounced seasonality of global groundwater recharge. Water Resources Research
733 50, 1–23. https://doi.org/http://dx.doi.org/10.1002/2014WR015809

734 Jiang, Z., Huete, A.R., Didan, K., Miura, T., 2008. Remote Sensing of Environment Development of a
735 two-band enhanced vegetation index without a blue band. Remote Sensing of Environment 112,
736 3833–3845. https://doi.org/10.1016/j.rse.2008.06.006

Khalaf, A., Donoghue, D., 2012. Estimating recharge distribution using remote sensing: A case study from the West Bank. Journal of Hydrology 414–415, 354–363. https://doi.org/10.1016/j.jhydrol.2011.11.006

Lakshmi, V., Fayne, J., Bolten, J., 2018. A comparative study of available water in the major river basins of the world. Journal of Hydrology 567, 510–532. https://doi.org/http://dx.doi.org/10.1016/j.jhydrol.2018.10.038

Lal, M., Mishra, S.K., Kumar, M., 2019. Reverification of antecedent moisture condition dependent runoff curve number formulae using experimental data of Indian watersheds. Catena 173, 48–58. https://doi.org/https://dx.doi.org/10.1016/j.catena.2018.09.002

Lal, M., Mishra, S.K., Pandey, A., Pandey, R.P., Meena, P.K., Chaudhary, A., Jha, R.K., Shreevastava, A.K., Kumar, Y., 2017. Evaluation of the Soil Conservation Service curve number methodology using data from agricultural plots. Hydrogeology Journal 25, 151–167. https://doi.org/http://dx.doi.org/10.1007/s10040-016-1460-5

Le, H.M., Sutton, J.R.P., Bui, D. Du, Bolten, J.D., Lakshmi, V., 2018. Comparison and bias correction of TMPA precipitation products over the Lower Part of Red–Thai Binh river basin of Vietnam. Remote Sensing 10, 1–21. https://doi.org/http://dx.doi.org/10.3390/rs10101582

Lenderink, G., Buishand, A., van Deursen, W., 2007. Estimates of future discharges of the river Rhine using two scenario methodologies: direct versus delta approach. Hydrology and Earth System Sciences 11, 1145–1159. https://doi.org/http://dx.doi.org/10.5194/hess-11-1145-2007

Lima, R.N. de S., Ribeiro, C.B. de M., 2018. Spatial variability of daily evapotranspiration in a mountainous watershed by coupling surface energy balance and solar radiation model with gridded weather dataset. Proceedings 2, 1–6. https://doi.org/http://dx.doi.org/10.3390/ecrs-2-05155

Lu, X., Tang, G., Wang, X., Liu, Y., Jia, L., Xie, G., Li, S., 2019. Correcting GPM IMERG precipitation data over the Tianshan Mountains in China. Journal of Hydrology 575, 1239–1252. https://doi.org/https://dx.doi.org/10.1016/j.jhydrol.2019.06.019

Lucas, M., Oliveira, P.T.S., Melo, D.C.D., Wendland, E., 2015. Evaluation of remotely sensed data for estimating recharge to an outcrop zone of the Guarani Aquifer System (South America). Hydrogeology Journal 23, 961–969. https://doi.org/10.1007/s10040-015-1246-1

MacDonald, A.M., Lark, R.M., Taylor, R.G., Abiye, T., Fallas, H.C., Favreau, G., Goni, I.B., Kebede, S., Scanlon, B., Sorensen, J.P.R., Tijani, M., Upton, K.A., West, C., 2021. Mapping groundwater recharge in Africa from ground observations and implications for water security. Environmental Research Letters 16, 034012. https://doi.org/10.1088/1748-9326/abd661

Maier, R., Krebs, G., Pichler, M., Muschalla, D., Gruber, G., 2020. Spatial Rainfall Variability in Urban Environments — High-Density Precipitation Measurements on a City-Scale. Water 12, 1157. https://doi.org/10.3390/w12041157

Malakar, P., Mukherjee, A., Bhanja, S.N., Scanlon, B.R., Verma, S., Rangarajan, R., 2019. Long-term groundwater recharge rates across India by in situ measurements. Hydrology and Earth System Sciences 23, 711–722. https://doi.org/10.5194/hess-23-711-2019

Mathias, S.A., Sorensen, J.P.R., Butler, A.P., 2017. Soil moisture data as a constraint for groundwater recharge estimation. Journal of Hydrology 552, 258–266. https://doi.org/http://dx.doi.org/10.1016/j.jhydrol.2017.06.040

Melo, D. de C.D., Wendland, E., Guanabara, R.C., 2015. Estimate of groundwater recharge based on Water Balance in the unsaturated soil zone. Revista Brasileira de Ciência do Solo 39, 1335–1343. https://doi.org/10.1590/01000683rbcs20140740

Melo, D.C.D., Anache, J.A.A., Almeida, C. das N., Coutinho, J. V., Ramos Filho, G.M., Rosalem, L.M.P., Pelinson, N.S., Ferreira, G.L.R.A., Schwamback, D., Calixto, K.G., Siqueira, J.P.G., Duarte-Carvajalino, J.C., Jhunior, H.C.S., Nóbrega, J.D., Morita, A.K.M., Leite, C.M.C., Guedes,

A.C.E., Coelho, V.H.R., Wendland, E., 2020. The big picture of field hydrology studies in Brazil. Hydrological Sciences Journal 02626667.2020.1747618. https://doi.org/10.1080/02626667.2020.1747618

Melo, D.C.D., Anache, J.A.A., Borges, V.P., Miralles, D.G., Martens, B., Fisher, J.B., Nóbrega, R.L.B., Moreno, A., Cabral, O.M.R., Rodrigues, T.R., Bezerra, B., Silva, C.M.S., Neto, A.A.M., Moura, M.S.B., Marques, T. v., Campos, S., Nogueira, J.S., Rosolem, R., Souza, R.M.S., Antonino, A.C.D., Holl, D., Galleguillos, M., Perez- Quezada, J.F., Verhoef, A., Kutzbach, L., Lima, J.R.S., Souza, E.S., Gassman, M.I., Perez, C.F., Tonti, N., Posse, G., Rains, D., Oliveira, P.T.S., Wendland, E., 2021. Are Remote Sensing Evapotranspiration Models Reliable Across South American Ecoregions? Water Resources Research 57. https://doi.org/10.1029/2020WR028752

Melo, D.C.D., Wendland, E., 2017. Shallow aquifer response to climate change scenarios in a small catchment in the Guarani Aquifer outcrop zone. Annals of the Brazilian Academy of Sciences 89, 391–406.

Minnig, M., Moeck, C., Radny, D., Schirmer, M., 2018. Impact of urbanization on groundwater recharge rates in Dübendorf, Switzerland. Journal of Hydrology 563, 1135–1146. https://doi.org/http://dx.doi.org/10.1016/j.jhydrol.2017.09.058

Moeck, C., Grech-Cumbo, N., Podgorski, J., Bretzler, A., Gurdak, J.J., Berg, M., Schirmer, M., 2020. A global-scale dataset of direct natural groundwater recharge rates: a review of variables, processes and relationships. Science of the Total Environment 717, 1–19. https://doi.org/https://dx.doi.org/10.1016/j.scitotenv.2020.137042

Moghim, S., McKnight, S.L., Zhang, K., Ebtehaj, A.M., Knox, R.G., Bras, R.L., Moorcroft, R., Wang, J., 2016. Bias-corrected data sets of climate model outputs at uniform space–time resolution for land surface modelling over Amazonia. International Journal of Climatology 37, 621–636. https://doi.org/http://dx.doi.org/10.1002/joc.4728

Mohan, C., Western, A.W., Wei, Y., Saft, M., 2018. Predicting groundwater recharge for varying land cover and climate conditions – a global meta-study. Hydrology and Earth System Sciences 22, 2689–2703. https://doi.org/https://dx.doi.org/10.5194/hess-22-2689-2018

Monteith, J.L., 1965. Evaporation and Environment, in: Symposium of the Society for Experimental Biology. pp. 205–234.

Mu, Q., Heinsch, F.A., Zhao, M., Running, S.W., 2007. Development of a global evapotranspiration algorithm based on MODIS and global meteorology data. Remote Sensing of Environment 111, 519–536.

Mu, Q., Zhao, M., Running, S.W., 2011. Improvements to a MODIS global terrestrial evapotranspiration algorithm. Remote Sensing of Environment 115, 1781–1800. https://doi.org/10.1016/j.rse.2011.02.019

Munch, Z., Conrad, J.E., Gibson, L.A., Palmer, A.R., Hughes, D., 2013. Satellite earth observation as a tool to conceptualize hydrogeological fluxes in the Sandveld, South Africa. Hydrogeology Journal 21, 1053–1070. https://doi.org/10.1007/s10040-013-1004-1

NRCS – Natural Resources Conservation Service, 2004. Hydrologic soil-cover complexes, in: Mockus, V., Moody, H.F., NRCS (Eds.), Part 630 Hydrology, National Engineering Handbook. USDA – United States Department of Agriculture, Washington, DC, pp. 1–20.

O'Driscoll, M., Clinton, S., Jefferson, A., Manda, A., McMillan, S., 2010. Urbanization effects on watershed hydrology and in-stream processes in the Southern United States. Water 2, 605–648. https://doi.org/http://dx.doi.org/10.3390/w2030605

Oliveira, L.M.M., Montenegro, S.M.G.L., Silva, B.B., Antonino, A.C.D. a, Moura, A.E.S.S., 2014. Real evapotranspiration in catchment area of northeastern Brazil through the SEBAL and MODIS products [Evapotranspiração real em bacia hidrográfica do Nordeste brasileiro por meio do SEBAL

e produtos MODIS]. Revista Brasileira de Engenharia Agricola e Ambiental 18, 1039–1046. https://doi.org/10.1590/1807-1929/agriambi.v18n10p1039-1046

Palharini, R.S.A., Vila, D.A., 2017. Climatological behavior of precipitating clouds in the northeast region of Brazil. Advances in Meteorology 17–21.

Ponce, V.M., Hawkins, R.H., 1996. Runoff Curve Number: Has It Reached Maturity? Journal of Hydrologic Engineering 1, 11–19. https://doi.org/10.1061/(ASCE)1084-0699(1996)1:1(11)

Reichle, R.H., de Lannoy, G.J.M., Liu, Q., Ardizzone, J. V., Colliander, A., Conaty, A., Crow, W., Jackson, T.J., Jones, L.A., Kimball, J.S., Koster, R.D., P.Mahanama, S., Smith, E.B., Berg, A., Bircher, S., Bosch, D., Caldwell, T.G., Cosh, M., González-Zamora, Á., Collins, C.D.H., Jensen, K.H., Livingston, S., Lopez-Baeza, E., Martínez-Fernández, J., McNairn, H., Moghaddam, M., Pacheco, A., Pellarin, T., Prueger, J., Rowlandson, T., Seyfried, M., Starks, P., Su, Z., Thibeault, M., van der Velde, R., Jeffrey Walker, Wu, X., Zeng, Y., 2017. Assessment of the SMAP Level-4 surface and root-zone soil moisture product using in situ measurements. Journal of Hydrometeorology 18, 2621–2645. https://doi.org/http://dx.doi.org/10.1175/JHM-D-17-0063.1

Reichle, R.H., Liu, Q., Koster, R.D., Ardizzone, J. v., Colliander, A., Crow, W.T., de Lannoy, G.J.M., Kimball, J.S., 2018. Soil Moisture Active Passive (SMAP) project assessment report for version 4 of the L4_SM sata product. Greenbelt, MD.

Rodell, M., Houser, P.R., Jambor, U., Gottschalck, J., Mitchell, K., Meng, C.-J., Arsenault, K., Cosgrove, B., Radakovich, J., Bosilovich, M., Entin, J.K., Walker, J.P., Lohmann, D., Toll, D., 2004. The Global Land Data Assimilation System. Bulletin of the American Meteorological Society 85, 381–394. https://doi.org/https://dx.doi.org/10.1175/BAMS-85-3-381

Rodríguez-Huerta, E., Rosas-Casals, M., Hernández-Terrones, L.M., 2020. A water balance model to estimate climate change impact on groundwater recharge in Yucatan Peninsula, Mexico. Hydrological Sciences Journal 65, 1–17. https://doi.org/https://dx.doi.org/10.1080/02626667.2019.1702989

Rossetti, D.F., Bezerra, F.H.R., Góes, A.M., Valeriano, M.M., Andrades-filho, C.O., Mittani, J.C.R., Tatumi, S.H., Brito-neves, B.B., 2011. Late Quaternary sedimentation in the Paraíba Basin, Northeastern Brazil: landform, sea level and tectonics in Eastern South America passive margin. Palaeogeography, Palaeoclimatology, Palaeoecology 300, 191–204. https://doi.org/http://dx.doi.org/10.1016/j.palaeo.2010.12.026

Rossetti, D.F., Góes, A.M., Bezerra, F.H.R., Valeriano, M.M., Brito-Neves, B.B., Ochoa, F.L., 2012. Contribution to the stratigraphy of the Onshore Paraíba Basin, Brazil. Anais da Academia Brasileira de Ciências 84, 313–333. https://doi.org/https://dx.doi.org/10.1590/S0001-37652012005000026

Ruhoff, A.L., Paz, A.R., Aragao, L.E.O.C., Mu, Q., Malhi, Y., Collischonn, W., Rocha, H.R., Running, S.W., 2013. Assessment of the MODIS global evapotranspiration algorithm using eddy covariance measurements and hydrological modelling in the Rio Grande basin. Hydrological Sciences Journal 58, 1658–1676. https://doi.org/10.1080/02626667.2013.837578

Running, S.W., Mu, Q., Zhao, M., Moreno, A., 2017. NASA Earth Observing System MODIS Land Algorithm User's Guide: MODIS Global Terrestrial Evapotranspiration (ET) Product (NASA MOD16A2/A3).

Salles, L., Satgé, F., Roig, H., Almeida, T., Olivetti, D., Ferreira, W., 2019. Seasonal effect on spatial and temporal consistency of the new GPM-based IMERG-v5 and GSMaP-v7 satellite precipitation estimates in Brazil's Central Plateau Region. Water 11, 668. https://doi.org/10.3390/w11040668

Sartori, A., Lombardi Neto, F., Genovez, A.M., 2005. Classificação hidrológica de solos brasileiros para a estimativa da chuva excedente com o método do Serviço de Conservação do Solo dos Estados Unidos Parte 1: Classificação. Revista Brasileira de Recursos Hídricos 10, 5–18. https://doi.org/http://dx.doi.org/10.21168/rbrh.v10n4.p5-18

878 Satgé, F., Xavier, A., Zolá, R.P., Hussain, Y., Timouk, F., Garnier, J., Bonnet, M.P., 2017. Comparative
879 assessments of the latest GPM mission's spatially enhanced satellite rainfall products over the main
880 bolivian watersheds. Remote Sensing 9, 1–16. https://doi.org/10.3390/rs9040369

881 Scanlon, B.R., Healy, R.W., Cook, P.G., 2002. Choosing appropriate techniques for quantifying
882 groundwater recharge. Hydrogeology Journal 10, 18–39.
883 https://doi.org/http:/dx.doi.org/10.1007/s10040-001-0176-2

884 Semire, F.A., Mohd-Mokhtar, R., Ismail, W., Mohamad, N., Mandeep, J.S., 2012. Ground validation of
885 space-borne satellite rainfall products in Malaysia. Advances in Space Research 50, 1241–1249.
886 https://doi.org/10.1016/j.asr.2012.06.031

887 Sharifi, E., Saghafian, B., Steinacker, R., 2019. Downscaling satellite precipitation estimates with
888 multiple linear regression, artificial neural networks, and spline interpolation techniques. Journal of
889 Geophysical Research: Atmospheres 124, 789–805.
890 https://doi.org/http:/dx.doi.org/10.1029/2018JD028795

891 Shi, Z.-H., Chen, L.-D., Fang, N.-F., Qin, D.-F., Cai, C.-F., 2009. Research on the SCS-CN initial
892 abstraction ratio using rainfall-runoff event analysis in the Three Gorges Area, China. CATENA 77,
893 1–7. https://doi.org/10.1016/j.catena.2008.11.006

894 Skofronick-Jackson, G., Kirschbaum, D., Petersen, W., Huffman, G., Kidd, C., Stocker, E., Kakar, R.,
895 2018. The Global Precipitation Measurement (GPM) mission's scientific achievements and societal
896 contributions: reviewing four years of advanced rain and snow observations. Quarterly Journal of
897 the Royal Meteorological Society. https://doi.org/10.1002/qj.3313

898 Skofronick-Jackson, G., Petersen, W.A., Berg, W., Kidd, C., Stocker, E.F., Kirschbaum, D.B., Kakar, R.,
899 Braun, S.A., Huffman, G.J., Iguchi, T., Kirstetter, P.E., Kummerow, C., Meneghini, R., Oki, R.,
900 Olson, W.S., Takayabu, Y.N., Furukawa, K., Wilheit, T., 2017. The Global Precipitation
901 Measurement (GPM) Mission for science and society. Bulletin of the American Meteorological
902 Society 98, 1679–1695. https://doi.org/10.1175/BAMS-D-15-00306.1

903 Souza, A.G.S.S., Ribeiro Neto, A., Rossato, L., Alvalá, R.C.S., Souza, L.L., 2018. Use of SMOS L3 soil
904 moisture data: validation and drought assessment for Pernambuco state, Northeast Brazil. Remote
905 Sensing 10, 1–19. https://doi.org/http://dx.doi.org/10.3390/rs10081314

906 Sur, C., Kang, S., Kim, J.S., Choi, M., 2015. Remote sensing-based evapotranspiration algorithm: A case
907 study of all sky conditions on a regional scale. GIScience and Remote Sensing 52, 627–642.
908 https://doi.org/10.1080/15481603.2015.1056288

909 Szilágyi, J., Kovács, Á., Józsa, J., 2012. Remote-sensing based groundwater recharge estimates in the
910 Danube-Tisza sand plateau region of Hungary. Journal of Hydrology and Hydromechanics 60, 64–
911 72. https://doi.org/http://dx.doi.org/10.2478/v10098-012-0006-3

912 Szilagyi, J., Zlotnik, V.A., Gates, J.B., Jozsa, J., 2011. Mapping mean annual groundwater recharge in the
913 Nebraska Sand Hills, USA. Hydrogeology Journal 19, 1503–1513. https://doi.org/10.1007/s10040-
914 011-0769-3

915 Tan, M.L., Duan, Z., 2017. Assessment of GPM and TRMM precipitation products over Singapore.
916 Remote Sensing 9, 1–16. https://doi.org/http://dx.doi.org/10.3390/rs9070720

917 Tang, G., Zeng, Z., Long, D., Guo, X., Yong, B., Zhang, W., Hong, Y., 2016. Statistical and Hydrological
918 Comparisons between TRMM and GPM Level-3 Products over a Midlatitude Basin: Is Day-1
919 IMERG a Good Successor for TMPA 3B42V7? Journal of Hydrometeorology 17, 121–137.
920 https://doi.org/10.1175/JHM-D-15-0059.1

921 Tapley, B.D., Bettadpur, S., Ries, J.C., Thompson, P.F., Watkins, M.M., 2004. GRACE measurements of
922 mass variability in the Earth System. Science 305, 503–5050.
923 https://doi.org/http://dx.doi.org/10.1126/science.1099192

Teixeira, A.H.D.C., Morris, S.-W., Hernandez, F.B.T., Andrade, R.G., Leivas, J.F., 2013. Large-scale water productivity assessments with MODIS images in a changing semi-arid environment: A Brazilian case study. Remote Sensing 5, 5783–5804. https://doi.org/10.3390/rs5115783

Usman, M., Liedl, R., Kavousi, A., 2015. Estimation of distributed seasonal net recharge by modern satellite data in irrigated agricultural regions of Pakistan. Environmental Earth Sciences 74, 1463–1486. https://doi.org/10.1007/s12665-015-4139-7

Valle Junior, L.C.G. do, Rodrigues, D.B.B., Oliveira, P.T.S. de, 2019. Initial abstraction ratio and Curve Number estimation using rainfall and runoff data from a tropical watershed. RBRH 24, 1–9. https://doi.org/10.1590/2318-0331.241920170199

Vasco, D.W., Farr, T.G., Jeanne, P., Doughty, C., Nico, P., 2019. Satellite-based monitoring of groundwater depletion in California's Central Valley. Scientific Reports 9, 16053. https://doi.org/10.1038/s41598-019-52371-7

Veeck, S., da Costa, F.F., Correia Lima, D.L., da Paz, A.R., Allasia Piccilli, D.G., 2020. Scale dynamics of the HIDROPIXEL high-resolution DEM-based distributed hydrologic modeling approach. Environmental Modelling & Software 127, 104695. https://doi.org/10.1016/j.envsoft.2020.104695

Verma, S., Verma, R.K., Mishra, S.K., Singh, A., Jayaraj, G.K., 2017. A revisit of NRCS-CN inspired models coupled with RS and GIS for runoff estimation. Hydrological Sciences Journal 62, 1891–1930. https://doi.org/10.1080/02626667.2017.1334166

Vu, H. V., Merkel, B.J., 2019. Estimating groundwater recharge for Hanoi, Vietnam. Science of the Total Environment 651, 1047–1057. https://doi.org/https://dx.doi.org/10.1016/j.scitotenv.2018.09.225

Wada, Y., van Beek, L.P.H., van Kempen, C.M., Reckman, J.W.T.M., Vasak, S., Bierkens, M.F.P., 2010. Global depletion of groundwater resources. Geophysical Research Letters 37, 1–5. https://doi.org/http://dx.doi.org/10.1029/2010GL044571

Wahr, J., Swenson, S., Zlotnicki, V., Velicogna, I., 2004. Time-variable gravity from GRACE: first results. Geophysical Research Letters 31, 1–14. https://doi.org/http://dx.doi.org/10.1029/2004GL019779

Walker, D., Parkin, G., Schmitter, P., Gowing, J., Tilahun, S.A., Haile, A.T., Yimam, A.Y., 2019. Insights from a multi-method recharge estimation comparison study. Groundwater 57, 245–258. https://doi.org/http://dx.doi.org/10.1111/gwat.12801

Weber, K., Stewart, M., 2004. A critical analysis of the cumulative rainfall departure concept. Ground water 42, 935–938. https://doi.org/10.1111/j.1745-6584.2004.t01-11-.x

Wendland, E., Barreto, C., Gomes, L.H., 2007. Water balance in the Guarani Aquifer outcrop zone based on hydrogeologic monitoring. Journal of Hydrology 342, 261–269. https://doi.org/10.1016/j.jhydrol.2007.05.033

Wiebe, A.J., Rudolph, D.L., 2020. On the sensitivity of modelled groundwater recharge estimates to rain gauge network scale. Journal of Hydrology 585, 1–14. https://doi.org/http://dx.doi.org/10.1016/j.jhydrol.2020.124741

Yin, L., Hu, G., Huang, J., Wen, D., Dong, J., Wang, X., Li, H., 2011. Groundwater-recharge estimation in the Ordos Plateau, China: Comparison of methods. Hydrogeology Journal 19, 1563–1575. https://doi.org/10.1007/s10040-011-0777-3

A satellite-based approach to estimating spatially distributed groundwater recharge rates in a tropical wet sedimentary region despite cloudy conditions

Luís Romero Barbosa[a,b,c,1], Victor Hugo R. Coelho[d,*,1], Ana Claudia V. e L. Gusmão[c], Lucila A. Fernandes[c], Bernardo B. da Silva[e], Carlos de O. Galvão[f], Nelson O. L. Caicedo[a], Adriano R. da Paz[a], Yunqing Xuan[g], Guillaume F. Bertrand[h], Davi de C. D. Melo[i], Suzana M. G. L. Montenegro[c], Sascha E. Oswald[b], Cristiano das N. Almeida[a]

[a] Department of Civil and Environmental Engineering, Federal University of Paraíba, João Pessoa, Brazil

[b] Institute of Environmental Science and Geography, University of Potsdam, Potsdam, Germany

[c] Department of Civil Engineering, Federal University of Pernambuco, Recife, Brazil

[d] Department of Geosciences, Federal University of Paraíba, João Pessoa, Brazil

[e] Department of Atmospheric Sciences, Federal University of Campina Grande, Campina Grande, Brazil

[f] Department of Civil Engineering, Federal University of Campina Grande, Campina Grande, Brazil

[g] College of Engineering, Swansea University, Swansea, UK

[h] Laboratory of Chrono-Environment, University of Bourgogne Franche-Comté, Besançon, France

[i] Department of Soils and Rural Engineering, Federal University of Paraíba, Areia, Brazil

[1] These authors contributed equally to this work.

*Corresponding author. Tel.: +55 83 32167432. E-mail address: victor.coelho@academico.ufpb.br

ABSTRACT: Groundwater recharge (GWR) is one of the most challenging water fluxes to estimate, as it relies on observed data that are often limited in many developing countries. This study developed an innovative water budget method using satellite products for estimating the spatially distributed GWR at monthly and annual scales in tropical wet sedimentary regions despite cloudy conditions. The distinctive features proposed in this study include the capacity to address 1) evapotranspiration estimations in tropical wet regions frequently overlaid by substantial cloud cover; and 2) seasonal root-zone water storage estimations in sedimentary regions prone to monthly variations. The method also utilises satellite-based information of the precipitation and surface runoff. The GWR was estimated and validated for the hydrologically contrasting years 2016 and 2017 over a tropical wet sedimentary region located in North-eastern Brazil, which has substantial potential for groundwater abstraction. This study showed that applying a cloud-cleaning procedure based on monthly compositions of biophysical data enables the production of a reasonable proxy for evapotranspiration able to estimate groundwater by the water budget method. The resulting GWR rates were 219 (2016) and 302 (2017) mm yr^{-1}, showing good correlations (CC = 0.68 to 0.83) and slight underestimations (PBIAS = -13 to -9%) when compared with the referenced estimates obtained by the water table fluctuation method for 23 monitoring wells. Sensitivity analysis shows that water storage changes account for +19% to -22% of our monthly evaluation. The satellite-based approach consistently demonstrated that the consideration of cloud-cleaned evapotranspiration and root-zone soil water storage changes are essential for a proper estimation of spatially distributed GWR in tropical wet sedimentary regions because of their weather seasonality and cloudy conditions.

Keywords: Remote sensing, water balance, groundwater recharge, water table fluctuation, tropical climate, sedimentary aquifer.

1. Introduction

Understanding the factors constraining groundwater recharge (GWR) is important for management and planning purposes of this water resource that is only slowly renewed (Cuthbert et al., 2019). In some regions, for instance, the abstracted groundwater over the past decades are taken from non-renewable groundwater (Döll et al., 2014), which increases, even more, the need for a better understanding of such factors. These abstractions need to be regionally regulated (Aeschbach-Hertig and Gleeson, 2012), since groundwater serves as the key strategic reserve for supplying water to societies during long-lasting droughts (Famiglietti, 2014). Such regulation, in turn, requires accurate information about the spatiotemporal distribution of natural GWR rates (Jasechko et al., 2014), including their variability and uncertainty in estimations, which are strongly sensitive to climate forcing factors, land uses and covers, watershed geomorphology and local hydrogeology (Moeck et al., 2020).

Since GWR is a key component used in many hydrological models to assess groundwater resource worldwide (Graaf et al., 2017; Wada et al., 2010), its accurate estimation constitutes a priority for stakeholders and a research challenge for the scientific community (Jasechko et al., 2014; Mohan et al., 2018). Many methods have been developed to estimate natural GWR at various spatiotemporal scales, with a wide range of complexity (Walker et al., 2019), given that GWR cannot be directly measured (Melo et al., 2015). Making use of these methods often depends on data availability, desired spatiotemporal resolution, and result representations (Walker et al., 2019).

The following five methods are commonly used to estimate GWR: 1) tracer techniques, which estimate aquifer renewal via substances in the water or specific concentrations of chemical elements, such as the chloride mass-balance method (e.g., Brunner et al., 2004; Hornero et al., 2016); 2) groundwater level monitoring in unconfined aquifers, which include examples such as water table fluctuation method (e.g., Cai and Ofterdinger, 2016; Wendland et al., 2007) and cumulative rainfall departure methods (e.g., Ahmadi et al., 2015; Weber and Stewart, 2004); 3) Darcy's law application, which allows calculating the velocity of soil water percolation and requires knowledge of hydraulic gradient and vertical hydraulic conductivity (e.g., Callahan et al., 2012; Yin et al., 2011); 4) numerical modelling, which consists of a mathematical representation of the GWR process (e.g., Melo et al., 2015; Melo and Wendland, 2017); and 5) the water balance method, which considers the main variables of the hydrological cycle as inputs and outputs of the system (e.g., Hornero et al., 2016; Wendland et al., 2007).

Most of the aforementioned methods are based on point-scale observations (e.g., meteorological stations or boreholes), which may cause serious issues when spatial variability in the regions of concern is great (e.g., Melo and Wendland, 2017). Although such a problem can be simply ignored for regions with extremely dense observation networks, it remains persistent in most regions worldwide, especially in developing countries. For instance, in Brazil, the national ground-based monitoring network consists of about 400 wells distributed over the country, complemented by a small number of observation wells monitored in only 21 active experimental basins (Melo et al., 2020). Therefore, the chief challenge for many hydrologists is to find and utilise alternative sources of data to estimate the spatial information of GWR (Brunner et al., 2007).

The use of cutting-edge satellite-derived remote sensing technology has played a crucial role in assimilating valuable distributed observation and in modelling water resources, which would otherwise be impossible with relatively sparse ground-based measurements alone (Famiglietti et al., 2015). However, the remote sensing contributions are rather inconsistent at quantifying and estimating GWR because all current data from satellite data can only detect patterns and processes related to water resources on and above the surface (Brunner et al., 2007; Coelho et al., 2017; Lucas et al., 2015). Satellite-based observations of time-variable gravity, such as the joint mission of the Gravity Recovery and Climate Experiment (GRACE), are sensitive to variations of terrestrial water storage, including the groundwater storage changes (Tapley et al., 2004; Vasco et al., 2019; Wahr et al., 2004). Unfortunately, the low spatial resolution of GRACE-derived data limits its ability to provide localised groundwater information at an appropriate scale (Alley and Konikow, 2015; Lakshmi et al., 2018). Thus, an innovative use of satellite data to estimate GWR at local and regional scales has been recently proposed, where most of data are applied to a simplified water budget approach that uses precipitation and evapotranspiration products (e.g., Crosbie et al., 2015; Gokmen et al., 2013; Lucas et al., 2015; Munch et al., 2013; Szilágyi et al., 2012; Szilagyi et al., 2011). This approach disregards other water balance components, such as surface runoff and soil water storage changes, which could considerably alter the estimation accuracy of GWR in some regions for short time scales (e.g., monthly).

In this context, some studies also have considered uniform surface runoff (Khalaf and Donoghue, 2012), as well as spatially distributed information about surface runoff (Coelho et al., 2017) and irrigation (Usman et al., 2015). The aforementioned studies used different remote sensing products and algorithms, but all of them were developed in regions with arid, semiarid, continental or Mediterranean climate

conditions where the cloud cover is limited (Coelho et al., 2017). For some tropical regions such as Brazil, the estimation of GWR using this approach remains challenging, mainly because of the difficulties in obtaining continuous information of actual evapotranspiration data by remote sensing without substantial cloud cover. In parallel, soil moisture information from satellite observations is currently available at the global scale and can provide valuable data to update the water budget approach with information regarding water storage changes in unsaturated soil layers (Reichle et al., 2018). Accounting for this component is particularly important for understanding GWR in sedimentary aquifers, where the unsaturated vadose zone width may vary from thin to thick soil layers (Rossetti et al., 2012). Unfortunately, some satellite-based datasets are only recently available, but some applications require earlier data.

Based on this information, this study develops an innovative water budget method using satellite-based data for estimating natural spatially distributed GWR rates at annual and monthly scales in tropical wet sedimentary regions, taking into account cloudy conditions. Accordingly, this study hypothesizes that such an approach enables local and regional scale perspectives in ungauged tropical wet regions. The general and transferable strategy would be relevant to account for 1) the substantial cloud cover and 2) the water storage changes in sedimentary regions prone to monthly variations. The method also utilises spatially distributed information on precipitation and surface runoff estimated from satellite products. The major limitation of this residual approach is that the accuracy of the GWR depends on the accuracy of the other components considered in the water balance (Scanlon et al., 2002), i.e., its application is appropriated when the errors of these components are small relative to the water flux. This limitation, when a satellite-based approach is considered, is mainly identified in regions that present ground-truth measurements discrepant with the estimated products used in the water balance, especially the main input (precipitation) and output (evapotranspiration) of the system. On the other hand, ground-based evaluations are punctual and representative of small areas, hardly integrating the spatial heterogeneity of meteorological processes, especially in urban areas (Maier et al., 2020). This study used ground-truth measurements to assess the two main estimated components of the water balance (i.e., precipitation and evapotranspiration) and the GWR rates.

2. Materials and methods

2.1 Study area

The study was carried out over an area of 1,032 km^2 in João Pessoa (JPA) (Paraíba, NE Brazil), which includes the metropolitan region and surrounding rural areas (Fig. 1). It consists in 1) the Gramame river basin (589.1 km^2; 57.1% of the area), and 2) the right bank of the Baixo Paraíba river basin (442.9 km^2; 42.9% of the area). The main source of water of the JPA metropolitan region (~1 million inhabitants) is the Gramame-Mamuaba reservoir, with maximum volume capacity of 56.9 hm^3. The water supply is complemented by more than 756 wells (CPRM – Geological Service of Brazil, 2020), pumped mostly for the public, industry, and irrigation, which are essential during periods of surface water shortage.

INSERT FIG. 1 HERE

Fig. 1. Location of (a) Brazil, (b) Paraíba state, and (c) João Pessoa (JPA) study area with the monitoring network, (d) land use and land cover, and (e) soil types.

The JPA has a tropical wet climate with a dry summer (i.e., As, according to the Köppen climate classification), with a mean temperature of 26°C and well-distinguished rainy and dry seasons (Alvares et al., 2013). The average annual precipitation is 1,700 mm, of which ~70% occurs from March to August during the austral autumn and winter. The potential evapotranspiration is relatively high in JPA, with mean annual values greater than 1,500 mm. The predominant land use and land cover (LULC) types in JPA are cropland (30.7%), Atlantic Forest (28.4%), pasture (26.3%), and urban areas (9.5%). The forest areas are Atlantic remnants, and the cropland areas contain mainly sugarcane and pineapple crops. Moreover, the main soil types in JPA are acrisols (58.7%), fluvisols (12.0%), podzols (10.8%), lixisols (9.1%) and histosols (5.5%). The fluvisols and histosols surround the rivers and the JPA urban area.

The hydrogeological framework mainly consists in 1) a coastal multi-layered sedimentary aquifer system near the littoral (i.e., the Paraíba Basin) and 2) a regional substratum that outcrops upstream in the more continental area (i.e., the Borborema Province). This latter corresponds to the crystalline regional basement that was affected by rifting processes due to the Cretaceos Atlantic aperture. This resulted in a graben that was progressively and sequentially filled by sediments as follows: 1) up to 360 m-thick fluvial sandstones of the Beberibe Formation from the Coniacian–Santonian age; 2) a 70 m-thick fossiliferous

calciferous sandstones and muddy siltstones of the Itamaracá Formation formed in marine transitional settings during the Santonian-Campanian age; 3) a 50-m thick phosphatic rocks and calciferous shales of the marine Gramame Formation from the Campanian-Maastrichtian age; and 4) a nearly 70 m-thick succession of fluvial sandstones and mudstones of the Barreiras Formation from the Early/Middle Miocene ages (Rossetti et al., 2012, 2011).

2.2 Satellite-based water budget approach

The actual GWR rates, defined as the rate at which water arrives at the table of an aquifer (Mathias et al., 2017), were spatially estimated from the residual terms of the water budget equation using satellite-based information. This estimation was performed for two hydrologically contrasting years 2016 and 2017, in which ground-based information was measured to evaluate the results. The GWR rates were then calculated at the monthly and annual scales by Eq. (1).

$$\mathrm{GWR} = \begin{cases} \mathrm{P} - \mathrm{ET} - \Delta\mathrm{S} - \mathrm{Q}\,, & \text{if } \mathrm{P} - \mathrm{ET} - \Delta\mathrm{S} - \mathrm{Q} > 0 \\ 0\,, & \text{if } \mathrm{P} - \mathrm{ET} - \Delta\mathrm{S} - \mathrm{Q} \leq 0 \end{cases} \quad (1)$$

where GWR is the groundwater recharge, P is the precipitation, ET is the actual evapotranspiration, ΔS is the water storage change at a root-zone scale (100-cm depth), and Q is the surface runoff. Other input and output water balance components were not investigated in this study because 1) they frequently represent relatively small contributions to the root zone (e.g., water pumping) or are implicitly considered in the aforementioned components (e.g., irrigation and interception), and 2) there are no reliable in situ data available for the JPA. Moreover, horizontal groundwater flow was also neglected because it refers to a slower GWR mechanism rather than the direct contribution of vertical infiltration (e.g., Coelho et al., 2017; Crosbie et al., 2015; Munch et al., 2013), since ~70% of the study area has terrain slope ranging from 0 to 92 m km^{-1}, which means that the topography predominantly presents weak slopes. All the used remote sensing products and other input data are summarised in Fig. 2 and described thoroughly in the next sub-items of this sub-section.

INSERT FIG. 2 HERE

Fig. 2. Satellite-based water budget approach showing the remote sensing products and other input data used to estimate the water balance components and groundwater recharge.

2.2.1 Precipitation

P was estimated by the Global Precipitation Measurement (GPM) mission, which is an international network of satellites undertaken by the National Aeronautics and Space Administration (NASA) of the USA and the Japanese Aerospace Agency (JAXA) (Huffman et al., 2018). This mission provides rainfall and snowfall information globally via the Integrated Multi-satellitE Retrievals for GPM (IMERG) products at 0.1° (~10 km) and 30-min resolutions (Huffman et al., 2018). IMERG is an algorithm that combines microwave and infrared estimates from the GPM constellation. This study used version V05B of the IMERG Final Run product. The IMERG Final Run product also incorporates monthly gauge observations from the Global Precipitation Climatology (GPCC) and other ancillary data to improve the satellite estimations (Skofronick-Jackson et al., 2017). This product is ready for use after 3.5 months of the data acquisition (Skofronick-Jackson et al., 2018). The advantage of IMERG is the high spatial resolution when compared to other satellite-based products. On the other hand, the weakness of this product is its latency (~3.5 months), which is inappropriate for real-time applications.

IMERG P is a valuable source of information for global and regional applications mainly because of its high spatiotemporal resolution. However, for medium- and small-scale hydrological studies, the spatial resolution of 0.1° of the IMERG product is still coarse (Sharifi et al., 2019). Due to the dimension of the study area, the IMERG data was downscaled to a resolution of 0.0045° (~500 m), similarly to Lu et al. (2019). The bilinear interpolation method was used to downscale the IMERG product, as it can provide consistent data disaggregation (Moghim et al., 2016). The 30-min IMERG data were accumulated aggregated to daily, monthly, and annual P scales.

The accuracy of remote sensing P products can be hampered by various factors, such as calculation algorithms and satellite sensor characteristics (Semire et al., 2012). The assessment carried out by Gadelha et al. (2019) found that in comparison with the ground-based rainfall data, the IMERG V05B effectively captures the P spatial patterns over most of the Brazilian territory, except for the entire coastal zone of NE Brazil, where underestimates occurs. For this reason, a linear-scaling bias correction procedure was applied (Lenderink et al., 2007), using a single correction factor per month calculated by the ratio between the monthly averages of rain gauges and the IMERG data (Le et al., 2018) rather than a grid-box correction (i.e., pixel-per-pixel) to preserve the original spatial distribution of the IMERG data.

P data measured from 16 rain gauges that are subjected to quality control were used for the IMERG bias correction and comparison purposes (Fig. 1c). The gridded observed rainfall data were estimated by inverse distance weighting interpolation. For comparison purposes, Quantile-Quantile plots between the bias-corrected IMERG interpolated data (henceforth IMERG-C) and ground-based interpolated data were built at the monthly and annual scales for every 10% percentiles (i.e., 0, 10, …, 90, 100%). Over these estimates, the linear regressions were plotted, and their slope and y-intersect values were calculated. Moreover, the rain gauges interpolated data were used as input to spatially estimate the runoff and the GWR from the water budget equation. The estimates were then compared with the estimated components obtained from the satellite-based approach.

2.2.2 Actual evapotranspiration

The ET was estimated using the Penman-Monteith equation (Monteith, 1965), which was also adopted by Mu et al. (2007) to create the first global ET product (MOD16). The MOD16 is a product from NASA based on the MODerate Resolution Imaging Spectroradiometer (MODIS) sensors installed on two satellites (Terra and Aqua), as well as reanalysis-derived meteorological inputs. Currently, the MOD16 dataset provides ET at the global scale with a spatial resolution of 500 m and three different timescales (8-d, monthly, and annual scales). Unlike the algorithm used by Mu et al. (2011) to generate the current MOD16 product, this study calculated the ET based on the algorithm developed by Mu et al. (2007), using the biome-property-look-up-table shown by Running et al. (2017). The algorithm proposed by Mu et al. (2007) was based on Eq. (2) and assumes that night-time ET is small and in turn negligible.

$$\Lambda E = \Lambda E_{transp} + \Lambda E_{soil} = \frac{\Delta A + \rho C_p (e_s - e_a)/r_a}{\Delta + \gamma(1 + \frac{r_s}{r_a})} \quad (2)$$

where Λ is the latent heat of evaporation (=2.45 MJ kg^{-1}), ΛE is the latent heat flux density (W m^{-2}) consisting of the plant transpiration (ΛE_{transp}) and soil evaporation (ΛE_{soil}), i.e., the total daily ET (mm) after multiplying by the conversion factor (=3.53×10^{-2} mm d^{-1} W^{-1} m^2); A is the available energy commonly determined as the daily net radiation of the land surface (Rn) (W m^{-2}); ρ is the air density (=1.2 kg m^{-3}); C_p is the specific heat capacity of air at constant pressure (=1005 J kg^{-1} $°C^{-1}$); r_a is the aerodynamic resistance (s m^{-1}), r_s is the surface resistance (s m^{-1}); e_a is the actual water vapour pressure (kPa); e_s is the saturated

water vapour pressure (kPa); Δ is the slope of the curve relating saturated water vapour pressure to the temperature (kPa $°C^{-1}$); and γ is the psychrometric constant (kPa $°C^{-1}$).

The MOD16 algorithm is only suitable to use under clear sky conditions, as MODIS satellite sensors cannot measure cloud base parameters (Sur et al., 2015). This occurs because the MOD16 generates the ET based on some 8-day MODIS products (i.e., pixels of the best observations from the last eight days) with 500-m spatial resolutions (e.g., MOD15A2H and MCD43A2/A3). These 8-d products remain insufficient to attenuate cloudy condition effects on ET estimations in some regions (Running et al., 2017).

The available MOD09Q1 (Terra) and MYD09Q1 (Aqua) reflectance products were used in this study due to their suitable 250-m and 8-d resolutions to obtain the biophysical data, namely, 1) the leaf area index (LAI) using the soil adjusted vegetation index (SAVI) (Bastiaanssen et al., 1998; Huete, 1988), 2) the vegetation cover fraction calculated by the enhanced vegetation index (EVI2) proposed by Jiang et al. (2008), and 3) the surface albedo (ALB) computed by the equation proposed by Teixeira et al. (2013). To address the shortcomings related to cloudy conditions, this study carried out monthly map compositions with 8-d grid biophysical inputs (i.e., EVI2, LAI, and ALB). The monthly compositions were based on the selection of pixels with higher values of LAI and EVI2 obtained from the eight images available per month (i.e., four MOD09Q1 and four MYD09Q1), assuming that lower or negative values of these two biophysical parameters were possibly contaminated by clouds. Conversely, for the monthly compositions of ALB, only the lower values per pixel from the eight images available per month were considered, assuming that higher values of albedo were possibly contaminated by clouds. These new data then assumed clear sky conditions to indicate fixed input parameters throughout a month and were used to generate daily ET data.

The MOD16 product also uses global LULC classification from MODIS land cover type (MCD12Q1) as an input to obtain information about canopy conductance and plant transpiration. However, the global representation of the MCD12Q1, which is associated with the limited number of classes (17), can misidentify some local and regional specificities of the vegetation and introduce considerable errors in the estimation of ET for medium and small areas (Ruhoff et al., 2013). Therefore, we used a regional LULC classification (SEEG/OC, 2015), namely, the MapBiomas Project (http://mapbiomas.org). MapBiomas provides Landsat-based annual LULC maps associated with 27 classes at a 30-m spatial resolution processed from 1985. In this study, MapBiomas LULC collection 3.1 was reclassified into six general classes (barren land, forest, cropland, pasture, urban, and water body) before being used to generate ET data.

The MOD16 product uses the global meteorological reanalysis data provided by NASA's Global Modelling and Assimilation Office (GMAO) at a 0.5° × 0.6° or 1.0° × 1.25° spatial resolution as inputs of the original algorithm (Mu et al., 2011, 2007; Running et al., 2017). GMAO incorporates ground- and satellite-based observations to provide information with a 6-h temporal resolution. Unlike the MOD16 product, this study used the GLDAS NOAH L4 V2.1 meteorological product provided by the NASA Global Land Data Assimilation System (GLDAS) (Rodell et al., 2004). It allowed providing the following meteorological data with 3-h and 0.25° resolutions: downward shortwave radiation, air pressure, air temperature, and specific humidity. The meteorological data were retrieved from four pixels covering most of JPA and were averaged and used as inputs for the ET estimation.

The daily mean estimated ET was tested against the Penman-Monteith equation, which is considered the universal standard approach for calculating daily reference evapotranspiration (ET_0) (Allen et al., 1998). Such a comparison does not validate the estimates but only assess if both evapotranspiration time series oscillate and peak with similar amplitudes and magnitudes, respectively. The meteorological data used to calculate the ET_0 were acquired from a meteorological station inside JPA, which belongs to the Brazilian National Institute of Meteorology (INMET, acronym in Portuguese) (Fig. 1c). Additionally, the mean 8-day ET data from the original MOD16A2 product was also used to check the daily estimates using the cloud-cleaning procedure combined with a more fine-tuned dataset.

2.2.3 Soil water storage changes

The soil water storage changes were calculated using root-zone moisture information of the Soil Moisture Active Passive (SMAP) mission from NASA, estimated each 2 to 3 days since 2015 (Reichle et al., 2018). The SMAP Level 4 (L4) provides global near-surface (0-5 cm) and root-zone (0-100 cm) soil moisture with the SMAP L4 Surface and Root Zone Soil Moisture Analysis Update (SPL4SMAU) product (Reichle et al., 2017). The 100-cm root-zone SPL4SMAU soil moisture product (3-h temporal and 9-km spatial resolution), whose data result from the assimilation of L-band brightness temperature data into the NASA Catchment land surface model, was used to obtain the soil water storage by the soil moisture difference from one day to another multiplied by the root zone depth of 1,000 mm (Reichle et al., 2018).

Based on the SMAP orbit revisit time, the soil moisture data were scheduled to be retrieved at 6:00 a.m. and 6:00 p.m. (at the Legal Local Time). However, since the satellite takes 2 to 3 days to map the

whole globe, some images over JPA were missing for a range of days of the year. Thus, similar to the study carried out by Souza et al. (2018), the soil moisture data were calculated in three ways: 1) if both orbits were completed on the same day, then both values were averaged; 2) if only one orbit had a valid value, then this value was considered for that day; and 3) if no valid value was obtained in any orbit, then the soil moisture calculated for the previous day was repeated. Finally, the soil water storage changes were calculated by summing (positive or negative) daily differences in the SPL4SMAU root-zone data at the monthly and annual scales, which was performed after interpolating their images from a 9-km to a 500-m resolution through bilinear interpolation (same as that for P).

2.2.4 Surface runoff

The surface runoff was estimated using the Natural Resources Conservation Service–Curve Number (NRCS–CN) method (Hawkins et al., 1985). The NRCS–CN method combines climatic and physiographic characteristics in empirical formulas that convert basic descriptive data into numeric values to estimate the excess P that was not intercepted, stored, or infiltrated (Deshmukh et al., 2013). We implemented this estimation spatially with daily P. The daily runoff estimates were then summed pixel by pixel at monthly and annual scales, thus avoiding the overestimation errors that stem from its direct calculation at monthly and annual scales (Awadallah et al., 2017). We choose the NRCS-CN method because of its simplicity, ease of use and widespread acceptance (Ponce and Hawkins, 1996; Verma et al., 2017), focusing on scarce data regions in developing countries but taking advantage of freely available remote sensing data.

The NRCS–CN method is based on a water budget equation that assumes that P must exceed the initial abstraction (I_a), being a soil-dependent fraction (λ) of the maximum water storage capacity (S), before any direct runoff (Q) is triggered. A fixed value of λ equals to 0.20 is recommended by the original method and widely adopted in the United States (Hawkins et al., 1985). However, the initial losses depend on the local and regional characteristics of the watershed. Many studies, including some carried out in Brazilian catchments, indicated that the value proposed by the original method is too high for many parts of the world and recommended λ values of about 0.05 or less (e.g., Ajmal and Kim, 2015; Durán-Barroso et al., 2017; Shi et al., 2009; Valle Junior et al., 2019; Veeck et al., 2020). Recently, the studies by Lal et al. (2019, 2017) reviewed the values of λ for 63 watersheds worldwide with various LULC, finding 0.03 as a

representative value, which was also used in our study. In this context, the new runoff and water storage capacity calculations under average wet conditions ($S_{II,\lambda=0.03}$) are shown in Eqs. (3) and (4).

$$Q = \begin{cases} \dfrac{\left(P - 0.03S_{II,\lambda=0.03}\right)^2}{\left(P + 0.97S_{II,\lambda=0.03}\right)} & , \quad \text{if } P \geq I_a = 0.03S \\ 0 & , \quad \text{if } P = 0 \end{cases} \tag{3}$$

$$S_{II,\lambda=0.03} = 0.654\left(\frac{25400}{CN_{II,\lambda=0.20}} - 254\right)^{1.248} \quad , \quad \text{for } 0 \leq CN_{II,\lambda=0.20} \leq 100 \tag{4}$$

CN values were selected from the (NRCS – Natural Resources Conservation Service, 2004) tables and spatially assigned to different hydrologic soil-cover complexes using a look-up table built in a GIS platform. The hydrologic soil-cover complexes refer to the different combinations of LULC and hydrological soil groups (HSGs) contained in a study area. The HSG information was created from the regional information about soil types provided by Araújo Filho et al. (2000). The HSG was assigned according to the soil type, following the methodology proposed by Sartori et al. (2005) that consists of 19 criteria based on a survey of 58 soil profiles and hydrodynamic data in Brazil. The LULC information was obtained from MapBiomas collection 3.1, the same used for estimating ET.

The potential runoff before a surface runoff event generated by the NRCS–CN method depends on the antecedent moisture condition (AMC) (Hawkins et al., 1985). The proper condition was identified through the 5-d antecedent cumulative P (P_{5d}, mm), which was calculated for each P grid cell. For this purpose, three intervals of P_{5d} were used, distinguishing between the growing season (GS, from March to July) and the dormant season (DS, from August to February) according to the AMC. Similar to those in Lal et al. (2017), the P_{5d} intervals in this study were defined as AMC-I (dry conditions): if $P_{5d} \leq 35.56$ mm (GS) or $P_{5d} \leq 12.7$ mm (DS); AMC-II (average conditions): if $35.56 < P_{5d} \leq 53.34$ mm (GS) or $12.70 < P_{5d} \leq 27.94$ mm (DS); and AMC-III (wet conditions): if $P_{5d} > 53.34$ mm (GS) or $P_{5d} > 27.94$ mm (DS). Moreover, the P_{5d} intervals of DS were considered for the urban and barren areas, whereas the P_{5d} intervals of GS were considered for the forest areas throughout all months of the year because of their active vegetation growing conditions. Finally, the CN_I and CN_{III} values were determined under AMC-I and AMC-III, respectively, based on Lal et al. (2019).

2.3 Evaluation of groundwater recharge estimates

The GWR rates were evaluated by the water table fluctuation (WTF) method (Healy and Cook, 2002; Scanlon et al., 2002). The ground-based GWR rates obtained from WTF (Eq. 5) were used to evaluate the spatially distributed GWR rates estimated by the water budget equation on a 1-km footprint around the wells to comprehensively consider the surrounding characteristics. Their absolute (GWR, mm) and relative (GWR/P, %) estimates were compared through linear regressions.

$$R_{WTF} = S_y \frac{\Delta H}{\Delta t} \quad (5)$$

where R_{WTF} denotes the estimated recharge rate (mm/time step) using WTF, S_y represents the aquifer specific yield coefficient, ΔH is the cumulated rising piezometric level changes (mm), and Δt is the time from the beginning of the rise to the peak. ΔH corresponds to the sum of the actual groundwater rise and the potential groundwater decline for the same period, with the latter being obtained by extrapolating the antecedent recession curve (Healy and Cook, 2002; Wendland et al., 2007).

The groundwater fluctuation data were manually collected every 45 days from 16 (in 2016) and 23 monitoring wells (in 2017) located in the Barreiras Formation (Fig. 1c). Seven additional wells were drilled in 2017 in the urban area. These monitoring wells are well-distributed throughout the study area and, therefore, capable to characterise the local groundwater since they cover several soil types, depths (from shallow to deep) and LULC, from the coastline to the headwater. This monitoring network was carefully selected so as to have no groundwater pumping in or nearby the monitoring wells. The temporal variations of groundwater fluctuations were also used to compare the overall behaviour of the monthly satellite-based GWR estimates. The values of S_y equal to 0.10 (16 wells) and 0.24 (7 wells) were estimated by pumping tests in four wells and assigned to the others based on their similar local characteristics, including the groundwater level patterns.

2.4 Statistical metrics

Three statistical metrics were selected to evaluate the goodness-of-fit of the results. The first metric was the correlation coefficient (CC, Eq. (6)), which describes the relationship between variations in simulated and observed values. The other two metrics were the percent bias (PBIAS, Eq. (7)) and the

relative root mean square error (RRMSE, Eq. (8)), both with perfect values equal to 0%, which were used to describe the bias and error between simulated and observed values, respectively.

$$\mathrm{CC}(-) = \frac{\sum_{i=1}^{n}(G_i - \overline{G})(S_i - \overline{S})}{\sqrt{\sum_{i=1}^{n}(G_i - \overline{G})^2}\sqrt{\sum_{i=1}^{n}(S_i - \overline{S})^2}} \quad (6)$$

$$\mathrm{PBIAS}(\%) = \frac{\sum_{i=1}^{n}(S_i - G_i)}{\sum_{i=1}^{n} G_i} \times 100 \quad (7)$$

$$\mathrm{RRMSE}(\%) = \frac{\sqrt{(1/n)\sum_{i=1}^{n}(S_i - G_i)^2}}{\overline{G}} \times 100 \quad (8)$$

where S_i and G_i are the satellite- and ground-based data, respectively, and $\overline{S}$ and $\overline{G}$ are the mean values of the satellite- and ground-based data, respectively.

3. Results and discussion

3.1 Precipitation

The first set of analyses assessed the spatiotemporal distributions of the main input of the water balance (i.e., P) obtained from IMERG-C data and compared these with the ground-based interpolated data (henceforth Gauge) (Fig. 3). Annual P based on IMERG-C data gradually decreased from east to west, varying from 1,120 to 1,600 mm in 2016 and 1,050 to 2,300 mm in 2017. The maximum P based on Gauge observations was 1,630 mm in 2016 and 2,070 mm in 2017. Similarly, (Lu et al., 2019) showed consistent spatial patterns and maximum values of IMERG P after performing bias correction using monitoring data. P obtained in JPA from the IMERG-C data occurred mostly within the regular rainy season (i.e., from March to July), corresponding to 71% in 2016 and 77% in 2017 of the annual totals. The monthly variations in P in 2016 from the IMERG-C and Gauge data were similar (Fig. 3e,f), whereas the IMERG-C variation was larger than the Gauge variation in some months of 2017, particularly in June and July, when the 10-90% percentile ranges were 60% higher and double, respectively. Despite such differences, the average values obtained by IMERG-C were similar to those from the Gauge in most of the months, showing that IMERG-C was able to detect the temporal variation of P.

385 **INSERT FIG. 3 HERE**

386 **Fig. 3.** Spatially distributed precipitation in 2016 and 2017 estimated using (a and d) ground-based
387 interpolated data and (b and e) IMERG-C data, with (c and f) monthly variations depicted by box plots with
388 10-90% percentiles. Histograms refer to the proportion of total cells.

389 The deviations between the IMERG-C and ground-based interpolated P were also assessed using
390 Quantile-Quantile plots (Fig. 4). At the monthly scale, a suitable correlation (CC = 0.97) and a reasonable
391 fit using linear regressions (slope = 1.01; y-intersect = -1.68) were found, with some deviations in March,
392 June, and July. Good correlations between the IMERG products and the observed dataset have been found
393 by other studies in tropical regions at the monthly scale (e.g., Satgé et al., 2017; Tan and Duan, 2017). The
394 monthly mean error was 23%, higher than the annual mean error (i.e., 8%). These values remained within
395 the acceptable ranges for satellite-based monthly P (Salles et al., 2019). Acceptable metrics were also found
396 at the annual scale, despite the slight deviation of the linear regression (slope = 1.20; y-intersect = -314
397 mm). Such a deviation probably occurred due to the larger variation of the ground-based P on the western
398 side of the study area in 2017, which likely stemmed from the limited number of rain gauges used on the
399 interpolation (see Fig. 1). According to Tang et al. (2016), the underestimation of this satellite-based P data
400 can occur over regions with wet climates and low latitudes. The results found in this analysis confirm that
401 the IMERG-C data enabled the mapping of the decreasing P gradient in the study area.

402 **INSERT FIG. 4 HERE**

403 **Fig. 4.** (a) Monthly and (b) annual Quantile-Quantile plots between the IMERG-C and ground-based
404 interpolated data at the 10% percentile. Shaded bounds: 95% confidence interval.

405 **3.2 Actual evapotranspiration**

406 The spatial ET distribution estimated by the modified MOD16 algorithm applying cloud cleaning
407 is shown in Fig. 5. Overall, the mean annual ET varied from 1,170 (in 2016) to 1,220 mm (in 2017). The
408 results were consistently distinguishable amongst the LULC types, with values smaller than 850 mm in the
409 urban areas and above 1,450 mm in the forest areas. At the monthly scale, the ranges of the average
410 estimates were similar between the studied years, varying from 73 to 119 mm in 2016 and 85 to 114 mm

411 in 2017. However, comparing the monthly mean estimates of 2017 with those of 2016, they were smaller
412 at the beginning, closer at the middle, and higher at the end of the year. In the rainy season, smaller
413 differences between high and low ET data were observed, showing monthly averages in the 10-90%
414 percentile ranges equal to 63 (in 2016) and 58 mm (in 2017) from April to August. On the other hand, larger
415 differences between high and low ET data occurred in the dry season, as shown by the monthly averages
416 in the 10-90% percentile ranges equal to 84 (in 2016) and 87 mm (in 2017) from September to March. Lima
417 and Ribeiro (2018) showed that such seasonable patterns can stem from the associations between
418 meteorological and evapotranspiration estimates by using the MapBiomas LULC and GLDAS
419 meteorological forcing data to calculate spatially distributed ET. Thus, variations in the ET throughout the
420 studied years in JPA were likely influenced by the combination of LULC diversity, weather seasonality and
421 cloudy conditions.

422 **INSERT FIG. 5 HERE**

423 **Fig. 5.** Spatially distributed actual evapotranspiration in (a) 2016 and (b) 2017, with (c) monthly variations
424 depicted by box plots with 10-90% percentiles. The MOD16 algorithm disregards the evaporation rates
425 from water bodies, which are white shown in the maps. Histograms refer to the proportion of total cells.

426 The mean daily ET obtained by the modified MOD16 algorithm ranged from 1.0 to 4.7 mm d^{-1}
427 during the whole study period, whereas the mean ET_0 varied from 3.0 to 7.0 mm d^{-1} (Fig. 6). The ET_0 was
428 as much as three times higher than the ET estimated by the proposed approach between August and
429 February (dry season) due to the lower soil water availability in these months. This difference is plausible
430 since ET_0 refers to the evapotranspiration of well-watered grass vegetation with active growth throughout
431 the year. Such a difference considerably shrunk during the rainy seasons, with the actual and reference
432 evapotranspiration following the same temporal behaviour, as expected.

433 **INSERT FIG. 6 HERE**

434 **Fig. 6.** Comparison between the daily actual evapotranspiration obtained by the modified MOD16
435 algorithm, the mean 8-day actual evapotranspiration data from the MOD16A2 product, and the daily
436 reference evapotranspiration.
437

The daily ET estimates obtained by the proposed methodology were greater than those acquired by the mean 8-day MOD16A2 product for the studied period, which ranged from 1.9 to 3.9 mm d^{-1} (Fig. 6). Consequently, the mean annual ET estimated by the MOD16A2 was lower than those obtained by the modified MOD16 algorithm for 2016 (895 mm) and 2017 (938 mm). The values of ET estimated by the MOD16A2 product was also lower than those found by other studies using the Surface Energy Balance Algorithm for Land (SEBAL) in river basins with similar characteristics in NE Brazil (e.g., Oliveira et al., 2014). Although slightly higher, the ET estimates presented the same temporal patterns observed by the original MOD16A2 product. The differences found between the original and the modified approaches can possibly be attributed to the following factors: 1) the missing data in some pixels of the MOD16A2 product because of the presence of cloud cover, 2) the use of a more fine-tuned LULC regional product, and 3) the use of a higher resolution input meteorological data. For instance, Ruhoff et al. (2013) identified that the misclassification of the LULC data used in the MOD16A2 product, combined with the low spatial resolution of the GMAO reanalysis meteorological information and the cloud cover contaminated pixels, were the largest contributors to over- or under-estimate the eddy covariance measurements in a humid tropical river basin located in south-eastern Brazil. Recently, a study carried by Melo et al. (2021) used 25 flux towers to evaluate four remote sensing-based ET algorithms in many ecoregions over South America, including the MOD16 model forced by ground-based meteorological data. An average uncertainty of ~10% was found for the MOD16 algorithm when considering all studied ecoregions, with relatively higher performance observed for wet climate regions. This overall uncertainty observed by Melo et al. (2021) for the MOD16 algorithm was similar to those found by Ruhoff et al. (2013) in two sites in Brazil after the MOD16 algorithm parameter fitting based on land use and land cover (i.e., without the use of the MOD12Q1 product).

3.3 Soil water storage changes

The annual water storage changes in the root zone throughout JPA varied from -27 to -6 mm during 2016 and from -40 to -12 mm during 2017 (Fig. 7). Annual water storage decreases suggest that the root zone released water during the studied period, which is in part due to vertical percolation to aquifers. Despite its original coarse resolution, SPL4SMAU consistently showed a water storage increase in the root zone mostly during the rainy season, likely because there is more water in the top layer after P. The water

increase in the root zone in December 2016 likely stemmed from substantial P (Fig. 3e) when the South Atlantic Convergence Zone was positioned further eastward (Palharini and Vila, 2017). Moreover, as expected, the urban areas featured large water decreases in the root zone in both years, likely because of the lower infiltration caused by soil imperviousness, whereas the rural areas featured a larger spatial variation in water decreases. These results show that an above-average rainy condition is required for an annual water increase in the root zone, implying a susceptibility in JPA to water shortage.

INSERT FIG. 7 HERE

Fig. 7. Spatially distributed soil water storage changes in (a) 2016 and (b) 2017, with (c) monthly variations depicted by box plots with 10-90% percentiles. Histograms refer to the proportion of total cells.

3.4 Surface runoff

The mean annual surface runoff estimated from the IMERG-C data varied from 220 (in 2016) to 300 (in 2017) mm (Fig. 8). Due to soil imperviousness, urban areas produced annual runoff estimates greater than 450 mm. In 2017, higher values of surface runoff from IMERG-C data also occurred outside the urban area in relation to that from Gauge because of the high P in June and July. In the regular rainy season (i.e., from March to July), the mean annual surface runoff estimated with IMERG-C data accounted for 200 mm in 2016 and 265 mm in 2017. The sources of uncertainties surrounding the NRCS-CN method were analysed by Durán-Barroso et al. (2017), which include: 1) a significant weakness to select representative events for simulation with the NRCS CN parameters; and 2) the impossibility of determining an optimum value for λ but lower values are recommended instead of the original value. For instance, the study carried out by Veeck et al. (2020) in a Brazilian catchment found fitted initial losses lower than the original value for almost all simulated events, with relative errors below 12%. However, quantifying uncertainties of rainfall-runoff is a very complex issue in Brazil due to the lack of data.

INSERT FIG. 8 HERE

Fig. 8. Spatially distributed surface runoff in 2016 and 2017 estimated using (a and d) rain gauge and (b and e) IMERG-C data, with (c and f) monthly variations depicted by box plots with 10-90% percentiles.

The surface runoff results over the water bodies were neglected in the NRCS–CN calculation, which are white shown in the maps. Histograms refer to the proportion of total cells.

3.5 Groundwater recharge

On average, the GWR rates ranged from 219 (in 2016) to 302 mm yr^{-1} (in 2017) (Fig. 9). These results remained within the range of the GWR rates of several tropical wet regions throughout the world (e.g., Malakar et al., 2019; Rodríguez-Huerta et al., 2020; Vu and Merkel, 2019). The urban area featured greater GWR rates than other areas despite its greater surface runoff, likely due to the combination of lower ET and sandy soils (Minnig et al., 2018; O'Driscoll et al., 2010), as well as to the higher P estimates for the coastline than for the headwaters. Consistently, Moeck et al. (2020) also showed that in the eastern part of Brazil, high GWR rates can occur despite the annual potential evapotranspiration being greater than 1,500 mm because of the large amount and seasonality of P. At the monthly scale, GWR rates using IMERG-C and Gauge data averaged 34.7 and 36.5 mm $month^{-1}$ in 2016 and 47.7 and 51.4 mm $month^{-1}$ in 2017, respectively. These monthly estimates using IMERG-C data were similar to the Gauge estimates, although the difference doubled in 2017 due to higher surface runoff estimated in June and July using IMERG-C data. The differing GWR rates obtained for the Gauge data were likely influenced by the sensitivity of modelled groundwater recharge estimates to the rain gauge network scale (Wiebe and Rudolph, 2020).

INSERT FIG. 9 HERE

Fig. 9. Spatially distributed GWR rates estimated in 2016 and 2017 by the water budget equation and WTF method, using (a and d) rain gauge and (b and e) IMERG-C data, with (c and f) monthly variations depicted by box plots with 10-90% percentiles. The GWR results over the water bodies were neglected in the water budget equation, which are white shown in the maps. Histograms refer to the proportion of total cells.

The differences caused by disregarding the soil water storage changes were negligible at the annual scale, reducing the mean relative GWR by less than -1% for the studied years, which likely occurred due to the compensation of the water increases and decreases in the root zone throughout the rainy and dry seasons. Conversely, at the monthly scale, neglecting the soil water storage changes would have considerably impacted the GWR values, increasing their mean relative estimates by as much as +19 (in 2016) and +12% (in 2017) during the rainy season and decreasing their mean relative estimates by -22 (in

518 2016) and -13% (in 2017) during the dry season. Therefore, although other studies considering long-term
519 average recharge (e.g., 10 year period) have claimed that satisfactory estimations can be obtained by simply
520 applying the difference between P and ET satellite products in some semiarid, continental and
521 Mediterranean regions (e.g., Crosbie et al., 2015; Gokmen et al., 2013; Munch et al., 2013; Szilagyi et al.,
522 2011), this study demonstrated that tropical wet sedimentary regions also require the consideration of
523 surface runoff and soil water storage changes on a monthly and annual basis because their water cycles are
524 stressed by weather seasonality and hydrologic soil-cover complexes.

525 The annual GWR rates estimated by the WTF method varied from 110 to 370 mm yr^{-1} in 2016,
526 corresponding to 10 and 24% of the mean annual P obtained by the Gauge data, respectively (Table 1). Half
527 of these estimates ranged from 100 to 200 mm yr^{-1}, mostly obtained from the observation wells located
528 upstream (Fig. 9). In 2017, the GWR rates varied from 90 to 550 mm yr^{-1}, corresponding to 7 and 29% of
529 the mean annual P obtained by the Gauge data, respectively. More than half of these estimates ranged from
530 300 to 550 mm yr^{-1}, mostly obtained from observation wells located downstream (urban area).

531 **INSERT TABLE 1 HERE**

532 **Table 1.** Absolute and relative GWR estimates calculated by the WTF method in 2016 and 2017.

533 For evaluation purposes, the absolute and relative estimates of the GWR obtained by the water
534 budget equation were plotted against the WTF results (Fig. 10). The correlations and mean errors of the
535 absolute and relative GWR estimates based on the IMERG-C data varied from 0.68 to 0.83 and from 30 to
536 34%, respectively. These correlations and mean errors were fairly similar to the GWR ranges estimated
537 using the Gauge data, whose correlations varied from 0.73 to 0.89, and the mean errors remained at 31%.
538 Szilagyi et al. (2011) compared the GWR rates estimated by a satellite-based approach with chloride mass-
539 balance rates, showing a spatial correlation of 0.57 at the annual scale. In our study, the GWR rates
540 estimated by the water budget equation using the IMERG-C data tended to slightly underestimate the WTF
541 data between -13 and -9%, whereas the Gauge scenario overestimated the WTF data between 8 and 11%.
542 However, a good fit was found for the IMERG-C data by using linear regressions, showing decent slope
543 and y-intersect values for the absolute (1.16 and -69 mm, respectively) and relative (0.82 and 0.79%,
544 respectively) GWR, which confirmed the low underestimations. These negative biases could have been
545 caused by neglecting the contribution of the irrigation input component in the water budget equation of this

546 study, which is practically nil in the wettest period but can be significant in some sugarcane cultivated areas
547 (i.e., corresponding to ~30% of the study area) during the four driest months. Usman et al. (2015) also
548 found negative bias by applying a satellite-based approach to estimate GWR rates, showing that the
549 consideration of irrigation considerably improves GWR estimates in comparison with WTF estimates. In
550 this study, the GWR estimates based on the IMERG-C data were slightly lower than those calculated based
551 on the WTF method, whose mean differences were 5 (in 2016) and -30 mm yr^{-1} (in 2017) at the absolute
552 scale, as well as -0.8 (in 2016) and -1.8% (in 2017) at the relative scale, respectively. Crosbie et al. (2015)
553 also found average underestimations of 45 mm yr^{-1} when comparing the GWR rates calculated by a satellite-
554 based approach with the chloride mass-balance and WTF estimates.

555 **INSERT FIG. 10 HERE**

556 **Fig. 10.** Evaluation based on the WTF method of the annual GWR rates, estimated from rain gauge and
557 IMERG-C data at (a, b, and e) absolute and (c, d, and f) relative scales.

558 Besides the biases possibly caused by disregarding the irrigation, the uncertainties in each water
559 balance component (i.e., P with ~8% according to comparisons with on-ground gauge measurements; ET
560 with ~10% based upon Melo et al. (2021); and Q with ~12% as found by Veeck et al. (2020)) used in the
561 proposed approach might propagate to the residual term (i.e., the GWR). Uncertainty in time series of GWR
562 estimated using the WTF method is associated with the difficulty in determining a representative Sy, which
563 has a dependence on the depth to water table (Crosbie et al., 2019). For instance, the uncertainty in the
564 GWR rates estimated from a satellite-based approach (P-ET) and the WTF method was analysed by Lucas
565 et al. (2015), which found uncertainties ranging from 24 to 42% of the annual mean GWR. Actually,
566 estimating GWR is a big challenge because it cannot be measured directly (Crosbie et al., 2019; Scanlon et
567 al., 2002). Therefore, it is still difficult to assess the accuracy of any method (Crosbie et al., 2019; Healy
568 and Cook, 2002), with no widely applicable methodology available that can directly and accurately quantify
569 the volume of rainwater that reaches the water table (MacDonald et al., 2021). Because of this, it has been
570 recommended over the last decades to use multiple methods when estimating the GWR (Crosbie et al.,
571 2019; Scanlon et al., 2002). Unfortunately, in most developing countries and remote regions, groundwater
572 measured data are scarce or unavailable, and rarely one or more than one method has been used to estimate
573 GWR (Lucas et al., 2015). For such areas, satellite-based approaches, as proposed in this study for tropical

wet regions, can be scientifically much more robust than considering, for instance, the estimations of GWR as a fixed percentage of rainfall, as often adopted by water managers in some tropical developing areas.

Fig. 11 shows the comparisons between the temporal variations of groundwater level fluctuations at 9 monitoring wells and the monthly satellite-based GWR estimates. The satellite-based GWR estimates presented similar peak variation patterns to those observed in the groundwater levels. This agreement between the peak variation patterns from the GWR and groundwater levels were observed to either shallower (e.g., W04, W9, and W13) and deeper (e.g., W15 and W16) monitoring wells. Although presenting similar peak variation patterns, it is possible to notice a monthly delay in the groundwater level fluctuations compared to the GWR amounts likely due to unsaturated zone transit which is not considered in the method, as it was already pointed out by Coelho et al. (2017) in a semiarid region.

INSERT FIG. 11 HERE

Fig. 11. Comparison between the observed groundwater levels and monthly groundwater recharge based on IMERG-C data and interpolated rain gauge data.

4. Summary and conclusions

This study developed and evaluated an innovative satellite-based approach based on the water budget equation to estimate the natural GWR over by only using freely available satellite-based data. The proposed distinctive features include the capacity to address 1) ET estimations (MOD16 algorithm) in tropical wet regions frequently overlaid by substantial cloud cover and 2) water storage change estimation in the root zone (SPL4SMAU product) in sedimentary regions seasonably prone to monthly variations. The proposed method, which also included P (IMERG product) and runoff (NRCS–CN method) information, was assessed for two hydrologically contrasting years. The spatially distributed GWR rates were compared with the measurements of groundwater levels and recharge estimates based on the WTF method applied to the monitoring wells over the study area. Overall, the results of the proposed satellite-based water budget approach performed consistently with the groundwater ground-based estimates. The monitoring wells used to evaluate the groundwater recharge rates covered different soil types, LULC, and depths (from shallow to deep). These features suggest that the proposed methodology may be reliable in characterising the spatial heterogeneity of the studied area.

Concerning ET, the use of a cloud-cleaning procedure based on monthly map compositions of biophysical data (i.e., LAI, EVI2, and ALB), combined with a more fine-tuned LULC regional product and a set of GLDAS meteorological forcing data, suggested the production of a reasonable proxy for ET despite cloudy conditions. The use of soil water storage changes calculated from the SPL4SMAU root-zone soil moisture product was shown to provide essential spatially distributed information to be included in the satellite-based approach, as the GWR estimates would vary considerably over JPA by disregarding this component at the monthly scale.

Therefore, the satellite-based approach consistently demonstrated that the consideration of soil water storage changes and the cloud cleaning procedure used to obtain ET are essential for a proper estimation of the spatially distributed GWR rates in tropical wet sedimentary regions because of their hydrologic soil-cover complexes, weather seasonality and cloudy conditions. However, some sources of uncertainty in the satellite-based approach still require a better assessment, which includes: 1) a more detailed comparison of each component of the water balance (e.g., runoff, ET, and soil moisture) with ground-based measurements to identify the errors accumulated in the residual term (i.e., GWR); and 2) the impact of interception, irrigation, and pumping demands in the GWR estimates. Also, a better representation of S_y across the region, together with an analysis of errors associated with its estimates, which contribute to the overall uncertainty of the WTF method, need to be accounted for in further studies.

Acknowledgements: The authors would like to acknowledge the financial support granted by 1) the Research Support Foundation of Paraíba State (FAPESQ-PB) (Grant REF: 88887.142311/2017-00), which also funded the contribution from Yunqing Xuan, supported in partnership with the Newton Fund, via CONFAP – The UK Academies Research Mobility 2017/2018 (Grant REF: 039/2018); 2) the Brazilian Coordination for Improvement of Higher Education Personnel (CAPES) – Finance Code 001 (Grant REF: 88887.161412/2017-00); 3) the Brazilian National Council for Scientific and Technological Development (CNPq) (Grant REF: 160043/2019-0), which also funds the Universal MCTI/CNPq No. 28/2018 (Grant REF: 433801/2018-2); 4) the Brazilian Innovation Agency (FINEP) for funding the Brazilian Managed Aquifer Recharge (BRAMAR) research project (Grant REF: 01.13.0340.00); and 5) the German Research Foundation (DFG) for funding the Cosmic Sense research project – Research Unit No. FOR 2694 (Grant REF: 357874777). The authors also acknowledge the two anonymous reviewers and the editor for the constructive comments that allowed improving the quality of the manuscript.

References

Aeschbach-Hertig, W., Gleeson, T., 2012. Regional strategies for the accelerating global problem of groundwater depletion. Nature Geoscience 5, 853–861. https://doi.org/10.1038/ngeo1617

Ahmadi, T., Ziaei, A.N., Rasoulzadeh, A., Davary, K., Esmaili, K., Izady, A., 2015. Mapping groundwater recharge areas using CRD and RIB methods in the semi-arid Neishaboor Plain, Iran. Arabian Journal of Geosciences 8, 2921–2935. https://doi.org/10.1007/s12517-014-1321-2

Ajmal, M., Kim, T.-W., 2015. Quantifying Excess Stormwater Using SCS-CN–Based Rainfall Runoff Models and Different Curve Number Determination Methods. Journal of Irrigation and Drainage Engineering 141, 1–12. https://doi.org/10.1061/(ASCE)IR.1943-4774.0000805

Allen, R.G., Pereira, L.S., Raes, D., Smith, M., 1998. Crop evapotranspiration - Guidelines for computing crop water requirements, in: FAO Irrigation and Drainage Paper 56. FAO - Food and Agriculture Organization of the United Nations, Rome, Italy, pp. 1–15.

Alley, W.M., Konikow, L.F., 2015. Bringing GRACE down to Earth. Groundwater 53, 826–829. https://doi.org/https://dx.doi.org/10.1111/gwat.12379

Alvares, C.A., Stape, J.L., Sentelhas, P.C., De Moraes Gonçalves, J.L., Sparovek, G., 2013. Köppen's climate classification map for Brazil. Meteorologische Zeitschrift 22, 711–728. https://doi.org/10.1127/0941-2948/2013/0507

Araújo Filho, J.C., Burgos, N., Lopes, O.F., Silva, F.H.B.B. Da, Medeiros, L.A.R., Melo Filho, H.F.R. De, Parahyba, R.D.B.V., Cavalcanti, A.C., Oliveira Neto, M.B. De, Silva, F.B.R.E., Leite, A.P., Santos, J.C.P. Dos, Souza Neto, N.C. De, Silva, A.B. Da, Luz, L.R.Qu.P. Da, Lima, P.C. De, Reis, R.M.G., Barros, A.H.C., 2000. Levantamento de reconhecimento de baixa e média intensidade dos solos do Estado de Pernambuco. … de Janeiro, Embrapa Solos 382.

Awadallah, A.G., Farahat, M.S., Haggag, M., 2017. Discussion of "Interfacing the geographic information system , remote sensing, and the soil conservation service-curve number method to estimate curve number and runoff volume in the ASIR region of Saudi Arabia" by Fawzi S . Mohammad, Jan Adamowski. Arabian Journal of Geosciences 10, 1–10. https://doi.org/http:/dx.doi.org/10.1007/s12517-017-2984-2

Bastiaanssen, W.G.M., Pelgrum, H., Wang, J., Ma, Y., Moreno, J.F., Roerink, G.J., van der Wal, T., 1998. A remote sensing surface energy balance algorithm for land (SEBAL), Part 1: Formulation. Journal of Hydrology 212–213, 213–229. https://doi.org/10.1016/S0022-1694(98)00254-6

Brunner, P., Bauer, P., Eugster, M., Kinzelbach, W., 2004. Using remote sensing to regionalize local precipitation recharge rates obtained from the Chloride Method. Journal of Hydrology 294, 241–250. https://doi.org/10.1016/j.jhydrol.2004.02.023

Brunner, P., Hendricks Franssen, H.J., Kgotlhang, L., Bauer-Gottwein, P., Kinzelbach, W., 2007. How can remote sensing contribute in groundwater modeling? Hydrogeology Journal 15, 5–18. https://doi.org/10.1007/s10040-006-0127-z

Cai, Z., Ofterdinger, U., 2016. Analysis of groundwater-level response to rainfall and estimation of annual recharge in fractured hard rock aquifers, NW Ireland. Journal of Hydrology 535, 71–84. https://doi.org/10.1016/j.jhydrol.2016.01.066

Callahan, T.J., Vulava, V.M., Passarello, M.C., Garrett, C.G., 2012. Estimating groundwater recharge in lowland watersheds. Hydrological Processes 26, 2845–2855. https://doi.org/10.1002/hyp.8356

Coelho, V.H.R., Montenegro, S., Almeida, C.N., Silva, B.B., Oliveira, L.M., Gusmão, A.C. V, Freitas, E.S., Montenegro, A.A.A., 2017. Alluvial groundwater recharge estimation in semi-arid environment using remotely sensed data. Journal of Hydrology 548, 1–15. https://doi.org/10.1016/j.jhydrol.2017.02.054

CPRM – Geological Service of Brazil, 2020. SIAGAS – Groundwater Information System [WWW Document]. Law No. 9.433/1997.

Crosbie, R.S., Davies, P., Harrington, N., Lamontagne, S., 2015. Ground truthing groundwater-recharge estimates derived from remotely sensed evapotranspiration: a case in South Australia. Hydrogeology Journal 23, 335–350. https://doi.org/10.1007/s10040-014-1200-7

Crosbie, R.S., Doble, R.C., Turnadge, C., Taylor, A.R., 2019. Constraining the Magnitude and Uncertainty of Specific Yield for Use in the Water Table Fluctuation Method of Estimating Recharge. Water Resources Research 55, 7343–7361. https://doi.org/10.1029/2019WR025285

Cuthbert, M.O., Taylor, R.G., Favreau, G., Todd, M.C., Shamsudduha, M., Villholth, K.G., MacDonald, A.M., Scanlon, B.R., Kotchoni, D.O.V., Vouillamoz, J.-M., Lawson, F.M.A., Adjomayi, P.A., Kashaigili, J., Seddon, D., Sorensen, J.P.R., Ebrahim, G.Y., Owor, M., Nyenje, P.M., Nazoumou, Y., Goni, I., Ousmane, B.I., Sibanda, T., Ascott, M.J., MacDonald, D.M.J., Agyekum, W., Koussoubé, Y., Wanke, H., Kim, H., Wada, Y., Lo, M.-H., Oki, T., Kukuric, N., 2019. Observed controls on resilience of groundwater to climate variability in sub-Saharan Africa. Nature 572, 230–234. https://doi.org/http://dx.doi.org/10.1038/s41586-019-1441-7

Deshmukh, D.S., Chaube, U.C., Ekube Hailu, A., Aberra Gudeta, D., Tegene Kassa, M., 2013. Estimation and comparision of curve numbers based on dynamic land use land cover change, observed rainfall-runoff data and land slope. Journal of Hydrology 492, 89–101. https://doi.org/10.1016/j.jhydrol.2013.04.001

Döll, P., Schmied, H.M., Schuh, C., Portmann, F.T., Eicker, A., 2014. Global-scale assessment of groundwater depletion and related groundwater abstractions: combining hydrological modeling with information from well observations and GRACE satellites. Water Resources Research 50, 5698–5720. https://doi.org/http://dx.doi.org/10.1002/2014WR015595

Durán-Barroso, P., González, J., Valdés, J.B., 2017. Sources of uncertainty in the NRCS CN model: Recognition and solutions. Hydrological Processes 31, 3898–3906. https://doi.org/10.1002/hyp.11305

Famiglietti, J.S., 2014. The global groundwater crisis. Nature Climate Change 4, 945–948. https://doi.org/http://dx.doi.org/10.1038/nclimate2425

Famiglietti, J.S., Cazenave, A., Eicker, A., Reager, J.T., Rodell, M., Velicogna, I., 2015. Satellites provide the big picture. Science 349, 684–685. https://doi.org/10.1126/science.aac9238

Gadelha, A.N., Coelho, V.H.R., Xavier, A.C., Barbosa, L.R., Melo, D.C.D., Xuan, Y., Huffman, G.J., Petersen, W.A., Almeida, C.N., 2019. Grid box-level evaluation of IMERG over Brazil at various space and time scales. Atmospheric Research 218, 231–244. https://doi.org/10.1016/j.atmosres.2018.12.001

Gokmen, M., Vekerdy, Z., Lubczynski, M.W., Timmermans, J., Batelaan, O., Verhoef, W., 2013. Assessing Groundwater Storage Changes Using Remote Sensing–Based Evapotranspiration and Precipitation at a Large Semiarid Basin Scale. Journal of Hydrometeorology 14, 1733–1753. https://doi.org/10.1175/JHM-D-12-0156.1

Graaf, I.E.M., Beek, R.L.P.H. Van, Gleeson, T., Moosdorf, N., Schmitz, O., Sutanudjaja, E.H., Bierkens, M.F.P., Engineering, C., 2017. Advances in Water Resources A global-scale two-layer transient groundwater model: Development and application to groundwater depletion. Advances in Water Resources 102, 53–67. https://doi.org/10.1016/j.advwatres.2017.01.011

Hawkins, R.H., Hjelmfelt, A.T., Members, A., Zevenbergen, A.W., 1985. Runoff probability, storm depth, and curve numbers. Journal of Irrigation and Drainage Engineering 111, 330–340. https://doi.org/http://dx.doi.org/10.1061/(ASCE)0733-9437(1985)111:4(330)

Healy, R.W., Cook, P.G., 2002. Using groundwater levels to estimate recharge. Hydrogeology Journal 10, 91–109. https://doi.org/10.1007/s10040-001-0178-0

Hornero, J., Manzano, M., Ortega, L., Custodio, E., 2016. Integrating soil water and tracer balances, numerical modelling and GIS tools to estimate regional groundwater recharge: Application to the Alcadozo Aquifer System (SE Spain). Science of the Total Environment 568, 415–432. https://doi.org/10.1016/j.scitotenv.2016.06.011

Huete, A.R., 1988. A soil-adjusted vegetation index (SAVI). Remote Sensing of Environment 25, 295–209. https://doi.org/10.1016/0034-4257(88)90106-X

Huffman, G.J., Bolvin, D.T., Nelkin, E.J., 2018. Integrated Multi-satellitE Retrievals for GPM (IMERG) Technical Documentation.

Jasechko, S., Birks, S.J., Gleeson, T., Wada, Y., Fawcett, P.J., Sharp, Z.D., McDonnell, J.J., Welker, J.M., 2014. The pronounced seasonality of global groundwater recharge. Water Resources Research 50, 1–23. https://doi.org/http://dx.doi.org/10.1002/2014WR015809

Jiang, Z., Huete, A.R., Didan, K., Miura, T., 2008. Remote Sensing of Environment Development of a two-band enhanced vegetation index without a blue band. Remote Sensing of Environment 112, 3833–3845. https://doi.org/10.1016/j.rse.2008.06.006

Khalaf, A., Donoghue, D., 2012. Estimating recharge distribution using remote sensing: A case study from the West Bank. Journal of Hydrology 414–415, 354–363. https://doi.org/10.1016/j.jhydrol.2011.11.006

Lakshmi, V., Fayne, J., Bolten, J., 2018. A comparative study of available water in the major river basins of the world. Journal of Hydrology 567, 510–532. https://doi.org/http://dx.doi.org/10.1016/j.jhydrol.2018.10.038

Lal, M., Mishra, S.K., Kumar, M., 2019. Reverification of antecedent moisture condition dependent runoff curve number formulae using experimental data of Indian watersheds. Catena 173, 48–58. https://doi.org/https://dx.doi.org/10.1016/j.catena.2018.09.002

Lal, M., Mishra, S.K., Pandey, A., Pandey, R.P., Meena, P.K., Chaudhary, A., Jha, R.K., Shreevastava, A.K., Kumar, Y., 2017. Evaluation of the Soil Conservation Service curve number methodology using data from agricultural plots. Hydrogeology Journal 25, 151–167. https://doi.org/http://dx.doi.org/10.1007/s10040-016-1460-5

Le, H.M., Sutton, J.R.P., Bui, D. Du, Bolten, J.D., Lakshmi, V., 2018. Comparison and bias correction of TMPA precipitation products over the Lower Part of Red–Thai Binh river basin of Vietnam. Remote Sensing 10, 1–21. https://doi.org/http://dx.doi.org/10.3390/rs10101582

Lenderink, G., Buishand, A., van Deursen, W., 2007. Estimates of future discharges of the river Rhine using two scenario methodologies: direct versus delta approach. Hydrology and Earth System Sciences 11, 1145–1159. https://doi.org/http://dx.doi.org/10.5194/hess-11-1145-2007

Lima, R.N. de S., Ribeiro, C.B. de M., 2018. Spatial variability of daily evapotranspiration in a mountainous watershed by coupling surface energy balance and solar radiation model with gridded weather dataset. Proceedings 2, 1–6. https://doi.org/http://dx.doi.org/10.3390/ecrs-2-05155

Lu, X., Tang, G., Wang, X., Liu, Y., Jia, L., Xie, G., Li, S., 2019. Correcting GPM IMERG precipitation data over the Tianshan Mountains in China. Journal of Hydrology 575, 1239–1252. https://doi.org/https://dx.doi.org/10.1016/j.jhydrol.2019.06.019

Lucas, M., Oliveira, P.T.S., Melo, D.C.D., Wendland, E., 2015. Evaluation of remotely sensed data for estimating recharge to an outcrop zone of the Guarani Aquifer System (South America). Hydrogeology Journal 23, 961–969. https://doi.org/10.1007/s10040-015-1246-1

MacDonald, A.M., Lark, R.M., Taylor, R.G., Abiye, T., Fallas, H.C., Favreau, G., Goni, I.B., Kebede, S., Scanlon, B., Sorensen, J.P.R., Tijani, M., Upton, K.A., West, C., 2021. Mapping groundwater recharge in Africa from ground observations and implications for water security. Environmental Research Letters 16, 034012. https://doi.org/10.1088/1748-9326/abd661

766 Maier, R., Krebs, G., Pichler, M., Muschalla, D., Gruber, G., 2020. Spatial Rainfall Variability in Urban
767 Environments — High-Density Precipitation Measurements on a City-Scale. Water 12, 1157.
768 https://doi.org/10.3390/w12041157

769 Malakar, P., Mukherjee, A., Bhanja, S.N., Scanlon, B.R., Verma, S., Rangarajan, R., 2019. Long-term
770 groundwater recharge rates across India by in situ measurements. Hydrology and Earth System Sciences
771 23, 711–722. https://doi.org/10.5194/hess-23-711-2019

772 Mathias, S.A., Sorensen, J.P.R., Butler, A.P., 2017. Soil moisture data as a constraint for groundwater
773 recharge estimation. Journal of Hydrology 552, 258–266.
774 https://doi.org/http://dx.doi.org/10.1016/j.jhydrol.2017.06.040

775 Melo, D. de C.D., Wendland, E., Guanabara, R.C., 2015. Estimate of groundwater recharge based on Water
776 Balance in the unsaturated soil zone. Revista Brasileira de Ciência do Solo 39, 1335–1343.
777 https://doi.org/10.1590/01000683rbcs20140740

778 Melo, D.C.D., Anache, J.A.A., Almeida, C. das N., Coutinho, J. V., Ramos Filho, G.M., Rosalem, L.M.P.,
779 Pelinson, N.S., Ferreira, G.L.R.A., Schwamback, D., Calixto, K.G., Siqueira, J.P.G., Duarte-
780 Carvajalino, J.C., Jhunior, H.C.S., Nóbrega, J.D., Morita, A.K.M., Leite, C.M.C., Guedes, A.C.E.,
781 Coelho, V.H.R., Wendland, E., 2020. The big picture of field hydrology studies in Brazil. Hydrological
782 Sciences Journal 02626667.2020.1747618. https://doi.org/10.1080/02626667.2020.1747618

783 Melo, D.C.D., Anache, J.A.A., Borges, V.P., Miralles, D.G., Martens, B., Fisher, J.B., Nóbrega, R.L.B.,
784 Moreno, A., Cabral, O.M.R., Rodrigues, T.R., Bezerra, B., Silva, C.M.S., Neto, A.A.M., Moura,
785 M.S.B., Marques, T. v., Campos, S., Nogueira, J.S., Rosolem, R., Souza, R.M.S., Antonino, A.C.D.,
786 Holl, D., Galleguillos, M., Perez- Quezada, J.F., Verhoef, A., Kutzbach, L., Lima, J.R.S., Souza, E.S.,
787 Gassman, M.I., Perez, C.F., Tonti, N., Posse, G., Rains, D., Oliveira, P.T.S., Wendland, E., 2021. Are
788 Remote Sensing Evapotranspiration Models Reliable Across South American Ecoregions? Water
789 Resources Research 57. https://doi.org/10.1029/2020WR028752

790 Melo, D.C.D., Wendland, E., 2017. Shallow aquifer response to climate change scenarios in a small
791 catchment in the Guarani Aquifer outcrop zone. Annals of the Brazilian Academy of Sciences 89, 391–
792 406.

793 Minnig, M., Moeck, C., Radny, D., Schirmer, M., 2018. Impact of urbanization on groundwater recharge
794 rates in Dübendorf, Switzerland. Journal of Hydrology 563, 1135–1146.
795 https://doi.org/http://dx.doi.org/10.1016/j.jhydrol.2017.09.058

796 Moeck, C., Grech-Cumbo, N., Podgorski, J., Bretzler, A., Gurdak, J.J., Berg, M., Schirmer, M., 2020. A
797 global-scale dataset of direct natural groundwater recharge rates: a review of variables, processes and
798 relationships. Science of the Total Environment 717, 1–19.
799 https://doi.org/https://dx.doi.org/10.1016/j.scitotenv.2020.137042

800 Moghim, S., McKnight, S.L., Zhang, K., Ebtehaj, A.M., Knox, R.G., Bras, R.L., Moorcroft, R., Wang, J.,
801 2016. Bias-corrected data sets of climate model outputs at uniform space–time resolution for land
802 surface modelling over Amazonia. International Journal of Climatology 37, 621–636.
803 https://doi.org/http://dx.doi.org/10.1002/joc.4728

804 Mohan, C., Western, A.W., Wei, Y., Saft, M., 2018. Predicting groundwater recharge for varying land
805 cover and climate conditions – a global meta-study. Hydrology and Earth System Sciences 22, 2689–
806 2703. https://doi.org/https://dx.doi.org/10.5194/hess-22-2689-2018

807 Monteith, J.L., 1965. Evaporation and Environment, in: Symposium of the Society for Experimental
808 Biology. pp. 205–234.

809 Mu, Q., Heinsch, F.A., Zhao, M., Running, S.W., 2007. Development of a global evapotranspiration
810 algorithm based on MODIS and global meteorology data. Remote Sensing of Environment 111, 519–
811 536.

Mu, Q., Zhao, M., Running, S.W., 2011. Improvements to a MODIS global terrestrial evapotranspiration algorithm. Remote Sensing of Environment 115, 1781–1800. https://doi.org/10.1016/j.rse.2011.02.019

Munch, Z., Conrad, J.E., Gibson, L.A., Palmer, A.R., Hughes, D., 2013. Satellite earth observation as a tool to conceptualize hydrogeological fluxes in the Sandveld, South Africa. Hydrogeology Journal 21, 1053–1070. https://doi.org/10.1007/s10040-013-1004-1

NRCS – Natural Resources Conservation Service, 2004. Hydrologic soil-cover complexes, in: Mockus, V., Moody, H.F., NRCS (Eds.), Part 630 Hydrology, National Engineering Handbook. USDA – United States Department of Agriculture, Washington, DC, pp. 1–20.

O'Driscoll, M., Clinton, S., Jefferson, A., Manda, A., McMillan, S., 2010. Urbanization effects on watershed hydrology and in-stream processes in the Southern United States. Water 2, 605–648. https://doi.org/http://dx.doi.org/10.3390/w2030605

Oliveira, L.M.M., Montenegro, S.M.G.L., Silva, B.B., Antonino, A.C.D. a, Moura, A.E.S.S., 2014. Real evapotranspiration in catchment area of northeastern Brazil through the SEBAL and MODIS products [Evapotranspiração real em bacia hidrográfica do Nordeste brasileiro por meio do SEBAL e produtos MODIS]. Revista Brasileira de Engenharia Agricola e Ambiental 18, 1039–1046. https://doi.org/10.1590/1807-1929/agriambi.v18n10p1039-1046

Palharini, R.S.A., Vila, D.A., 2017. Climatological behavior of precipitating clouds in the northeast region of Brazil. Advances in Meteorology 17–21.

Ponce, V.M., Hawkins, R.H., 1996. Runoff Curve Number: Has It Reached Maturity? Journal of Hydrologic Engineering 1, 11–19. https://doi.org/10.1061/(ASCE)1084-0699(1996)1:1(11)

Reichle, R.H., de Lannoy, G.J.M., Liu, Q., Ardizzone, J. V., Colliander, A., Conaty, A., Crow, W., Jackson, T.J., Jones, L.A., Kimball, J.S., Koster, R.D., P.Mahanama, S., Smith, E.B., Berg, A., Bircher, S., Bosch, D., Caldwell, T.G., Cosh, M., González-Zamora, Á., Collins, C.D.H., Jensen, K.H., Livingston, S., Lopez-Baeza, E., Martínez-Fernández, J., McNairn, H., Moghaddam, M., Pacheco, A., Pellarin, T., Prueger, J., Rowlandson, T., Seyfried, M., Starks, P., Su, Z., Thibeault, M., van der Velde, R., Jeffrey Walker, Wu, X., Zeng, Y., 2017. Assessment of the SMAP Level-4 surface and root-zone soil moisture product using in situ measurements. Journal of Hydrometeorology 18, 2621–2645. https://doi.org/http://dx.doi.org/10.1175/JHM-D-17-0063.1

Reichle, R.H., Liu, Q., Koster, R.D., Ardizzone, J. v., Colliander, A., Crow, W.T., de Lannoy, G.J.M., Kimball, J.S., 2018. Soil Moisture Active Passive (SMAP) project assessment report for version 4 of the L4_SM sata product. Greenbelt, MD.

Rodell, M., Houser, P.R., Jambor, U., Gottschalck, J., Mitchell, K., Meng, C.-J., Arsenault, K., Cosgrove, B., Radakovich, J., Bosilovich, M., Entin, J.K., Walker, J.P., Lohmann, D., Toll, D., 2004. The Global Land Data Assimilation System. Bulletin of the American Meteorological Society 85, 381–394. https://doi.org/https://dx.doi.org/10.1175/BAMS-85-3-381

Rodríguez-Huerta, E., Rosas-Casals, M., Hernández-Terrones, L.M., 2020. A water balance model to estimate climate change impact on groundwater recharge in Yucatan Peninsula, Mexico. Hydrological Sciences Journal 65, 1–17. https://doi.org/https://dx.doi.org/10.1080/02626667.2019.1702989

Rossetti, D.F., Bezerra, F.H.R., Góes, A.M., Valeriano, M.M., Andrades-filho, C.O., Mittani, J.C.R., Tatumi, S.H., Brito-neves, B.B., 2011. Late Quaternary sedimentation in the Paraíba Basin, Northeastern Brazil: landform, sea level and tectonics in Eastern South America passive margin. Palaeogeography, Palaeoclimatology, Palaeoecology 300, 191–204. https://doi.org/http://dx.doi.org/10.1016/j.palaeo.2010.12.026

Rossetti, D.F., Góes, A.M., Bezerra, F.H.R., Valeriano, M.M., Brito-Neves, B.B., Ochoa, F.L., 2012. Contribution to the stratigraphy of the Onshore Paraíba Basin, Brazil. Anais da Academia Brasileira de Ciências 84, 313–333. https://doi.org/https://dx.doi.org/10.1590/S0001-37652012005000026

Ruhoff, A.L., Paz, A.R., Aragao, L.E.O.C., Mu, Q., Malhi, Y., Collischonn, W., Rocha, H.R., Running, S.W., 2013. Assessment of the MODIS global evapotranspiration algorithm using eddy covariance measurements and hydrological modelling in the Rio Grande basin. Hydrological Sciences Journal 58, 1658–1676. https://doi.org/10.1080/02626667.2013.837578

Running, S.W., Mu, Q., Zhao, M., Moreno, A., 2017. NASA Earth Observing System MODIS Land Algorithm User's Guide: MODIS Global Terrestrial Evapotranspiration (ET) Product (NASA MOD16A2/A3).

Salles, L., Satgé, F., Roig, H., Almeida, T., Olivetti, D., Ferreira, W., 2019. Seasonal effect on spatial and temporal consistency of the new GPM-based IMERG-v5 and GSMaP-v7 satellite precipitation estimates in Brazil's Central Plateau Region. Water 11, 668. https://doi.org/10.3390/w11040668

Sartori, A., Lombardi Neto, F., Genovez, A.M., 2005. Classificação hidrológica de solos brasileiros para a estimativa da chuva excedente com o método do Serviço de Conservação do Solo dos Estados Unidos Parte 1: Classificação. Revista Brasileira de Recursos Hídricos 10, 5–18. https://doi.org/http://dx.doi.org/10.21168/rbrh.v10n4.p5-18

Satgé, F., Xavier, A., Zolá, R.P., Hussain, Y., Timouk, F., Garnier, J., Bonnet, M.P., 2017. Comparative assessments of the latest GPM mission's spatially enhanced satellite rainfall products over the main bolivian watersheds. Remote Sensing 9, 1–16. https://doi.org/10.3390/rs9040369

Scanlon, B.R., Healy, R.W., Cook, P.G., 2002. Choosing appropriate techniques for quantifying groundwater recharge. Hydrogeology Journal 10, 18–39. https://doi.org/http:/dx.doi.org/10.1007/s10040-001-0176-2

Semire, F.A., Mohd-Mokhtar, R., Ismail, W., Mohamad, N., Mandeep, J.S., 2012. Ground validation of space-borne satellite rainfall products in Malaysia. Advances in Space Research 50, 1241–1249. https://doi.org/10.1016/j.asr.2012.06.031

Sharifi, E., Saghafian, B., Steinacker, R., 2019. Downscaling satellite precipitation estimates with multiple linear regression, artificial neural networks, and spline interpolation techniques. Journal of Geophysical Research: Atmospheres 124, 789–805. https://doi.org/http:/dx.doi.org/10.1029/2018JD028795

Shi, Z.-H., Chen, L.-D., Fang, N.-F., Qin, D.-F., Cai, C.-F., 2009. Research on the SCS-CN initial abstraction ratio using rainfall-runoff event analysis in the Three Gorges Area, China. CATENA 77, 1–7. https://doi.org/10.1016/j.catena.2008.11.006

Skofronick-Jackson, G., Kirschbaum, D., Petersen, W., Huffman, G., Kidd, C., Stocker, E., Kakar, R., 2018. The Global Precipitation Measurement (GPM) mission's scientific achievements and societal contributions: reviewing four years of advanced rain and snow observations. Quarterly Journal of the Royal Meteorological Society. https://doi.org/10.1002/qj.3313

Skofronick-Jackson, G., Petersen, W.A., Berg, W., Kidd, C., Stocker, E.F., Kirschbaum, D.B., Kakar, R., Braun, S.A., Huffman, G.J., Iguchi, T., Kirstetter, P.E., Kummerow, C., Meneghini, R., Oki, R., Olson, W.S., Takayabu, Y.N., Furukawa, K., Wilheit, T., 2017. The Global Precipitation Measurement (GPM) Mission for science and society. Bulletin of the American Meteorological Society 98, 1679–1695. https://doi.org/10.1175/BAMS-D-15-00306.1

Souza, A.G.S.S., Ribeiro Neto, A., Rossato, L., Alvalá, R.C.S., Souza, L.L., 2018. Use of SMOS L3 soil moisture data: validation and drought assessment for Pernambuco state, Northeast Brazil. Remote Sensing 10, 1–19. https://doi.org/http://dx.doi.org/10.3390/rs10081314

Sur, C., Kang, S., Kim, J.S., Choi, M., 2015. Remote sensing-based evapotranspiration algorithm: A case study of all sky conditions on a regional scale. GIScience and Remote Sensing 52, 627–642. https://doi.org/10.1080/15481603.2015.1056288

Szilágyi, J., Kovács, Á., Józsa, J., 2012. Remote-sensing based groundwater recharge estimates in the Danube-Tisza sand plateau region of Hungary. Journal of Hydrology and Hydromechanics 60, 64–72. https://doi.org/http://dx.doi.org/10.2478/v10098-012-0006-3

905 Szilagyi, J., Zlotnik, V.A., Gates, J.B., Jozsa, J., 2011. Mapping mean annual groundwater recharge in the
906 Nebraska Sand Hills, USA. Hydrogeology Journal 19, 1503–1513. https://doi.org/10.1007/s10040-011-
907 0769-3

908 Tan, M.L., Duan, Z., 2017. Assessment of GPM and TRMM precipitation products over Singapore.
909 Remote Sensing 9, 1–16. https://doi.org/http://dx.doi.org/10.3390/rs9070720

910 Tang, G., Zeng, Z., Long, D., Guo, X., Yong, B., Zhang, W., Hong, Y., 2016. Statistical and Hydrological
911 Comparisons between TRMM and GPM Level-3 Products over a Midlatitude Basin: Is Day-1 IMERG a
912 Good Successor for TMPA 3B42V7? Journal of Hydrometeorology 17, 121–137.
913 https://doi.org/10.1175/JHM-D-15-0059.1

914 Tapley, B.D., Bettadpur, S., Ries, J.C., Thompson, P.F., Watkins, M.M., 2004. GRACE measurements of
915 mass variability in the Earth System. Science 305, 503–5050.
916 https://doi.org/http://dx.doi.org/10.1126/science.1099192

917 Teixeira, A.H.D.C., Morris, S.-W., Hernandez, F.B.T., Andrade, R.G., Leivas, J.F., 2013. Large-scale water
918 productivity assessments with MODIS images in a changing semi-arid environment: A Brazilian case
919 study. Remote Sensing 5, 5783–5804. https://doi.org/10.3390/rs5115783

920 Usman, M., Liedl, R., Kavousi, A., 2015. Estimation of distributed seasonal net recharge by modern
921 satellite data in irrigated agricultural regions of Pakistan. Environmental Earth Sciences 74, 1463–1486.
922 https://doi.org/10.1007/s12665-015-4139-7

923 Valle Junior, L.C.G. do, Rodrigues, D.B.B., Oliveira, P.T.S. de, 2019. Initial abstraction ratio and Curve
924 Number estimation using rainfall and runoff data from a tropical watershed. RBRH 24, 1–9.
925 https://doi.org/10.1590/2318-0331.241920170199

926 Vasco, D.W., Farr, T.G., Jeanne, P., Doughty, C., Nico, P., 2019. Satellite-based monitoring of
927 groundwater depletion in California's Central Valley. Scientific Reports 9, 16053.
928 https://doi.org/10.1038/s41598-019-52371-7

929 Veeck, S., da Costa, F.F., Correia Lima, D.L., da Paz, A.R., Allasia Piccilli, D.G., 2020. Scale dynamics of
930 the HIDROPIXEL high-resolution DEM-based distributed hydrologic modeling approach.
931 Environmental Modelling & Software 127, 104695. https://doi.org/10.1016/j.envsoft.2020.104695

932 Verma, S., Verma, R.K., Mishra, S.K., Singh, A., Jayaraj, G.K., 2017. A revisit of NRCS-CN inspired
933 models coupled with RS and GIS for runoff estimation. Hydrological Sciences Journal 62, 1891–1930.
934 https://doi.org/10.1080/02626667.2017.1334166

935 Vu, H. V., Merkel, B.J., 2019. Estimating groundwater recharge for Hanoi, Vietnam. Science of the Total
936 Environment 651, 1047–1057. https://doi.org/https://dx.doi.org/10.1016/j.scitotenv.2018.09.225

937 Wada, Y., van Beek, L.P.H., van Kempen, C.M., Reckman, J.W.T.M., Vasak, S., Bierkens, M.F.P., 2010.
938 Global depletion of groundwater resources. Geophysical Research Letters 37, 1–5.
939 https://doi.org/http://dx.doi.org/10.1029/2010GL044571

940 Wahr, J., Swenson, S., Zlotnicki, V., Velicogna, I., 2004. Time-variable gravity from GRACE: first results.
941 Geophysical Research Letters 31, 1–14. https://doi.org/http://dx.doi.org/10.1029/2004GL019779

942 Walker, D., Parkin, G., Schmitter, P., Gowing, J., Tilahun, S.A., Haile, A.T., Yimam, A.Y., 2019. Insights
943 from a multi-method recharge estimation comparison study. Groundwater 57, 245–258.
944 https://doi.org/http://dx.doi.org/10.1111/gwat.12801

945 Weber, K., Stewart, M., 2004. A critical analysis of the cumulative rainfall departure concept. Ground
946 water 42, 935–938. https://doi.org/10.1111/j.1745-6584.2004.t01-11-.x

947 Wendland, E., Barreto, C., Gomes, L.H., 2007. Water balance in the Guarani Aquifer outcrop zone based
948 on hydrogeologic monitoring. Journal of Hydrology 342, 261–269.
949 https://doi.org/10.1016/j.jhydrol.2007.05.033

950 Wiebe, A.J., Rudolph, D.L., 2020. On the sensitivity of modelled groundwater recharge estimates to rain
951 gauge network scale. Journal of Hydrology 585, 1–14.
952 https://doi.org/http://dx.doi.org/10.1016/j.jhydrol.2020.124741

953 Yin, L., Hu, G., Huang, J., Wen, D., Dong, J., Wang, X., Li, H., 2011. Groundwater-recharge estimation in
954 the Ordos Plateau, China: Comparison of methods. Hydrogeology Journal 19, 1563–1575.
955 https://doi.org/10.1007/s10040-011-0777-3

956

957

Figure 1

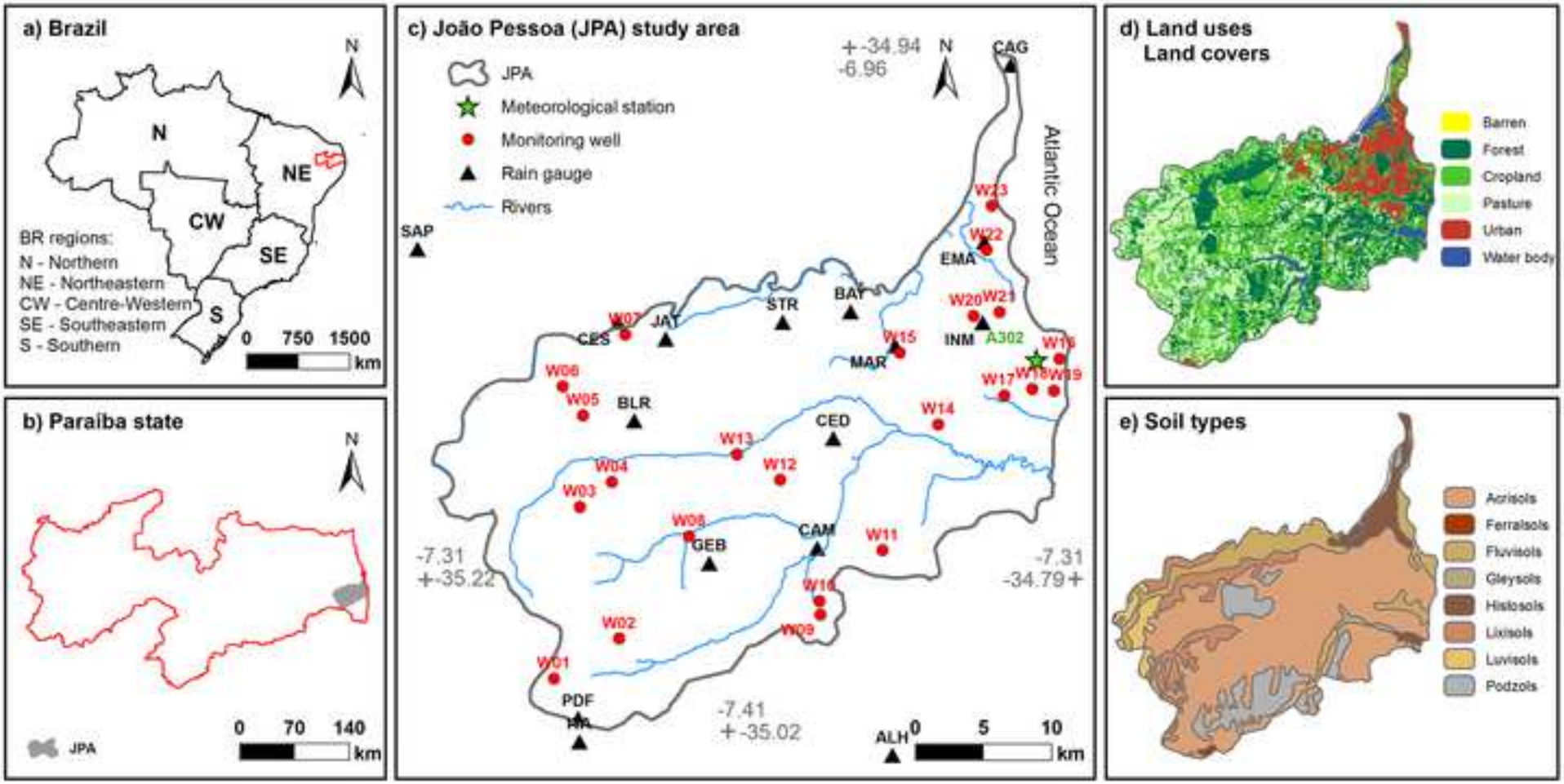
a) Brazil
N
NE
CW
SE
S
BR regions:
N - Northern
NE - Northeastern
CW - Centre-Western
SE - Southeastern
S - Southern
0 750 1500
km
b) Paraiba state
N
JPA
0 70 140
km
c) João Pessoa (JPA) study area
JPA
Meteorological station
Monitoring well
Rain gauge
Rivers
+-34.94
-6.96
-7.31
+-35.22
-7.31
-34.79+
-7.41
+-35.02
Atlantic Ocean
SAP
CAG
EMA
BAY
STR
JAT
CES
MAR
INM
A302
BLR
CED
CAM
GEB
ALH
PDF
W01
W02
W03
W04
W05
W06
W07
W08
W09
W10
W11
W12
W13
W14
W15
W16
W17
W18
W19
W20
W21
W22
W23
0 5 10
km
d) Land uses
Land covers
Barren
Forest
Cropland
Pasture
Urban
Water body
e) Soil types
Acrisols
Ferralsols
Fluvisols
Gleysols
Histosols
Lixisols
Luvisols
Podzols

Figure 2

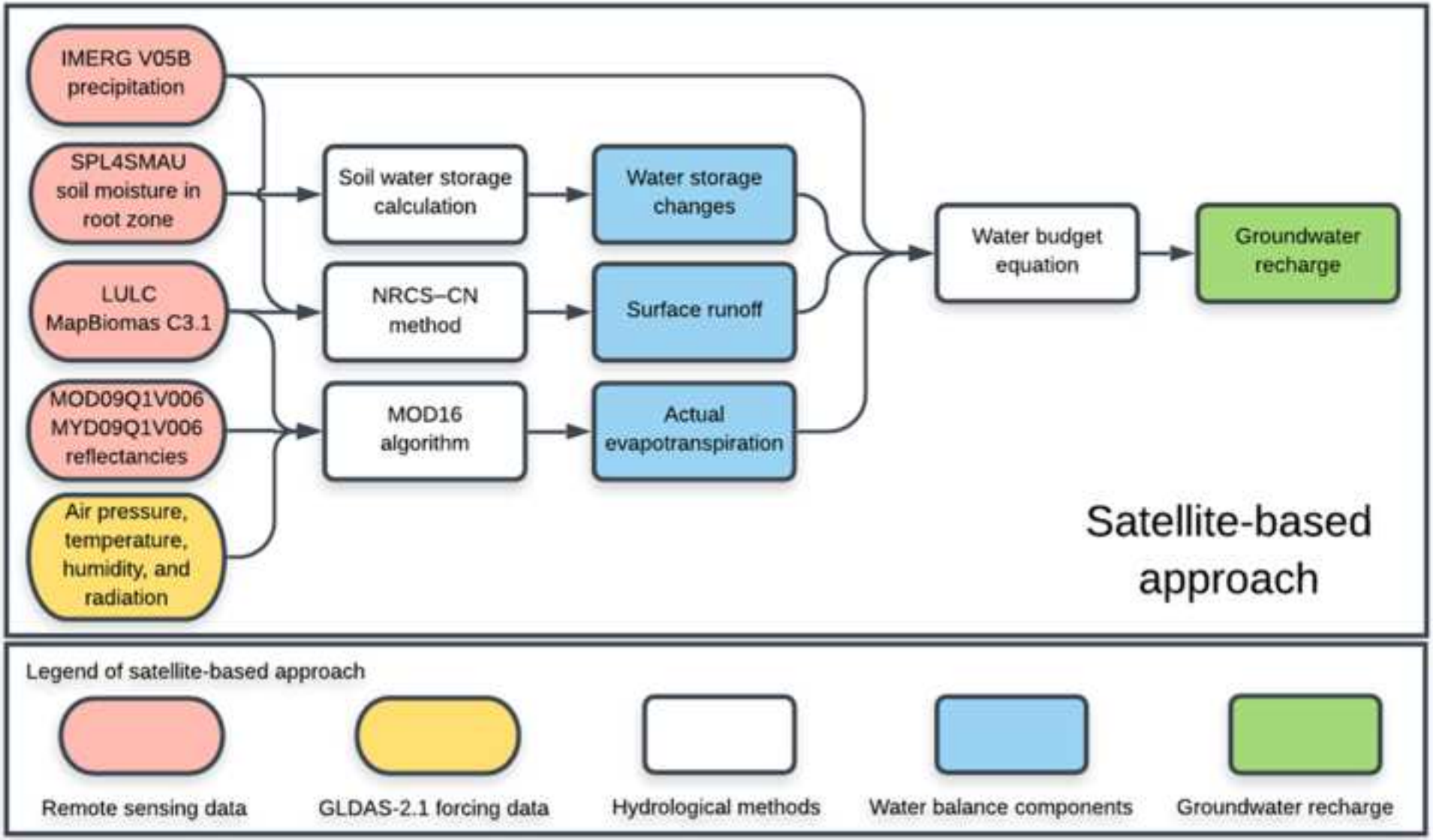

Figure 3

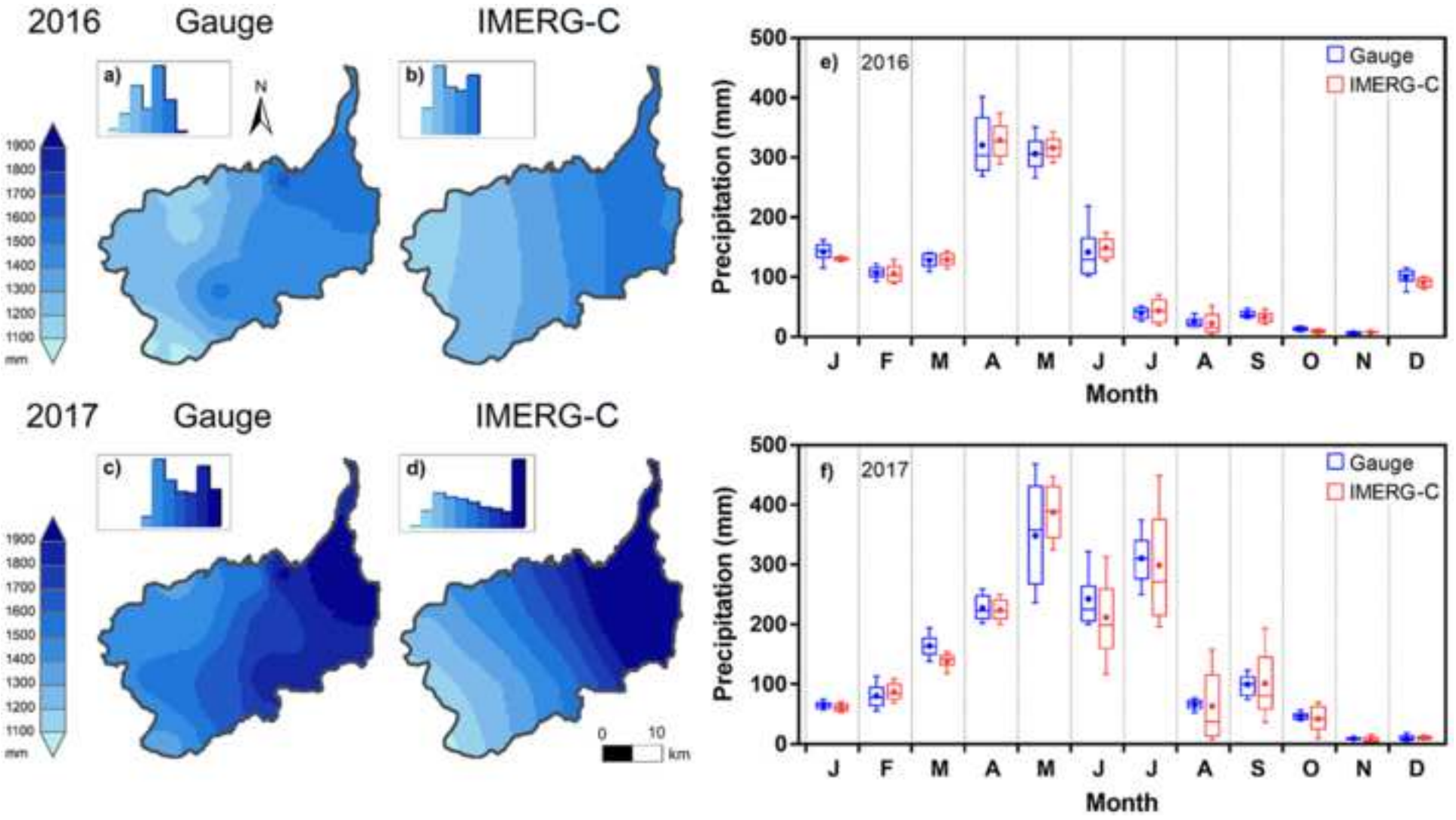

Figure 4

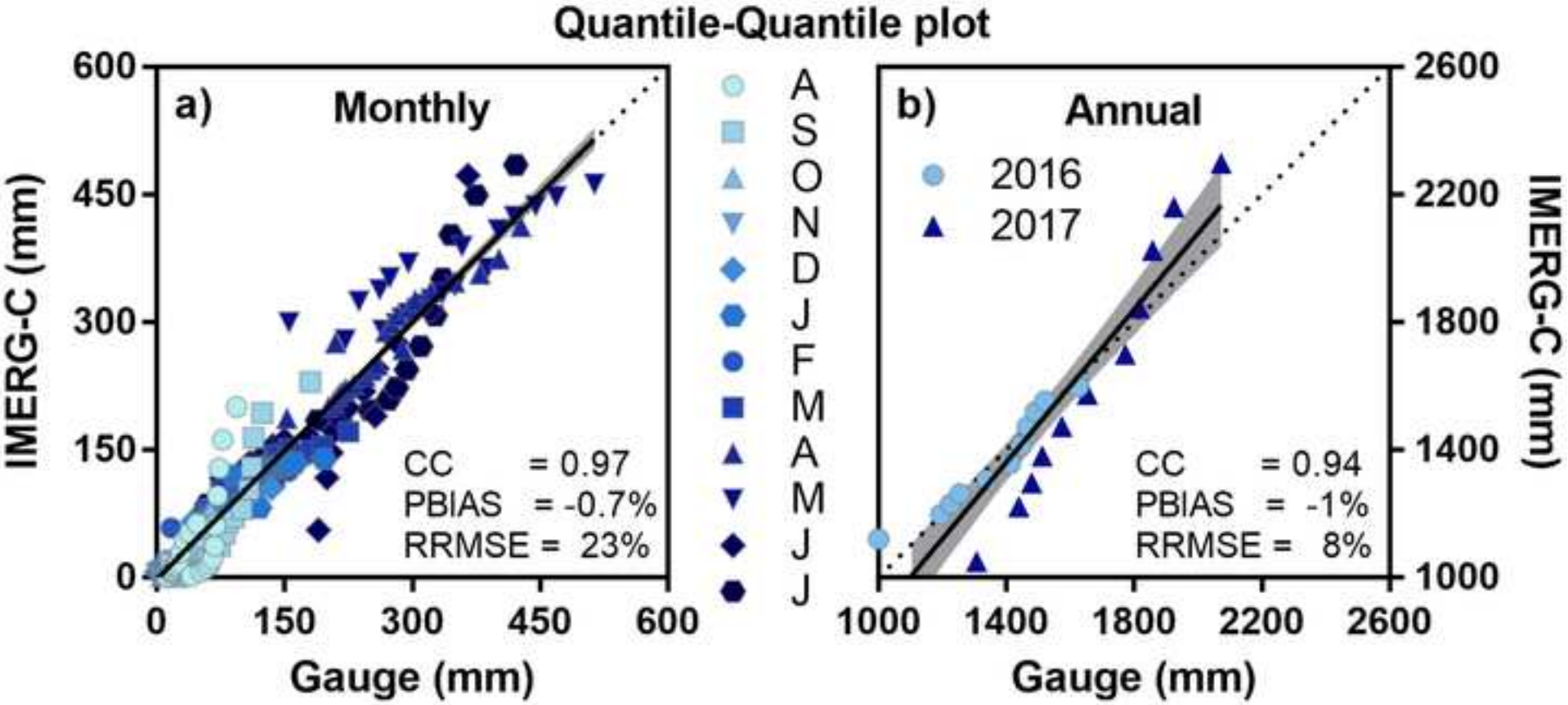

Figure 5

Click here to access/download;Figure;Fig_5__17cm_double_column_300dpi.tif

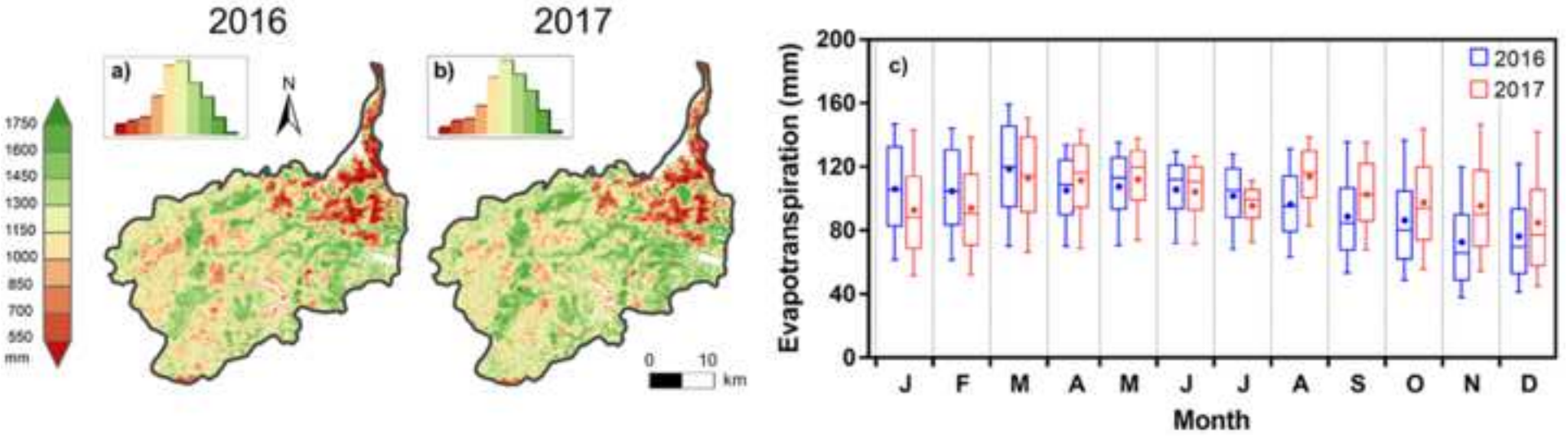

Figure 6

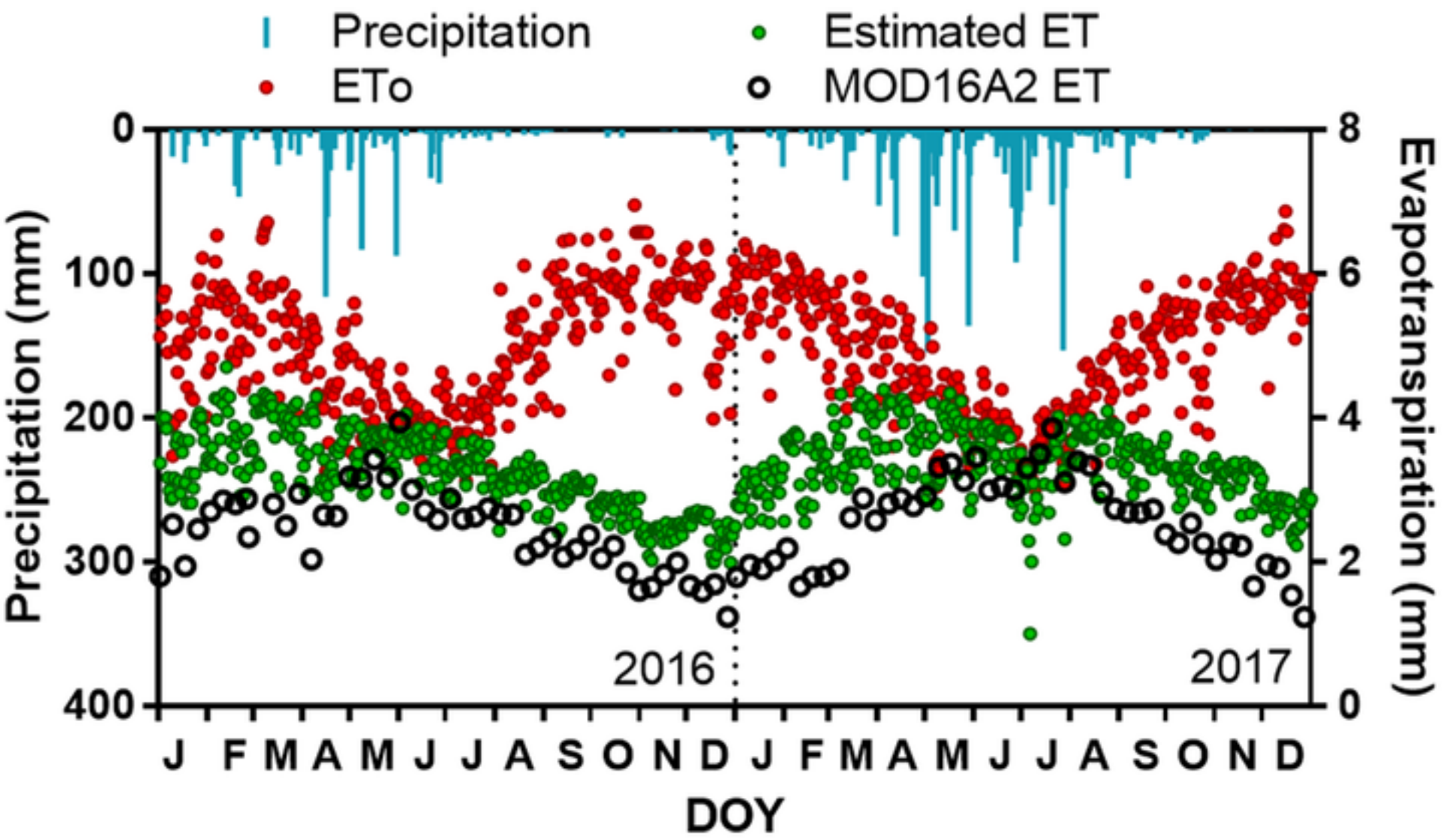

Figure 7

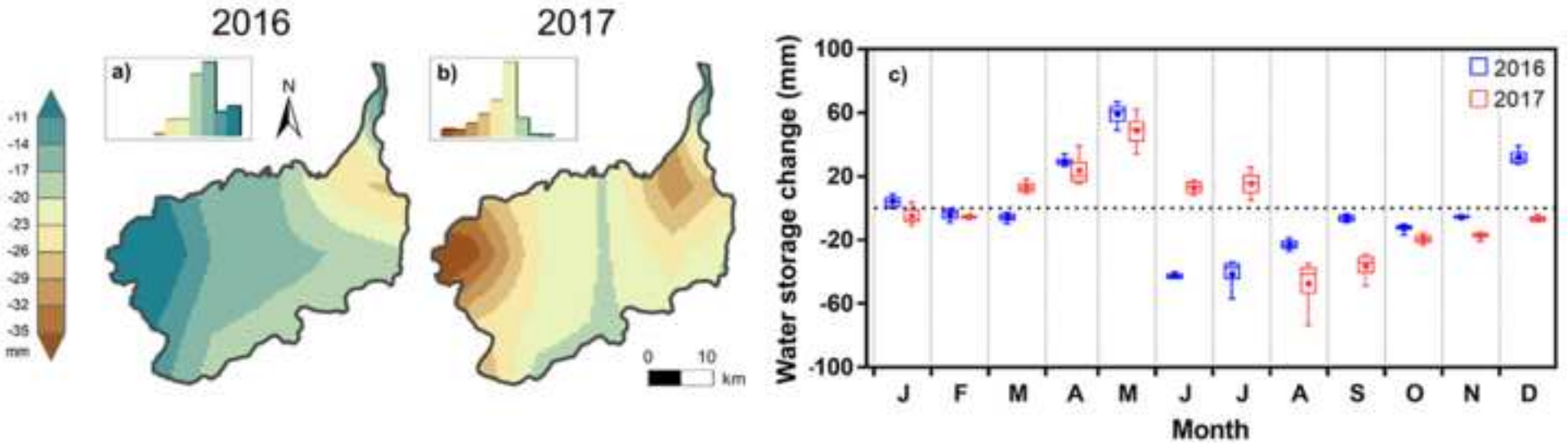

Figure 8

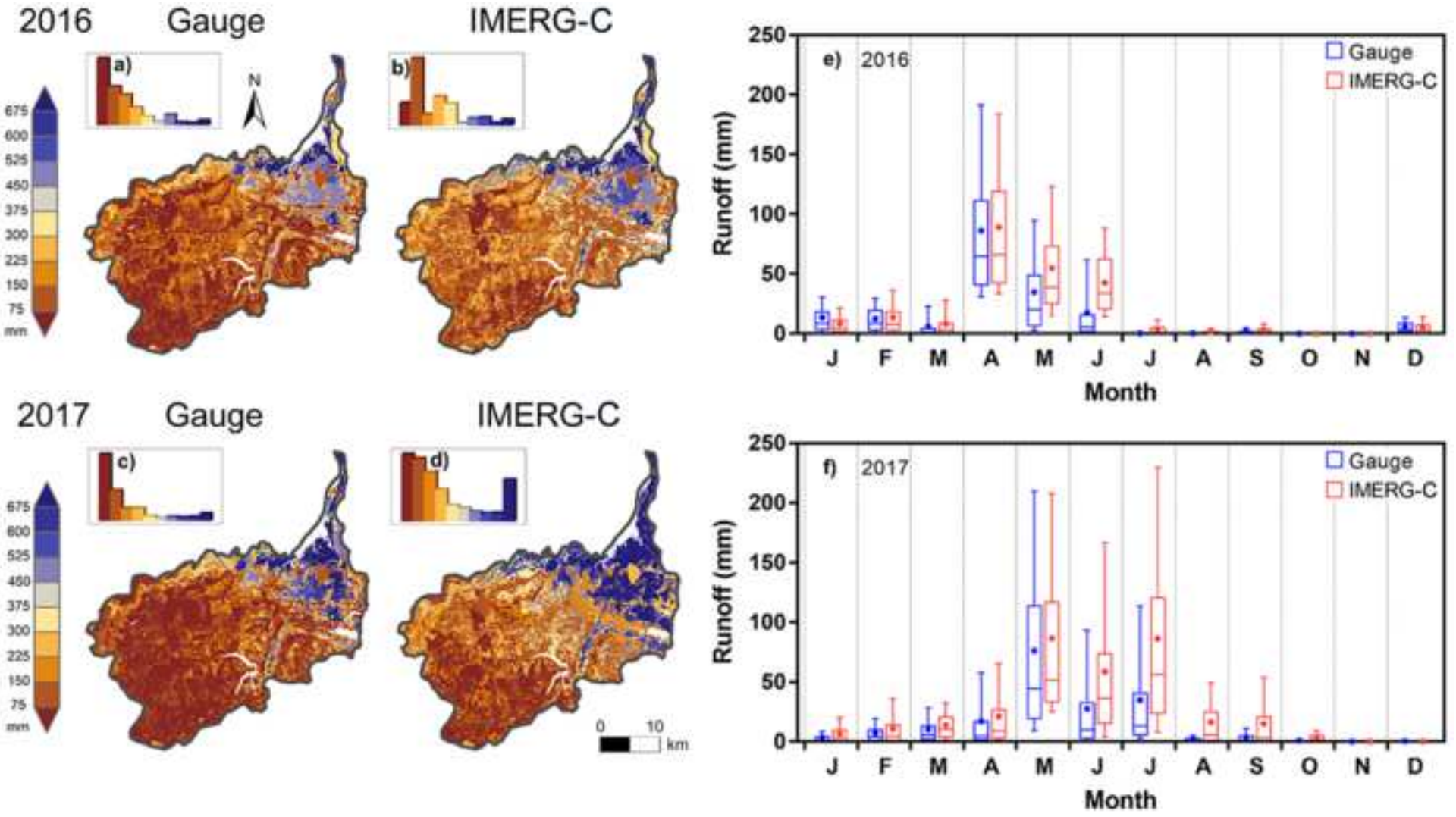
2016
Gauge
IMERG-C
a)
b)
N
675
600
525
450
375
300
225
150
75
mm
2017
Gauge
IMERG-C
c)
d)
0
10
km
e) 2016
Gauge
IMERG-C
Runoff (mm)
250
200
150
100
50
0
J
F
M
A
M
J
J
A
S
O
N
D
Month
f) 2017
Gauge
IMERG-C
Runoff (mm)
250
200
150
100
50
0
J
F
M
A
M
J
J
A
S
O
N
D
Month

Figure 9

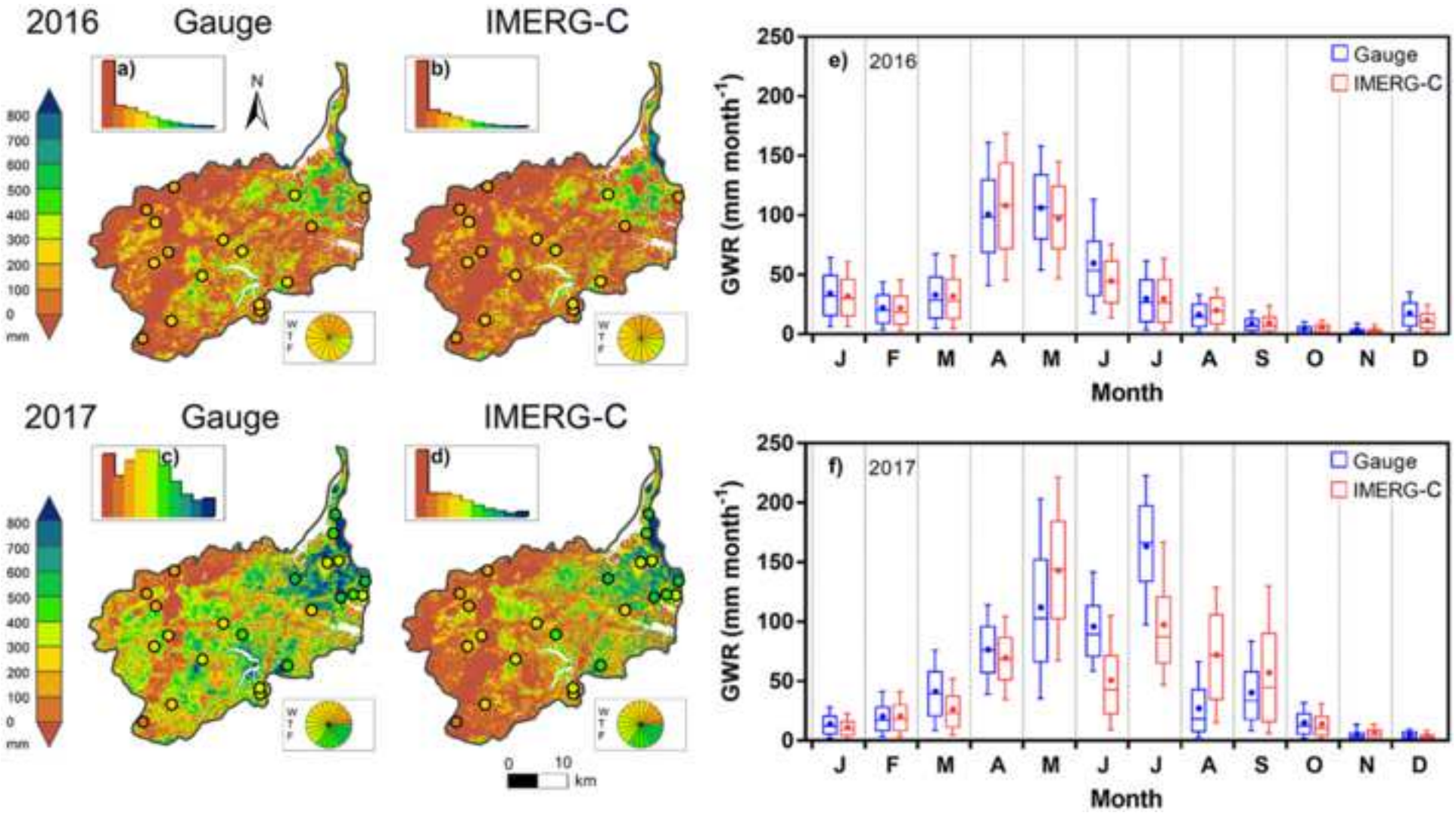
2016
Gauge
IMERG-C
a)
b)
N
800
700
600
500
400
300
200
100
0
mm
W
T
F
2017
Gauge
IMERG-C
c)
d)
0
10
km
e) 2016
f) 2017
Gauge
IMERG-C
GWR (mm month-1)
250
200
150
100
50
0
J
F
M
A
M
J
J
A
S
O
N
D
Month

Figure 10

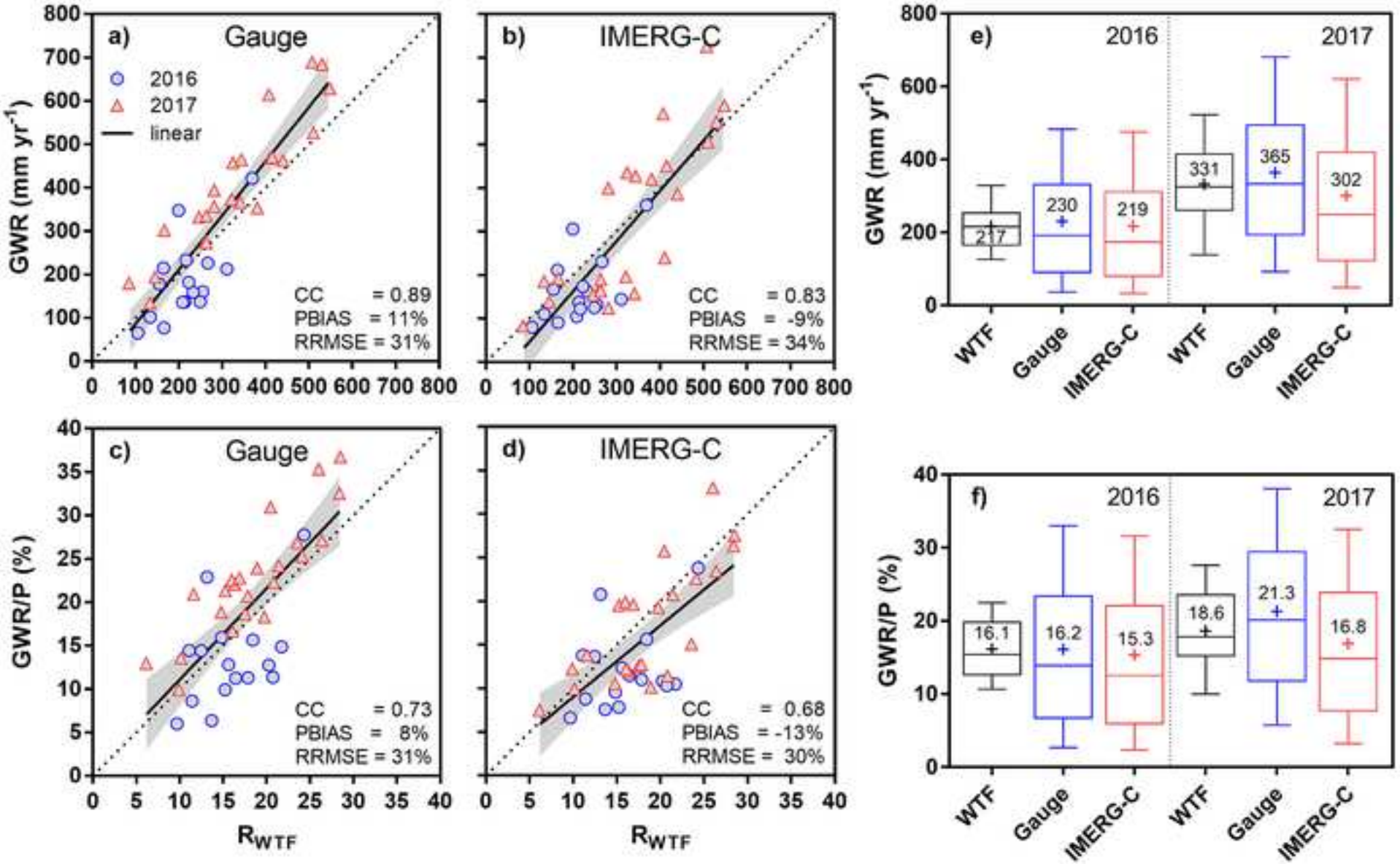
a)
Gauge
2016
2017
linear
CC = 0.89
PBIAS = 11%
RRMSE = 31%
GWR (mm yr-1)
b)
IMERG-C
CC = 0.83
PBIAS = -9%
RRMSE = 34%
c)
Gauge
CC = 0.73
PBIAS = 8%
RRMSE = 31%
GWR/P (%)
RWTF
d)
IMERG-C
CC = 0.68
PBIAS = -13%
RRMSE = 30%
RWTF
e)
2016
2017
GWR (mm yr-1)
217
230
219
331
365
302
WTF
Gauge
IMERG-C
WTF
Gauge
IMERG-C
f)
2016
2017
GWR/P (%)
16.1
16.2
15.3
18.6
21.3
16.8
WTF
Gauge
IMERG-C
WTF
Gauge
IMERG-C

Figure 11

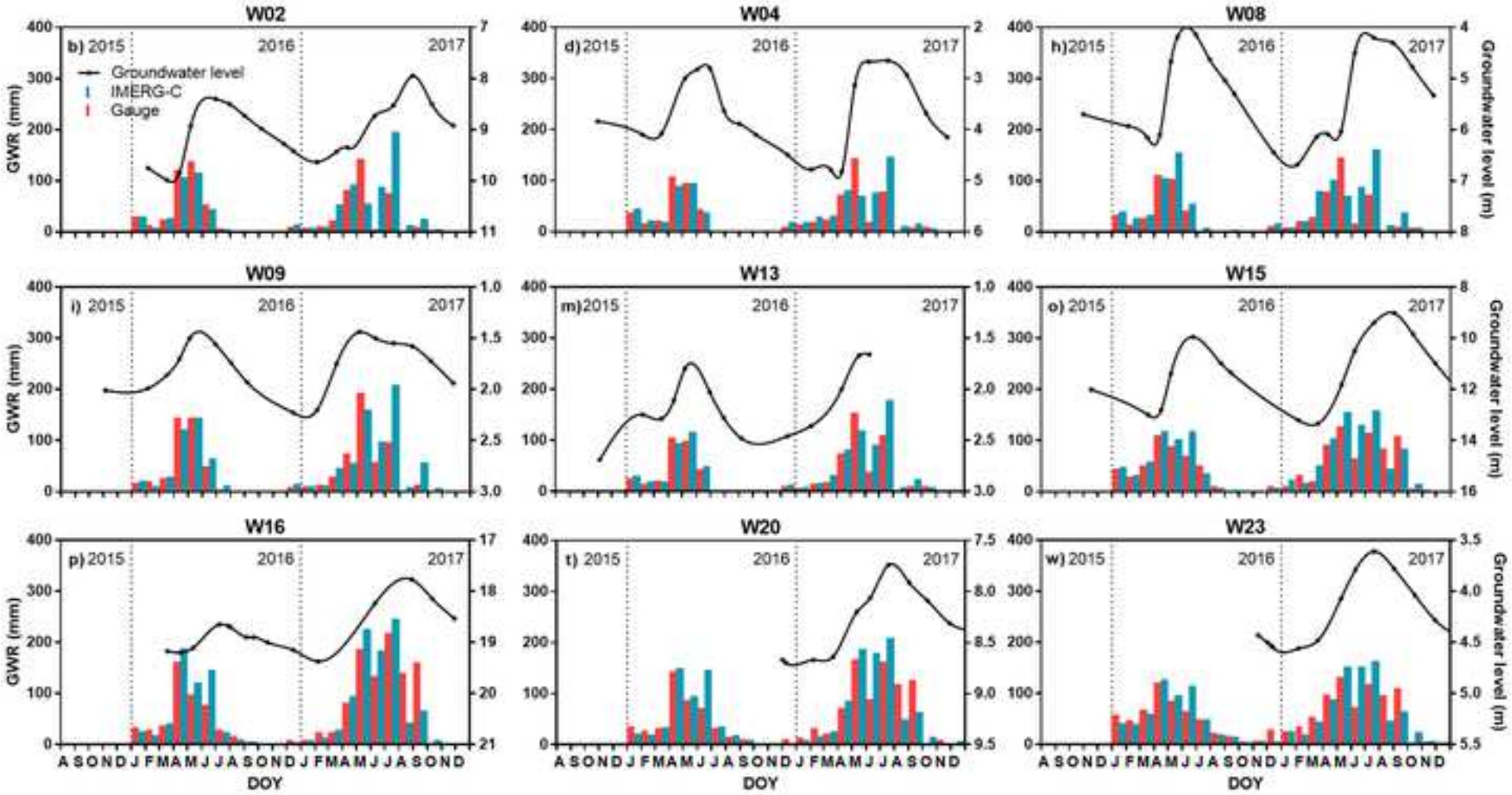
W02
b) 2015
2016
2017
Groundwater level
IMERG-C
Gauge
GWR (mm)
W04
d) 2015
W08
h) 2015
W09
i) 2015
W13
m) 2015
W15
o) 2015
W16
p) 2015
W20
t) 2015
W23
w) 2015
Groundwater level (m)
A S O N D J F M A M J J A S O N D J F M A M J J A S O N D J F M A M J J A S O N D
DOY

Table 1 – GWR rates obtained over JPA by the WTF method in 2016 and 2017.

id	S_y	P_{2016}	ΔH_{2016}	$R_{WTF,2016}$		P_{2017}	ΔH_{2017}	$R_{WTF,2017}$	
(-)	(-)	(mm)	(m)	(mm)	(%)	(mm)	(m)	(mm)	(%)
W01	0.10	1096	1.1	110	10.0	1388	0.9	90	6.5
W02	0.10	1196	2.1	210	17.6	1489	2.8	280	18.8
W03	0.10	1257	2.6	260	20.7	1508	2.5	250	16.6
W04	0.10	1244	1.6	160	12.9	1491	2.6	260	17.4
W05	0.10	1203	2.5	250	20.8	1442	1.7	170	11.8
W06	0.10	1209	1.7	170	14.1	1432	1.5	150	10.5
W07	0.10	1176	1.3	130	11.1	1349	1.3	130	9.6
W08	0.10	1463	2.2	220	15.0	1639	3.4	340	20.7
W09	0.24	1415	1.0	240	17.0	1780	1.1	264	14.8
W10	0.10	1424	2.2	220	15.4	1804	3.2	320	17.7
W11	0.24	1447	1.1	264	18.2	1827	1.8	432	23.6
W12	0.10	1431	3.1	310	21.7	1743	4.1	410	23.5
W13	0.10	1369	2.1	210	15.3	1639	2.6	260	15.9
W14	0.10	1484	1.6	160	10.8	1844	2.8	280	15.2
W15	0.10	1517	3.7	370	24.4	1861	5.3	530	28.5
W16	0.24	1520	0.8	192	12.6	1950	2.1	504	25.8
W17	0.24	-	-	-	-	1935	2.1	504	26.0
W18	0.10	-	-	-	-	1939	4.2	420	21.7
W19	0.10	-	-	-	-	1929	3.8	380	19.7
W20	0.24	-	-	-	-	2037	1.4	336	16.5
W21	0.10	-	-	-	-	2027	3.2	320	15.8
W22	0.24	-	-	-	-	1992	1.7	408	20.5
W23	0.24	-	-	-	-	1930	2.3	552	28.6